

LONG-PERIOD SEISMICITY AT SHISHALDIN VOLCANO, ALASKA

A

THESIS

Presented to the Faculty
of the University of Alaska Fairbanks
in Partial Fulfillment of the Requirements
for the Degree of

DOCTOR OF PHILOSOPHY

By

Tanja Petersen, Dipl. Geophys.

Fairbanks, Alaska

December 2006

UMI Number: 3251427

INFORMATION TO USERS

The quality of this reproduction is dependent upon the quality of the copy submitted. Broken or indistinct print, colored or poor quality illustrations and photographs, print bleed-through, substandard margins, and improper alignment can adversely affect reproduction.

In the unlikely event that the author did not send a complete manuscript and there are missing pages, these will be noted. Also, if unauthorized copyright material had to be removed, a note will indicate the deletion.

UMI[®]

UMI Microform 3251427

Copyright 2007 by ProQuest Information and Learning Company.

All rights reserved. This microform edition is protected against unauthorized copying under Title 17, United States Code.

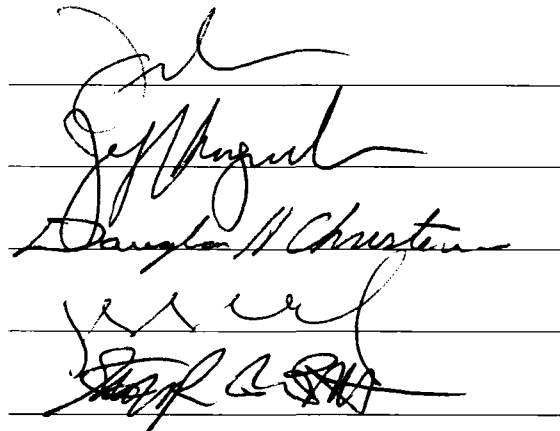
ProQuest Information and Learning Company
300 North Zeeb Road
P.O. Box 1346
Ann Arbor, MI 48106-1346

LONG-PERIOD SEISMICITY AT SHISHALDIN VOLCANO, ALASKA

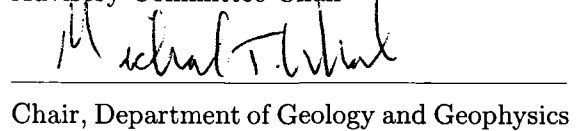
By

Tanja Petersen

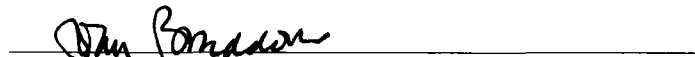
RECOMMENDED:

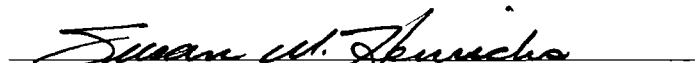


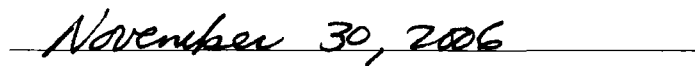
Advisory Committee Chair


Chair, Department of Geology and Geophysics

APPROVED:


Dean, College of Natural Science and Mathematics


Dean of the Graduate School


Date

Abstract

Since it last erupted in 1999, Shishaldin Volcano, Aleutian Islands, Alaska, has been characterized by a continuous and extremely high level of seismicity. The activity consists of many hundreds to thousands long-period (LP; 1–2 Hz) earthquakes per day. The rate of one LP event every 0.5–5 minutes has remained more or less constant for the last 7 years. A high rate of LP seismicity has been associated with pre-eruptive activity at many other volcanoes presented in the volcano seismology literature. Shishaldin, however, shows no other signs of volcanic unrest except for a ~200 m high steam plume that nearly always emanates from the volcano's summit and occasional weak thermal anomalies observed in satellite imagery. This thesis investigates the nature of Shishaldin's unusual volcanic behavior, and provides a case-study that mainly focuses on seismic data recorded by the short-period monitoring network surrounding the volcano, but also integrates local infrasound data, visual observations and SO₂ measurements. The observations suggest a steady-state volcanic process within an open conduit system that is capable of releasing a large amount of energy, approximately equivalent to at least one magnitude 1.8–2.6 earthquake per day. Shishaldin infrasound signals recorded by a pressure sensor co-located with a seismic instrument are used to confine the source locations of the LP events to a depth of 240 ± 200 m below the crater rim. The seismo-acoustic data suggest that the LP earthquakes are associated with degassing explosions, created by complex gas volume ruptures from a fluid-air interface. Measurements of the SO₂ flux within the puffing summit plume have revealed low values (58 tons/day), suggestive of a hydrothermal system. Four time periods of increased earthquake amplitudes, which each lasted about 1–2 months, have been analyzed. The periods of elevated seismicity are characterized by an abundance of LP events with highly similar waveforms that represent a spatially confined, repetitive, and non-destructive source process. A mechanism, known as *choked flow*, fulfills all the requirements implied by the observed repeating events and provides a plausible trigger mechanism for Shishaldin's LP events. The observations suggest that the hydrothermal system at Shishaldin is multi-fractured, regulating a pressure gradient within the gas flow through the uppermost conduit.

Table of Contents	Page
Signature Page	i
Title Page	ii
Abstract	iii
Table of Contents	iv
List of Figures	vii
List of Tables	ix
Acknowledgements	x
Chapter 1 Introduction	1
1.1 Volcano monitoring	1
1.2 Overview of thesis contents	2
1.2.1 The main chapters	2
1.2.2 The appendix	3
Chapter 2 Sustained long-period seismicity at Shishaldin Volcano, Alaska	5
2.1 Abstract	5
2.2 Introduction	6
2.3 Geologic setting	8
2.4 Limited visual and satellite observations	9
2.5 Seismic Network	11
2.6 Classification of event types	12
2.7 Overview of Shishaldin seismicity	16
2.8 Estimation of magnitudes and energy	19
2.9 Repeating LP events at Shishaldin	20
2.10 Locations	22
2.11 Constraints on allowable source models	27
2.12 Discussion and conclusions	29
2.13 Acknowledgements	31

References	32
Chapter 3 Seismo-acoustic signals associated with degassing explosions recorded at Shishaldin Volcano, Alaska, 2003–2004	38
3.1 Abstract	38
3.2 Introduction	39
3.3 Seismo-acoustic data	42
3.4 Depth constraints using seismo-acoustic data	47
3.5 Discussion and concluding remarks	54
3.6 Acknowledgments	56
References	57
Chapter 4 Swarms of repeating long-period earthquakes at Shishaldin Volcano, Alaska, 2001–2004	62
4.1 Abstract	62
4.2 Introduction	63
4.3 Methodology	67
4.3.1 Data selection	67
4.3.2 Event extraction	68
4.3.3 Event classification	69
4.3.4 Family detection	74
4.4 Results	76
4.5 Implications and discussion	91
4.6 Conclusions	95
References	97
Chapter 5 General conclusions	101
Appendix Local infrasound observations of large ash explosions at Augustine Volcano, Alaska, during January 11–28, 2006	106
A.1 Abstract	106
A.2 Introduction	107

A.3	Data acquisition	108
A.4	Acoustic data	110
A.5	Discussion	116
A.6	Acknowledgements	117
	References	118

	List of Figures	Page
2.1	a) Map of Unimak Island, easternmost island in the Aleutian Arc	7
2.2	Section of helicorder record showing 8 hours of data	8
2.3	a) A volcanic plume is typically emitted as discrete puffs	10
2.4	Seismograms and normalized power spectra for earthquake types	13
2.5	Example of pseudohelicorder plot showing 24 hours of continuous	17
2.6	Filtered digital daily (<i>pseudohelicorder</i>) counts for Shishaldin	18
2.7	Detailed helicorder counts for seven different days	21
2.8	Examples of repeating events at Shishaldin.	23
2.9	Waveforms and normalized power spectra of reference events	24
2.10	Epicenters for LP and coupled events at Shishaldin since 1997	25
2.11	Illustration of how the depth of explosion events can be estimated	26
3.1	Alaska Volcano Observatory (AVO) monitoring network	39
3.2	Example of seismo-acoustic data recorded at station SSLN	43
3.3	Acoustic and seismic traces with corresponding spectrograms	44
3.4	Example of a Shishaldin coupled earthquake	46
3.5	Shishaldin explosion examples selected from a subset	48
3.6	a) Seismo-acoustic amplitude ratios for the subset of 153 events.	50
3.7	Schematic diagram of Shishaldin Volcano	52
4.1	Daily number of earthquakes with magnitudes $M \geq 1.1$	67
4.2	Similarity matrix of 738 extracted events recorded at station SSLN	70
4.3	Example for a master event and the corresponding normalized	71
4.4	Histogram of correlation coefficients for the January 3, 2002	71
4.5	Similarity matrix of the repeating events selected on	72
4.6	Histogram of correlation coefficients for events recorded on	73
4.7	Distribution of maximum amplitudes of repeating events	74
4.8	Overlay of the 588 repeating events recorded on January 3, 2002	76

4.9	Daily stacks for Swarm A. The number of events included	77
4.10	Similarity matrix for Swarm A daily stacks.	78
4.11	Spectral amplitudes for Swarm A daily stacks.	79
4.12	Daily stacks for Swarm B. Each stack is composed	80
4.13	Similarity matrix for Swarm B.	81
4.14	Similarity matrix for extracted events recorded on 21-Nov-2002	82
4.15	The zero-to-peak amplitude distribution of the repeating events	83
4.16	Daily stacks for Swarm C.	84
4.17	Similarity matrix for repeating events of Swarm C.	85
4.18	Daily stacks for Swarm D.	86
4.19	Similarity matrix for repeating events of Swarm D.	87
4.20	Repeating event overlays and stacks for the representative days	88
4.21	Spectral amplitudes for daily stacks of repeating events	89
4.22	Similarity matrix for the 97 daily stacks from all swarms.	90
4.23	Schematic illustration of Shishaldin's multi-fractured hydrothermal system.	95
A.1	Map of Augustine Volcano showing the permanent AVO	109
A.2	Zero-to-peak pressures of the 13 acoustic signals	112
A.3	Examples of traces and cumulative energies of acoustic signals	113
A.4	Spectrograms for two of the impulsive pressure signals	114
A.5	The acoustic pulse associated with the initial vent-clearing event	115

List of Tables

Page

4.1	Family classification for representative days within each swarm.	75
A.1	Parameters of Augustine January 11–28, 2006 explosive eruption events . .	111

Acknowledgements

A large number of people have contributed to this work in one way or another. Most importantly, I would like to thank my advisor, Stephen R. McNutt, who brought me to Alaska and handed me a beautiful and challenging volcano to work on. He shared his great knowledge of volcano seismology, while at the same time giving me great independence to discover the highs and lows of conducting scientific research myself. I am very grateful for the many fieldwork and conference opportunities he approved. I am also very thankful to the other members of my advisor committee: Jeff T. Freymueller, Douglas Christensen, Jacqueline “Jackie” Caplan-Auerbach and Jessica Larsen, who never failed to provide support, encouragement and advice. I would like to give additional credits to Jackie, who may have provided the most significant contribution to my understanding of science by reviewing my manuscripts in an extensive, thorough and extremely critical way. It never took her long to plaster my manuscripts with a huge amount of useful comments. Many thanks! Many thanks also to Silvio De Angelis, who has been a very helpful and fun colleague during the last two years. My Ph.D. would probably have taken a lot longer without his wise and encouraging words about my ideas. I feel lucky that we shared the fortunate experience of participating in the response of the Alaska Volcano Observatory to the eruption of Augustine Volcano - we eventually had “a volcano that works”. I also highly appreciate the helpful support by my computer heroes Mitch Robinson and Lovro Valcic, as well as Mike West and Celso Reyes. I’ve had great colleagues at the Alaska Volcano Observatory - thanks to you all!

I have done lots of fieldwork since I came to Alaska. I would like to thank every one of the wonderful people I worked with, especially Guy Tytgat and John Paskievitch from whom I learned a lot about installing seismic stations surrounded by the magic beauty of the remote Aleutian Islands. I also had the privilege to experience the amazing field trips to Katmai and Kamchatka with Alaska Volcano Observatory. Many thanks to John Eichelberger! Many thanks also to the glacier people for adopting me into their daily lunch circle and to Leslie Almberg for being a great office mate - Vielen Dank für die Schokolade!

I've learned much more than science during my five years in Alaska and I'm more than happy about all the great adventures I've experienced, especially together with Dan Elsberg - you, "mein Sonnenschein", will always stay a big part of my beloved Alaska! Special thanks also go to my family and my dearest friends in Germany who haven't forgotten me and never stopped sending German chocolate. I've enjoyed living in Fairbanks together with wonderful friends: spending most enjoyable times at "Belfair", the "Ski Hut", the "Hobbit Hole", Robin's sauna and even at Fairbanksian bars. The cabin life, the Aurora, beautiful clear skies, and especially the many many times I went skiing together with my three "Mafia" dogs on the frozen Tanana river and through drunken forests made up for being so far away from the ocean. I will deeply miss Alaska and its people!

Chapter 1

Introduction

1.1 Volcano monitoring

Monitoring of volcanic activity is primarily focused on hazard assessment of specific volcanoes, but it also provides opportunities for research that contributes to a broader understanding of the physical processes inside volcanic systems and the great diversity in volcanic behavior worldwide. Volcano seismology probably is, next to deformation studies, the most widely applied and most extensively used monitoring technique today. The seismic monitoring of volcanoes provides an evaluation of the general, or *background*, state of activity of individual volcanoes and uses variations in local earthquake activity to detect changes in volcanic systems as possible precursors for volcanic eruptions. Although volcano seismology has proven itself as a useful tool for eruption forecasting, it is not always suitable for assessing the vigor or even the existence of explosive gas release from a volcanic system. The combination of visual or satellite observations and volcano seismology would provide a superior monitoring tool, however, in reality these observations are often limited. Volcano infrasound is a relatively young science that studies acoustic signals originated at volcanoes, and when combined with seismic data offers good potential of remotely determining the explosive degassing behavior of a volcano.

Tectonic subduction zones are associated with the world's most dangerous type of volcanic activity. The Aleutian Arc, Alaska, signifies the subduction of the Pacific Plate beneath the North American Plate by hosting about 40 volcanoes that have been active in historic times. Shishaldin Volcano, located on the easternmost island of the Aleutians, is one of them. Shishaldin exhibits a seismic behavior that stands out from many other monitored volcanoes anywhere in the world. The volcano produces a continuously high level of long-period earthquake activity commonly seen as an indicator for volcanic unrest and a potential precursor for volcanic eruptions. This is troubling for an organization such as the Alaska Volcano Observatory, which is responsible for eruption forecasting and hazard assessment. The primary objective of this dissertation is to provide a multi-parameter data

analysis that incorporates both seismic and infrasound data, in order to illuminate the internal state of Shishaldin and to enable greater understanding of the driving forces behind its unusual seismic activity.

1.2 Overview of thesis contents

1.2.1 The main chapters

The main part of this dissertation consists of three scientific chapters (Chapter 2, 3 and 4), along with this introduction and general conclusions, which focus on the seismicity recorded at Shishaldin Volcano. Chapters 2 and 3 have been individually prepared for publication in scientific journals and were published in 2006. The name of the journal and the co-authors are listed at the beginning of each chapter.

Chapter 2 presents a quantitative overview of the continuous and extremely high level of seismicity at Shishaldin, occurring a few months after the volcano last erupted in 1999 through April 2004. In this part of my dissertation, I discuss the different observation methods used to monitor Shishaldin's volcanic activity and classify the earthquake types recorded by the Shishaldin permanent seismic network operated by the Alaska Volcano Observatory. The vast majority of Shishaldin's seismic activity is composed of discrete long-period events; therefore I focus my studies on this particular earthquake type. I apply an earthquake counting method that allows me to estimate the amount of seismic energy produced by Shishaldin. I also discuss the difficulty of determining hypocentral locations for Shishaldin long-period earthquakes and show that the source is likely located within the conduit system at very shallow depth. I describe various allowable source models involving fluid and gas and propose a possible scenario leading to the steady-state post-eruption regime of Shishaldin's activity. The main conclusion of the chapter is that Shishaldin exhibits a behavior that is unusual among volcanoes in its long-lasting high level of seismicity without preceding or accompanying eruptive activity.

Chapter 3 focuses on infrasonic and seismic signals recorded at Shishaldin between July 2003 and November 2004. The nature of the observed acoustic waveforms suggests that the

infrasound source is located at the fluid-air interface within an open-vent system. I combine seismic and acoustic data in order to improve source locations, and relate Shishaldin's long-period seismicity to degassing explosions. I propose that, since the 1999 eruption, Shishaldin's conduit has changed to a hydrothermal system with magmatic gases leaking through, which is responsible for the sustained seismic activity presented in Chapter 2.

In Chapter 4 I expand the studies of Shishaldin's long-period earthquakes recorded during 2001–2004. I use waveform cross-correlation to identify highly repetitive earthquakes, investigate the nature of these events and discuss their implications. I consider several source models and propose that the choked flow model provides a plausible trigger mechanism for Shishaldin's repeating events. I conclude that the hydrothermal system, driving the generation of long-period events observed at Shishaldin, is a multi-fractured system with complex dynamics.

1.2.2 The appendix

Between January 11–28, 2006, Augustine Volcano, Alaska, exhibited several large explosive eruption events that generated strong infrasonic signals. The signals were recorded by a local microphone that was newly installed by the Alaska Volcano Observatory. The eruption provided a great opportunity for me to apply the experience gained by analyzing Shishaldin infrasound data (see Chapter 3) to a different volcano. Although the impulsive infrasonic signals produced by these two volcanoes show similarities in some aspects as they are both related to explosive degassing, they are associated with significantly different types of volcanic activity. Shishaldin's infrasonic signals were explained by frequent gas volume ruptures from a fluid-air interface. In contrast, the waveforms recorded at Augustine, which are extremely large compared to the ones recorded at Shishaldin, were associated with the vigorous and continuous degassing activity during an energetic Vulcanian-type eruption.

In Appendix A, a supplementary chapter of my dissertation, the acoustic waveforms associated with the explosive eruption sequence at Augustine are presented. The Augustine infrasound data reveal a large variety of waveforms reflecting substantial differences in

degassing behavior between the individual eruptive explosions that occurred during January 11–28, 2006. The acoustic data are used to characterize the impulsivity of the degassing sources and to distinguish between precursory sub-surface seismicity and the actual explosion events. Appendix A was published by *Geophysical Research Letters*, with T. Petersen, S. De Angelis, G. Tytgat and S. R. McNutt as the authors.

Chapter 2

Sustained long-period seismicity at Shishaldin Volcano, Alaska ¹

2.1 Abstract

From September 1999 through April 2004, Shishaldin Volcano, Aleutian Islands, Alaska, exhibited a continuous and extremely high level of background seismicity. This activity consisted of many hundreds to thousands of long-period (LP; 1–2 Hz) earthquakes per day, recorded by a 6-station monitoring network around Shishaldin. The LP events originate beneath the summit at shallow depths (0–3 km). Volcano tectonic events and tremor have rarely been observed in the summit region. Such a high rate of LP events with no eruption suggests that a steady state process has been occurring ever since Shishaldin last erupted in April–May 1999. Following the eruption, the only other signs of volcanic unrest have been occasional weak thermal anomalies and an omnipresent puffing volcanic plume. The LP waveforms are nearly identical for time spans of days to months, but vary over longer time scales. The observations imply that the spatially close source processes are repeating, stable and non-destructive. Event sizes vary, but the rate of occurrence remains roughly constant. The events range from magnitude ~ 0.1 to 1.8, with most events having magnitudes < 1.0 . The observations suggest that the conduit system is open and capable of releasing a large amount of energy, approximately equivalent to at least one magnitude 1.8–2.6 earthquake per day. The rate of observed puffs (1 per minute) in the steam plume is similar to the typical seismic rates, suggesting that the LP events are directly related to degassing processes. However, the source mechanism, capable of producing one LP event about every 0.5–5 minutes, is still poorly understood. Shishaldin's seismicity is unusual in its sustained high rate of LP events without accompanying eruptive activity. Every indication is that the high rate of seismicity will continue without reflecting a hazardous state. Sealing of the conduit and/or change in gas flux, however, would be expected to change Shishaldin's behavior.

¹Published under the same title with authors T. Petersen, J. Caplan-Auerbach, and S. R. McNutt in *Journal of Volcanology and Geothermal Research*, 151, 365–381, 2006.

2.2 Introduction

In September 1999, a few months after it last erupted [Nye *et al.*, 2002], Shishaldin Volcano, Aleutian Arc, Alaska (Figure 2.1), started to exhibit a long-lasting continuous and extremely high level of background seismicity. This consists of many hundreds to approximately two thousand long-period (LP) earthquakes per day (Figure 2.2) originating beneath the summit at shallow depths. The unusually high and continuous earthquake rate is 2–3 orders of magnitude higher than that observed at any of the other 26 volcanoes monitored by the Alaska Volcano Observatory (AVO) [Dixon *et al.*, 2003]. A high rate of LP seismicity has often been associated with pre-eruptive behavior at many other volcanoes, including Mount Redoubt [Chouet *et al.*, 1994], Galeras Volcano [Gil Cruz and Chouet, 1997], El Chichon [Havskov *et al.*, 1983], and Mount Pinatubo [Harlow *et al.*, 1997]. Shishaldin, however, shows no other signs of volcanic unrest except for an omnipresent volcanic plume and occasional weak hotspots in thermal satellite imagery when viewing conditions are optimal. Shishaldin’s seismic activity is almost exclusively composed of discrete LP events; volcano tectonic events are rare in the summit region. Another relevant feature of the seismic activity at Shishaldin is the extreme similarity between some of the events over long time scales of up to several months. At the beginning of May 2004, the seismicity radically changed to tremor and the extended earthquake swarm ended. The high rate of LP events over a 4.6-year time period, together with the lack of eruptive behavior makes Shishaldin unusual among volcanoes anywhere in the world.

In this paper, we present an overview of the seismicity at Shishaldin with a focus on LP earthquakes. We chose to end the time period of this study before the nature of seismicity changed in May 2004. Our purposes are to describe the Shishaldin’s events in detail, and to document and quantify the main aspects of the events. Shishaldin’s unusual behavior makes it difficult to forecast eruptive activity and evaluate volcanic hazards. While other volcanoes monitored by AVO would be likely categorized into an elevated eruption alert level if they had such high rates, Shishaldin’s seismicity is considered to be at background level. The observations made at Shishaldin permit us to place constraints on allowable

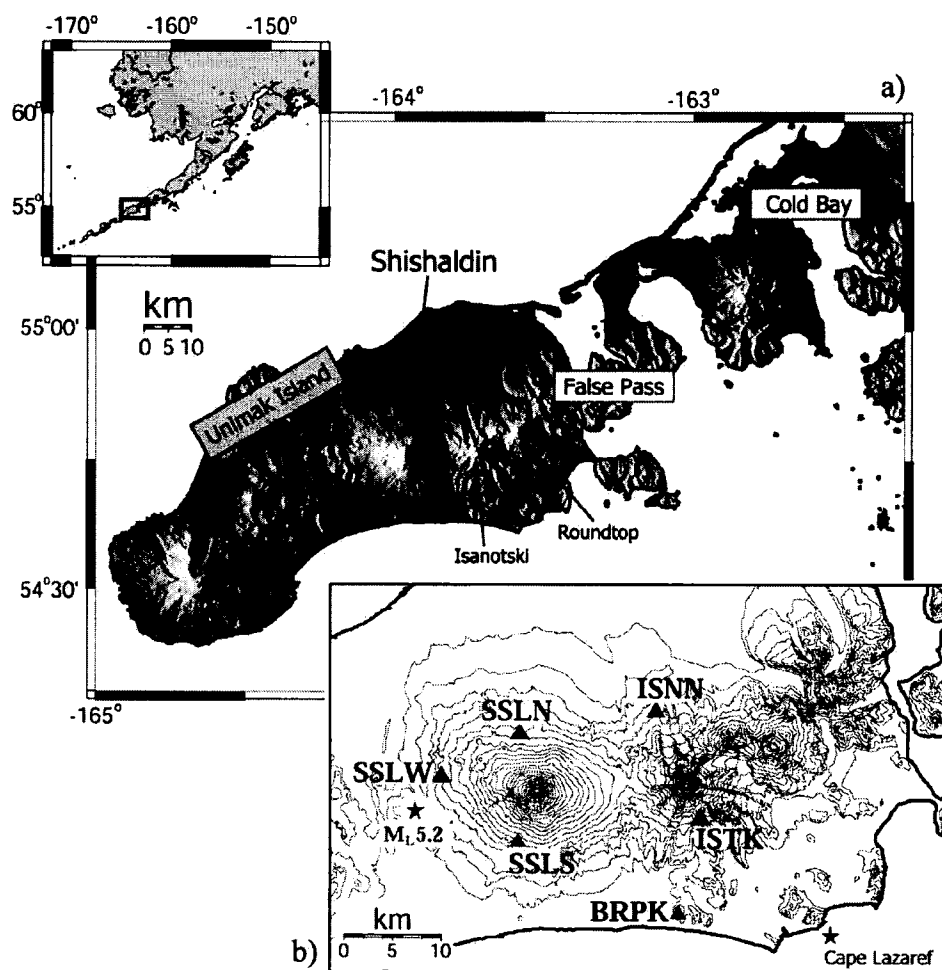


Figure 2.1. a) Map of Unimak Island, easternmost island in the Aleutian Arc, Alaska. False Pass and Cold Bay are the nearest population centers to Shishaldin Volcano. Roundtop and Isanotski volcanoes block the view from False Pass to Shishaldin, but the volcano is visible from Cold Bay. b) Seismic network around Shishaldin and Isanotski volcanoes. The locations of the six short-period seismometers are marked by triangles. All stations are vertical, short-period (L-4C, 1 Hz) seismometers, except SSLS, which is a three-component L-22 with natural frequency of 2 Hz. The distances of the stations to the summit are: 6.3 km (SSLN), 9.8 km (SSLW), 5.3 km (SSLS), 19.0 km (BRPK), 17.0 km (ISTK) and 14.8 km (ISNN). The pressure sensor is co-located with station SSLN. The area where the M_L 5.2 earthquake and its aftershock sequence are located is indicated by a star. Another cluster area for VT events is located southeast of Isanotski off of Cape Lazaref. The base map was produced using Generic Mapping Tools (GMT) and 15-min Digital Elevation Model (DEM) data from the U.S.G.S.

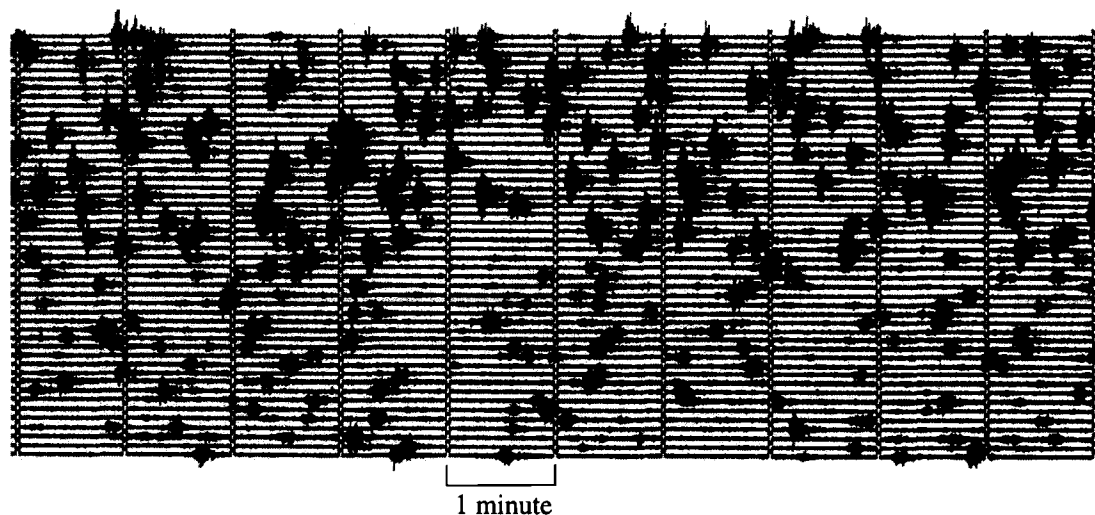


Figure 2.2. Section of helicorder record showing 8 hours of data recorded at station SSLN on November 21, 2002. Tick marks represent 1-minute intervals. A long-period event occurs every 1–2 minutes. Event amplitudes decrease in the middle of the section, but the number of events remains high. A detailed count of all events in the 8-hour section with signal-to-noise ratio ≥ 2 results in 160 events before and 138 after the decrease in amplitudes.

source models, but the 6-station monitoring network is not adequate to fully model source characteristics. We emphasize instead the unusual nature of Shishaldin's seismicity.

2.3 Geologic setting

Shishaldin Volcano is one of five volcanoes located on Unimak Island, the easternmost of the Aleutian Islands, Alaska (Figure 2.1). The 2857 m high stratovolcano with pronounced conical symmetry is primarily composed of basalt and basaltic andesite. The cone is about 16 km in diameter at its base, and snowfields and small glaciers cover two-thirds of it year-round. At almost all times, a volcanic plume is emitted from the ~ 60 m wide vent that is embedded in a small (about 100 m diameter) summit crater (Figure 2.3). The relative contribution of meteoric and magmatic gas is unknown, but blue haze and sulfur smell indicates that magmatic gases, such as SO_2 , are at least partly involved in the plume activity. Field observations have shown that the plume emanates from the summit crater

in the form of discrete puffs (Figure 2.3).

With 29 eruptions reported since 1775 [Miller *et al.*, 1998; Nye *et al.*, 2002], Shishaldin is one of the most active volcanoes in the Aleutian Islands. The eruptions have mostly been of Strombolian type, creating small ash and steam plumes, but 11 Subplinian eruptions in the Holocene have also been identified based on the study of tephra deposits [Beget *et al.*, 1998]. Shishaldin last erupted in April–May 1999, exhibiting both Strombolian and Subplinian behavior with a plume that reached heights up to 16 km [Nye *et al.*, 2002] and produced 43 million cubic meters of tephra [Stelling *et al.*, 2002].

2.4 Limited visual and satellite observations

Visual observations of Shishaldin's volcanic activity are limited by its remote setting. The volcano is located 1098 km southwest of the AVO office in Anchorage, Alaska, making field observations conducted by AVO relatively rare. Shishaldin is not visible from the nearest population center False Pass, located ~60 km to the east, although the summit is visible from Cold Bay, a community located ~92 km to the ENE. Occasionally local pilots provide AVO with reports about the ongoing plume activity. Visual observations are further limited by the poor weather conditions, typical for the Aleutian Islands. Therefore, AVO relies heavily on telemetered data, in particular seismic and satellite data, for monitoring the volcano.

Between September 2000 and April 2004, the only thermal anomalies observed in satellite imagery occurred on 2 days in January 2004 and on one day in April 2004 [J. Dehn, *written communication*, 2004]. This rare observation may or may not be due to the geometry of Shishaldin's crater. The steep slopes of the crater (Figure 2.3) shield part of the volcano from satellites; hence the satellite has to be more or less directly above the volcano in order to detect heat sources within the deeper parts of the conduit system. Dense meteorological clouds and the volcanic plume itself also frequently limit the satellite imagery.

Interferometric synthetic aperture radar (InSAR) imaging corresponding to the 1999 eruption shows no significant deformation at Shishaldin [Lu *et al.*, 2003]. This might be

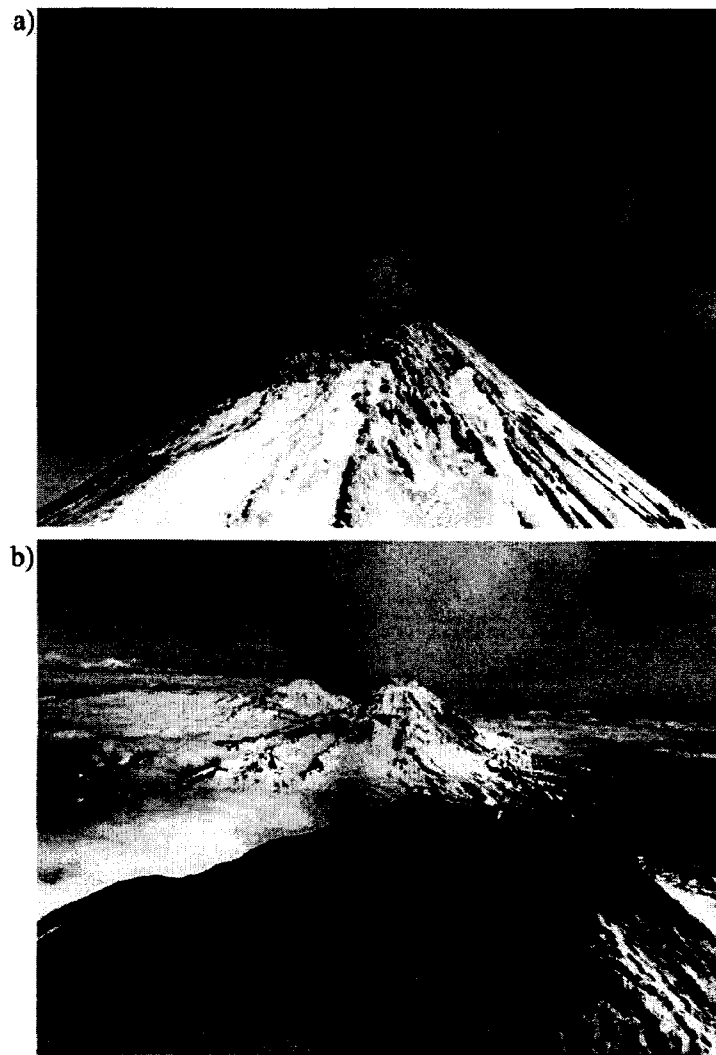


Figure 2.3. a) A volcanic plume is typically emitted as discrete puffs of gas from the summit crater of the 2857 m high stratovolcano Shishaldin. Photo shows the upper 500 m of the volcano. b) Shishaldin's summit crater, ~ 100 m in diameter. The crater walls steeply slope towards the ~ 60 m wide vent. Isanotski and Round Top volcanoes are visible in the background. View from the west. Photos taken by Tanja Petersen, July 2003.

due to the steep, snow and ice covered summit area, which does not maintain coherence. A deformation source at shallow depth right beneath the summit would produce more localized deformation on the upper flanks of the volcano and therefore would be undetectable [Mann, 2002]. Other possible scenarios are that any inflation was balanced by successive deflation or simply that no significant deformation took place [Lu *et al.*, 2003]. Data from October 2000 to July 2001 show a ~ 3 cm shallow inflation slightly northwest of Shishaldin's cone [Mann, 2002]. However, Mann [2002] further notes that subtle signals such as the one fringe of inflation seen in the Shishaldin interferogram may be due to atmospheric effects rather than deformation of the volcano. Available images were not sufficient to verify the inflation.

The remote setting of Shishaldin volcano allows no definitive information on fluctuations in the strength of the omnipresent summit plume and its possible correlation with the intensity of the seismic activity.

2.5 Seismic Network

In summer 1997, AVO installed a network of six short-period seismic stations around Shishaldin at distances of 5.3–19 km from the vent (Figure 2.1). Five of the stations are vertical, short-period L-4C instruments with 1 Hz natural frequency. Station SSLS is a three-component L-22 instrument with a natural frequency of 2 Hz. In July 2003, station SSLN was supplemented with a Chaparral Model 2 microphone. The pressure sensor has a flat response from 0.1 to 200 Hz. The data from all instruments are telemetered to AVO in Fairbanks, where they are displayed as helicorder records on drum recorders and also digitized at a sampling rate of 100 samples/s using a 12-bit digitizer.

Station ISNN suffers from a poor telemetry link, which makes it unreliable especially in the winter months. Stations BRPK and ISTK are located too far from Shishaldin's vent to exhibit reasonable signal-to-noise ratios for small signals; hence they rarely show clear arrivals for LP events. Station SSLN retains the best signal-to-noise ratio when weather conditions are poor, although, until July 2003 the data clipped at low amplitude. The clipping, caused by a dysfunction in the recording system, modified the information on fre-

quency content and restricted magnitude estimates. However, on quiet days with relatively high signal-to-noise ratios five P-wave first arrival time picks are available for locating larger LP earthquakes; four picks are more common. Because LP events commonly lack clear S-waves, P-wave arrivals are the only phases available for the vast majority of events. Even though there are some limitations of the network, the seismic data recorded at Shishaldin provide a high number of clear signals, which can be selected for additional analyses.

2.6 Classification of event types

The vast majority of Shishaldin's earthquake types can be classified by using schemes similar to the ones developed by *Chouet et al.* [1994] and *Lahr et al.* [1994]. This classification is based on more general ideas about the physical processes associated with the seismic source. The literature presents a much greater variety of distinct source mechanisms for each event type. However, the earthquake types most commonly observed in volcanic regions include volcanic tremor, volcano-tectonic events, long-period events and hybrids. Event types observed at Shishaldin are described below.

Volcano-tectonic (VT) events are high-frequency earthquakes representing the brittle failure of rocks due to stress changes in volcanic regions. VT events represent a purely elastic source and show characteristics similar to common double-couple tectonic earthquakes located in non-volcanic regimes. They have clear P- and S phases with peak frequencies above 5 Hz and a variety of first motions [*Lahr et al.*, 1994]. VT earthquakes occur within or near the volcanic edifice and may or may not be associated with magmatic activity. In March 1999, a shallow (about 1 km below the surface) M_L 5.2 strike-slip earthquake occurred 16 km to the west of Shishaldin (Figure 2.1), followed by a several months long aftershock sequence [*Moran et al.*, 2002]. Since then the few VT events detected, are almost exclusively restricted to the area 10–15 km west of the summit. Another VT cluster is located southeast of the adjacent volcano Isanotski near Cape Lazaref (Figure 2.1). An exception to this steady-state behavior was a small swarm of VT events at shallow depths beneath the summit region on 6–7 February 2000.

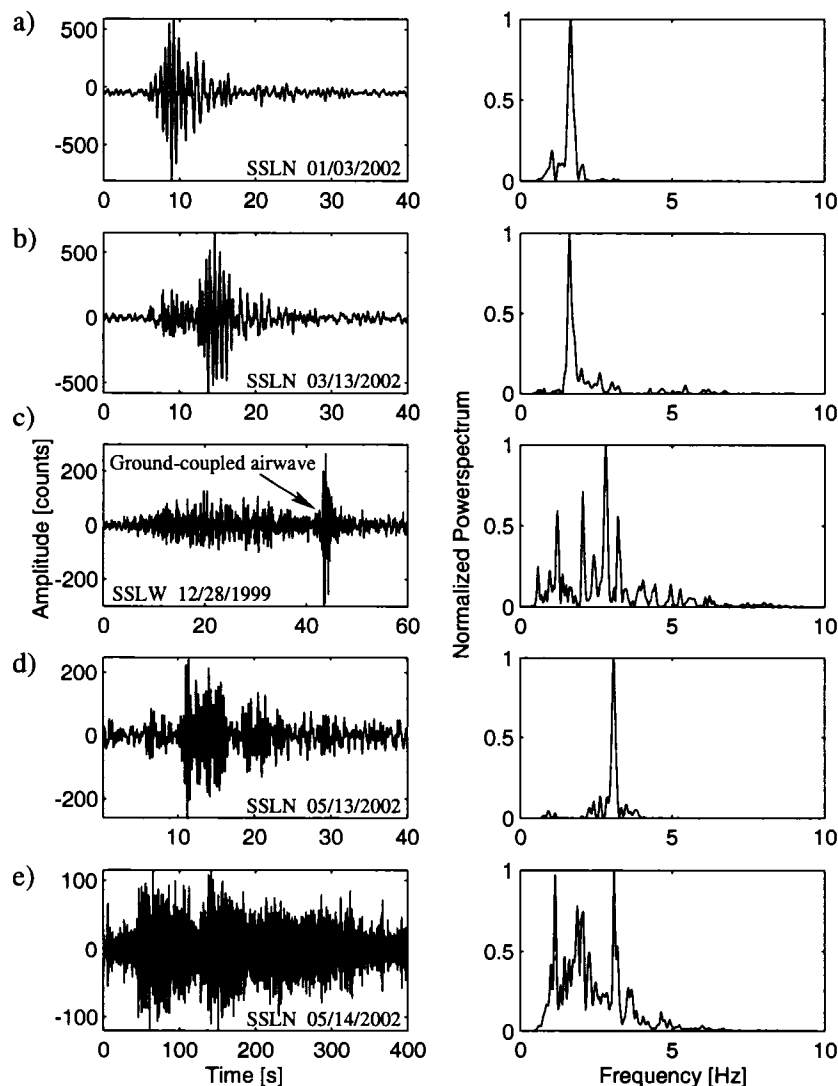


Figure 2.4. Seismograms and normalized power spectra for earthquake types commonly seen at Shishaldin. Each spectrum is obtained from a window enclosing the signal. a) LP event recorded at station SSLN. LP events belong to the most common type of earthquakes seen at Shishaldin. The spectrum exhibits a dominant spectral peak at 1.6 Hz. b) Coupled event recorded at station SSLN. Note that the low-frequency part of the waveforms is similar to event a). The preceding higher frequency (4–7 Hz) portion is the distinctive characteristic for the coupled events observed at Shishaldin. c) Explosion event recorded on station SSLW at 10.1 km from the summit. The airwave also arrived at station SSLS and SSLN, but there the acoustic signal coupled less strongly into the ground. The initial part of the waveform is low-frequency, while the airwave has dominant frequencies between 5–7 Hz. d) DLP event recorded at station SSLN in May 2002. The event exhibits a dominant spectral peak at 3 Hz. e) Volcanic tremor recorded at station SSLN in May 2002. The tremor burst was recorded across the entire network.

Long-period (LP) events produce discrete low-frequency seismic signals and are commonly associated with gas and liquid phases within the volcanic conduit [Lahr *et al.*, 1994]. They are characterized by emergent onsets due to a gradual increase of fluid-driven oscillation [Lahr *et al.*, 1994]. The waveforms are monochromatic with extended codas lasting several tens of seconds. The S-waves of LP events are not distinct. A possible reason for this is that LP events represent a volumetric source that has less excitation of S-waves than an earthquake generated by shear faulting. Short arrival time differences between P, S and surface waves and a finite duration of the source time function enhance the lack of distinct S-waves. At Shishaldin, the vast majority of earthquakes are discrete low-frequency signals with a fairly narrow frequency band between 0.8 and 4 Hz and dominant spectral amplitudes between 1 and 2 Hz (Figure 2.4a). These LP events occur at intervals of about 0.5–5 minutes.

The timing between consecutive puffs in the omnipresent summit plume has been measured with precision over a time period of 20 minutes based on visual observations from station SSLS on July 13, 2003. It ranges between 15 and 100 s. The LP events recorded during the observation time occur at a similar rate. These short time intervals make it impossible to assign a puff to a specific seismic signal without ambiguity, mainly because the delay between the formation of a puff and its arrival at the crater rim is likely to vary from event to event. A puff produced by an LP event located deep within the conduit is likely to have a larger delay time than puffs induced by a shallower earthquake. Also a weak seismic event may not produce a plume strong enough to be seen as discrete puff. However, the similarity between time intervals of observed puffs and LP events suggests, together with the ubiquity of the summit plume, that the seismic events at Shishaldin are related to degassing processes.

Explosion events are discrete low-frequency earthquakes with an airwave phase. The airwaves are acoustic waves, propagating through the atmosphere at about 331 m/s and couple back into the ground near the seismometer. The deeper the explosion events occur in the conduit, the larger is the seismic arrival compared to the airwave phase (e.g. Mori *et al.*

[1989]). During 1999 and 2000, high-frequency signals identified as ground-coupled airwaves were occasionally observed at Shishaldin [McNutt *et al.*, 2000]. McNutt *et al.* [2000] further document that these explosion events were partly accompanied by weak thermal anomalies. Figure 2.4c shows an explosion event recorded at Shishaldin.

Hybrid events typically have an impulsive higher frequency onset followed by a low-frequency coda with the same frequency content as LP events [Neuberg *et al.*, 1998]. They commonly exhibit a variety of first motions characteristic for VT events [Lahr *et al.*, 1994]. The model most commonly used to explain the different phases involve both shear faulting and resonance of an intersecting fluid-filled crack [Lahr *et al.*, 1994]. At Shishaldin, events with a hybrid appearance, termed *coupled events*, dominated the March–November 2002 activity [Caplan-Auerbach and Petersen, 2005]. They consist of a short-period (4–7 Hz) phase, followed by a long-period (1–2 Hz) signal of larger amplitude. The waveform of the long-period portion is similar to the LP events described earlier. This similarity suggests that LP events and the LP phase of coupled events share common source processes and have nearby origins. The two portions of the coupled events are both highly repetitive, indicating a stable, non-destructive source process for each part [Caplan-Auerbach and Petersen, 2005]. Unlike traditional hybrid events, the time separation between the two parts of the signal is highly variable, from 3 to 15 seconds, a behavior that has been related to temporal changes in gas content [Caplan-Auerbach and Petersen, 2005]. Figure 2.4b shows an example of a coupled event.

Volcanic tremor is identified by its continuous signal with a low-frequency spectral content of 0.8–8 Hz, typically peaked at 2–3 Hz [McNutt, 1992]. Models for volcanic tremor include the response of fluid-filled conduits to sustained pressure fluctuations [Chouet, 1996; Neuberg *et al.*, 2000] and degassing processes of magma [Chouet, 1985; Ripepe *et al.*, 1996, 2001]. Fehler [1983], Havskov *et al.* [1983] and Malone [1983] consider volcanic tremor to be composed of a sustained sequence of LP events, i.e. tremor and LP events are both generated by similar fluid dynamical processes but with different excitation mechanisms [Almendros *et al.*, 2001]. Ripepe and Gordeev [1999] present a model, in which tremor is

generated by the continuous bursting of small gas bubbles. *Julian [1994]* proposes that tremor oscillations are excited by a nonlinear interaction of a single-phased fluid with the irregular conduit through which it is flowing. Extensive volcanic tremor was observed at Shishaldin in relation with the 1999 eruption, and was discussed by *Thompson et al. [2002]*. The only other time volcanic tremor was observed at Shishaldin was in May 2002 when several tremor bursts lasting 3–5 minutes accompanied a deep long-period event at Shishaldin (Figure 2.4e).

Deep long-period (DLP) events occur at about 10–50 km depth and are characterized by emergent onsets, extended codas and strong spectral peaks between 2 and 4 Hz (Figure 2.4f; *Power et al. [2002]*). DLP events have been associated with magma movement, are often highly clustered in time and accompanied by volcanic tremor [*Power et al., 2002*]. Since AVO started monitoring Shishaldin, about 13 DLP events, spread out over much of the eastern half of the island, have been located, five of which may have been precursors to the 1999 eruption [*Power et al., 2002*]. In May 2002, a DLP appeared as a M_L 1.8 earthquake at a depth of 47 km with an epicenter some 7 km east of Shishaldin’s summit [*Dixon et al., 2003*]; approximately 150 larger LP events located within the shallow summit region were recorded on the same day.

2.7 Overview of Shishaldin seismicity

AVO uses several methods for monitoring the level of seismicity at Shishaldin, including the *Earthworm* acquisition system that uses a short-term-average/long-term-average trigger algorithm to detect earthquakes. However, the only counting method that provides a continuous quantitative overview of the seismicity throughout the time period since the eruption is referred to as *pseudohelicorder counts*. In this paper we use pseudohelicorder counts, or simply *counts*, to present the number of events per day with the maximum amplitude exceeding a certain threshold (≥ 6 mm peak-to-peak) on digitally filtered helicorder records (Figure 2.5). The 0.8–5 Hz bandpass filter reduces the influence of seismic noise by removing low frequency surf noise and high frequency wind and rainfall noise. The counts

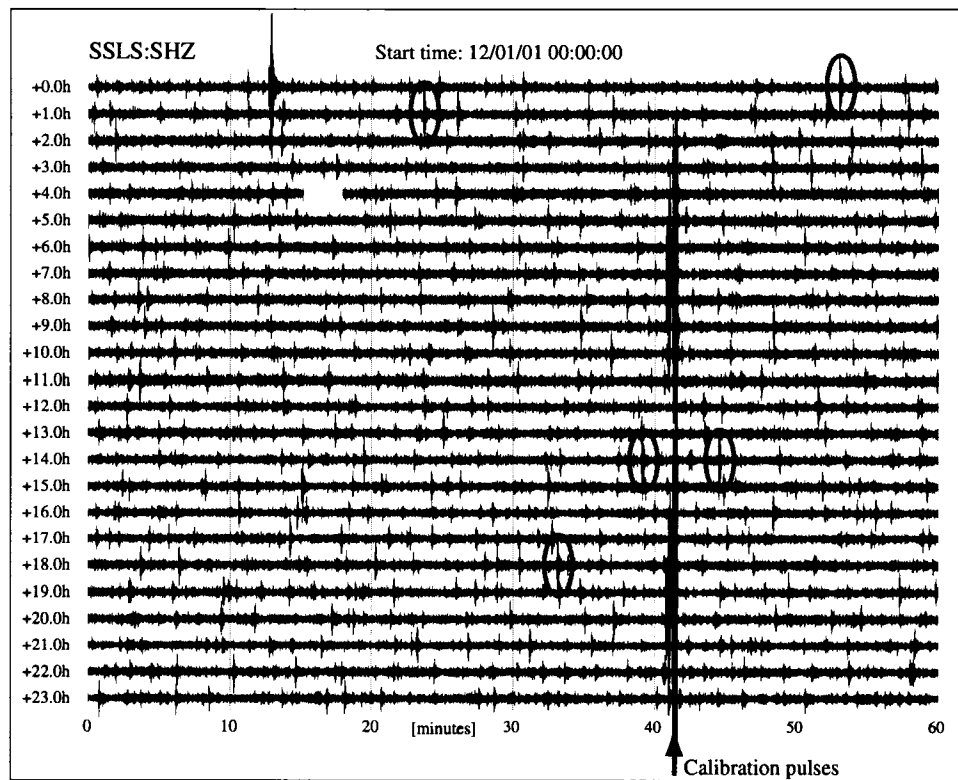


Figure 2.5. Example of pseudohelicorder plot showing 24 hours of continuous data (December 3, 2001; station SSLS, vertical component). The data have been bandpass filtered between 0.8–5 Hz to reduce noise. In order to be included in the pseudohelicorder counts, the event has to be a local earthquake and the maximum amplitude has to contact the two adjacent lines. The threshold value is equivalent to local magnitude $M_L 1.1$. Earthquakes are considered as being local if the P- and S-wave arrivals are not clearly distinguishable from each other on the pseudohelicorder plots; ambiguous events are resolved using helicorder records, which have higher temporal resolution. Ovals mark the five events included in the pseudohelicorder counts for that day.

are performed on data recorded by an L-22 seismometer. Since this type of instrument is not optimal for recording low frequencies, the number of Shishaldin events that will meet the counting criteria has already been reduced. The vast majority of the events recorded at Shishaldin have very small amplitudes, thus a large number of events fall below the counting criteria. Figure 2.6 presents the systematic overview of Shishaldin seismicity provided by

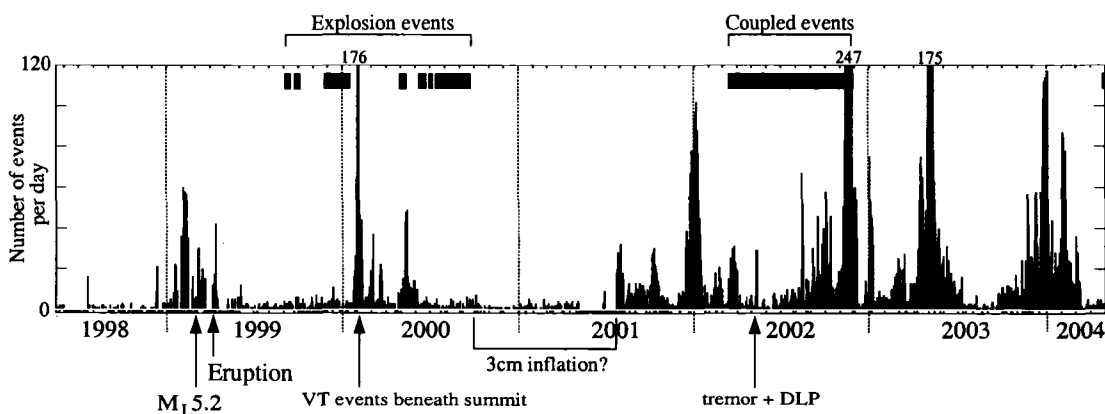


Figure 2.6. Filtered digital daily (*pseudohelicorder*) counts for Shishaldin plotted from May 1998 through April 2004. The interval between two tick marks on the time axis (top) represents one month. The vertical bars show the number of events per day included in the counts. Negative values indicate days for which no counts are available due to wind noise. The horizontal bars at the top mark periods during which *explosion events* and *coupled events* occurred (see text). The $M_L 5.2$ earthquake in March 1999 and Shishaldin's most recent eruption in April–May 1999 are labeled. A small swarm of VT events at shallow depths beneath the summit region occurred February 6–7, 2000 (2 days after 176 events were included in the counts). InSAR data from October 2000 to July 2001 show a potential ~ 3 cm shallow inflation at the northwest flank of Shishaldin. Tremor bursts and a DLP event were recorded in May 2002.

pseudohelicorder counts.

During the first year of network operation, from 1997 to 1998, Shishaldin was seismically relatively quiet, except for a few brief swarms of small LP events and a few deep long-period (DLP) events [Power *et al.*, 2002]. In early 1999, the counts became more complex (Figure 2.6): tremor episodes preceding and accompanying the eruption in April–May 1999 and an $M_L 5.2$ strike-slip earthquake on March 4 and its aftershock sequence dominated the seismic data through May 1999. After the eruption, seismicity was low through early September. Then it increased again in September 1999, composed exclusively of LP and explosion events. Since that time, the background seismicity has remained high but variable. An episode of very high counts with up to 176 counted events per day occurred in February 2000. A small swarm of VT events beneath the summit was observed for 2 days at the beginning of this episode. Since July 2001 the average number in counts per day has

increased resulting in a mean value greater by a factor of three. Four episodes of very high counts have been observed since then. During these episodes, 6–10 months apart, the counts remained very high for several weeks reaching up to 247 counted events per day. Overall, since 1999, Shishaldin seismic activity has had a rate that is almost three orders of magnitude higher than that seen at other volcanoes monitored by AVO and at Shishaldin during 1997–1998. Pseudohelicorder counts for Akutan Volcano, one of the most active volcanoes in the Aleutian arc, for example, show about one event per week. The counts for Shishaldin vary between one (occasionally 0, but only for up to a couple of days at a time) and 247 events per day. It must be noted that these values reflect only the larger events; there are always several hundreds to about 1500 smaller events every day that do not meet the selection criteria.

2.8 Estimation of magnitudes and energy

In order to relate the seismicity observed at Shishaldin to other volcanic regions, earthquake counts have to be further quantified. The first step is to determine the magnitudes of counted events. We can then estimate the amount of energy released per day.

The determination of magnitudes for LP events is not easy because the location of most of these events is not always possible. Furthermore, the source mechanisms for earthquakes generated by fluid processes are still poorly understood, hence the local magnitude scale, M_L , developed for tectonic earthquakes by *Richter* [1935], may not be appropriate for LP events. However, because at present there is no known way to quantify the size of LP events more accurately, the magnitudes for the thousands of located LP events at Shishaldin are local Richter magnitudes computed by HYPOELLIPSE [*Lahr*, 1999] using a measure of peak amplitude. These magnitudes vary between 0.4 and 1.8. Assuming that the unlocated LP events also originate in the summit region we can provide estimates of the magnitudes of these events. The similarity in waveforms between located and unlocated events supports this assumption. The located events provide a reasonable reference for scaling pseudohelicorder and helicorder records. The vast majority of LP events have magnitudes < 1.0 . The

amplitude threshold value for the pseudohelicorder counts is equivalent to $M_L 1.1$, hence a significant number of events are not included in the counts.

The energy, E , of the seismic source can be estimated using an empirical formula for local earthquakes, $\log E = 9.9 + 1.9M_L - 0.024M_L^2$ [Gutenberg and Richter, 1956], where M_L is the local magnitude. This magnitude scale may not be reasonable for LP events and does not provide absolute values, but can be used as a consistent mean of looking at energy release over time. The number of events per day and their magnitudes are needed to approximate the amount of energy released per day. In order to extrapolate pseudohelicorder counts to the overall number of earthquakes per day, *detailed counts* have been accomplished for a few days with very low wind noise. Detailed counts are performed on helicorder records, including all events with a signal-to-noise ratio of ≥ 2 . The amplitudes are measured by hand; hence this method is very time consuming and has only been done for a few selected days. The smallest events included in the detailed counts have an estimated magnitude of M_L 0.03. The total number of events per day counted for the seven selected days varies from 349 to 1505 (Figure 2.7). The counted events had magnitudes as large as M_L 1.2. The seismic energy released per day, calculated from the detailed counts, ranges from 1.86×10^{13} to 5.75×10^{14} ergs, which is equivalent to one M_L 1.8–2.6 earthquake. The relation between the number of larger ($M \geq 1.1$) events and smaller ($M < 1.1$) events is not consistent. The ratio of small-to-larger events varies by a factor between three and 185; hence we are unable to extrapolate total daily energy release from the pseudohelicorder counts. The observed variation in the relative abundance of small events compared to larger ones itself needs further investigation and shall be addressed in future studies.

2.9 Repeating LP events at Shishaldin

Visual inspection of seismic records exposed repetitive LP events with extremely similar waveforms. We use a technique based on waveform cross-correlation [Caplan-Auerbach and Petersen, 2005] to identify and extract repeating events. In this method a *reference event*, a section of an event with a good signal-to-noise ratio, is cross-correlated with segments

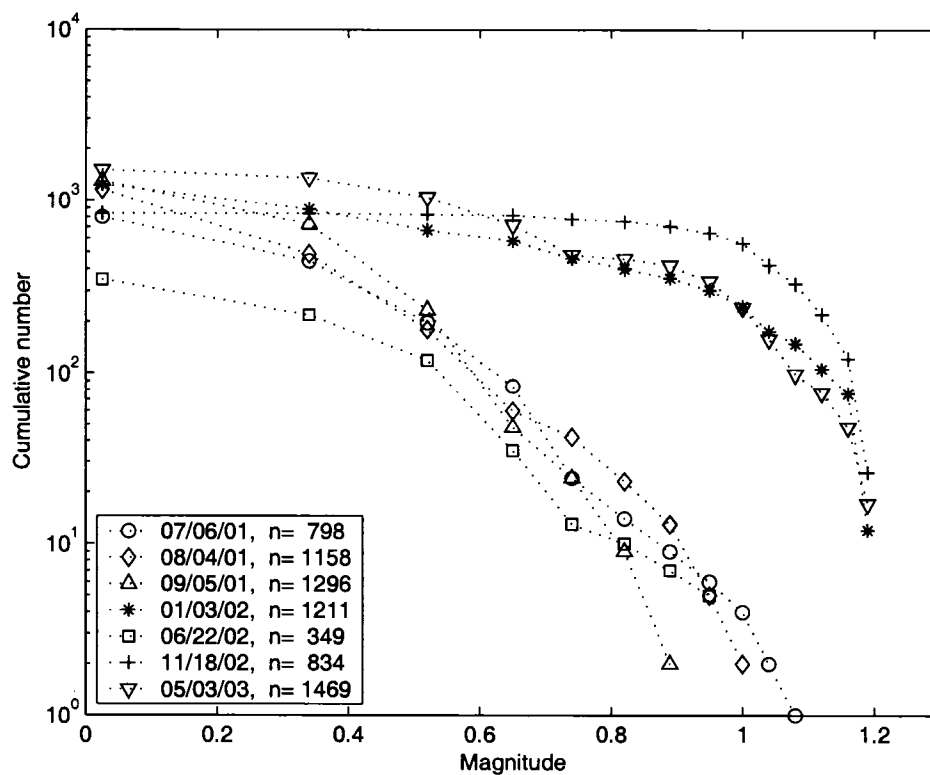


Figure 2.7. Detailed helicorder counts for seven different days plotted as frequency-magnitude distributions. The *estimated magnitude* for unlocatable low-frequency events has been calculated relative to located events using Richter's local magnitude scale and assuming that all low-frequency events originate in the summit region. The total number of events per day (n) is listed in the legend. Note that when the number of large events increases, the number of small events does not change significantly.

of the continuous data. The selected reference event is 8 s long, which is an appropriate duration of the strong part of the signal (Figure 2.4a). The time at which two signals show the maximum cross-correlation value defines the beginning of a data segment. The spectral-coherence between the reference event and each data segment is calculated and averaged over a frequency band between 0.5 and 4 Hz. Events with a mean coherence exceeding a threshold of 0.9 are extracted and aligned in time series. We chose to use the coherence as a measure of how well two signals correlate rather than using correlation coefficients because the monochromatic nature of LP waveforms often causes misalignment

by an integer number of wavelengths. Figure 2.8 shows events exceeding a minimum spectral coherence of 0.9, which were extracted as *repeating events*, i.e., events with highly similar waveforms. The waveform similarity is also seen at other stations; hence the similarity is due to source rather than path or site effects. In order to produce similar waveforms at a seismic station the source locations of the individual events can only vary within ~ 500 m ($1/4$ of the approximated dominant wavelength; e.g., *Geller and Mueller* [1980]). The source process has to be stable and non-destructive in order to act repeatedly. At any given time there is generally only one major family of repeating events, dominating Shishaldin's seismic activity for several days up to several months [*Caplan-Auerbach and Petersen*, 2005]. These different repeating events exhibit subtle differences in event waveforms and power spectra (Figure 2.9).

2.10 Locations

Determining the locations of LP events using traditional arrival time methods is usually difficult or impossible because of their emergent onsets and the lack of clear S-waves. At Shishaldin, the large distance (5.3–19 km) between the source region and the local seismic network, and the small size of the events, results in a low signal-to-noise ratio for the majority of events. Because it is already difficult to locate LP events due to their emergent onsets, small amplitudes make it even more difficult to identify or define the P-wave arrivals precisely. Furthermore, the noise levels on network stations due to wind and telemetry problems sometimes leave only a few readings available for earthquake locations. Therefore, at Shishaldin only a small percentage ($< 10\%$) of the events that triggered the Earthworm data acquisition system are locatable [*Dixon et al.*, 2003]. The velocity structure around Shishaldin is poorly constrained. The velocity model used by AVO was originally constructed for Pavlof volcano [*McNutt and Jacob*, 1986], located 160 km to the ENE of Shishaldin. Shishaldin's seismic stations span a ~ 400 m difference in elevation. These factors, together with the lack of S-waves and the difficulties of picking P-wave arrivals with accuracy, combine to produce a severely limited depth resolution. Although precise

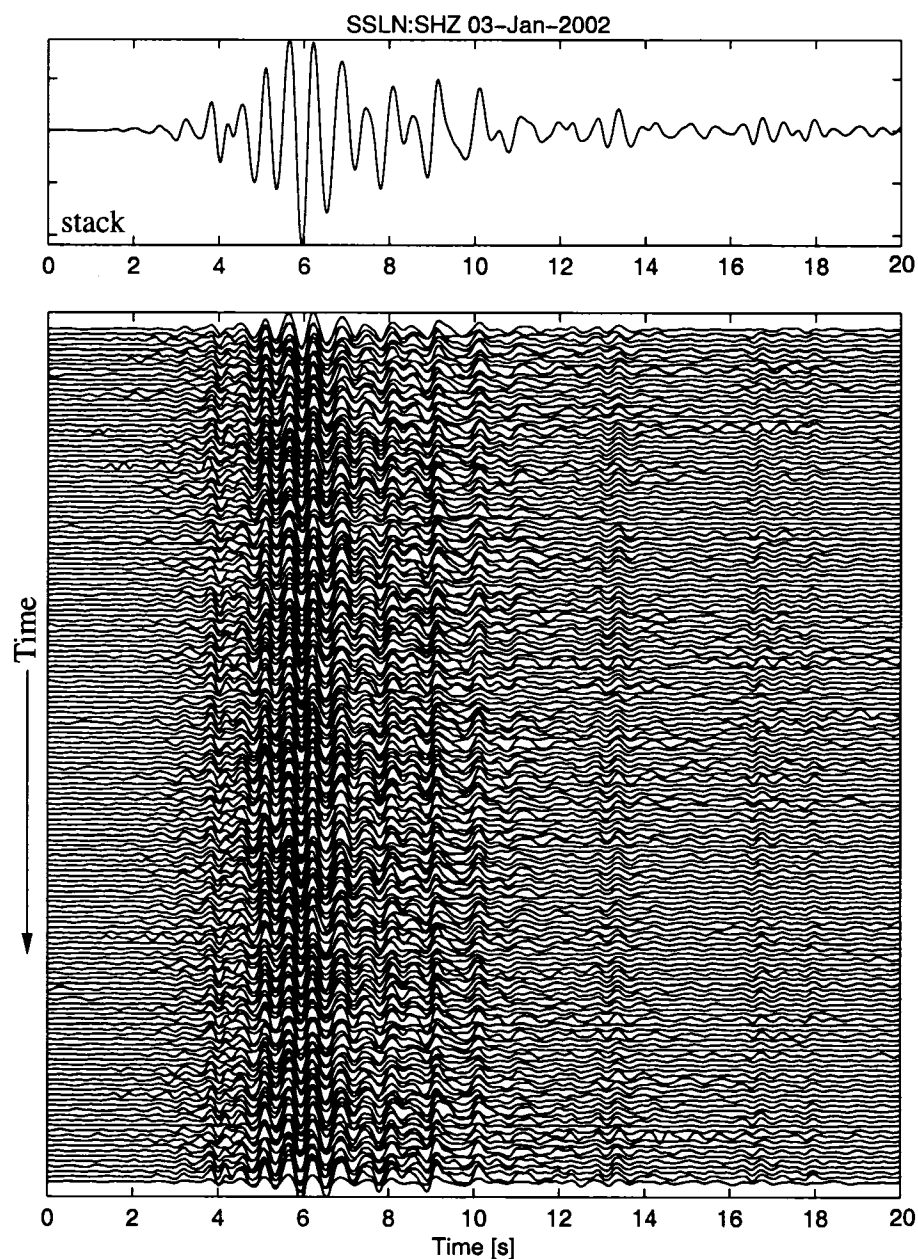


Figure 2.8. Examples of repeating events at Shishaldin. LP events recorded at station SSLN on January 3, 2002. The cluster was extracted by cross-correlation. The spectral-coherence values for these events are ≥ 0.9 . The upper part of the plot shows a stack of all events in the lower part. The waveform similarity between the events is also seen on other stations.

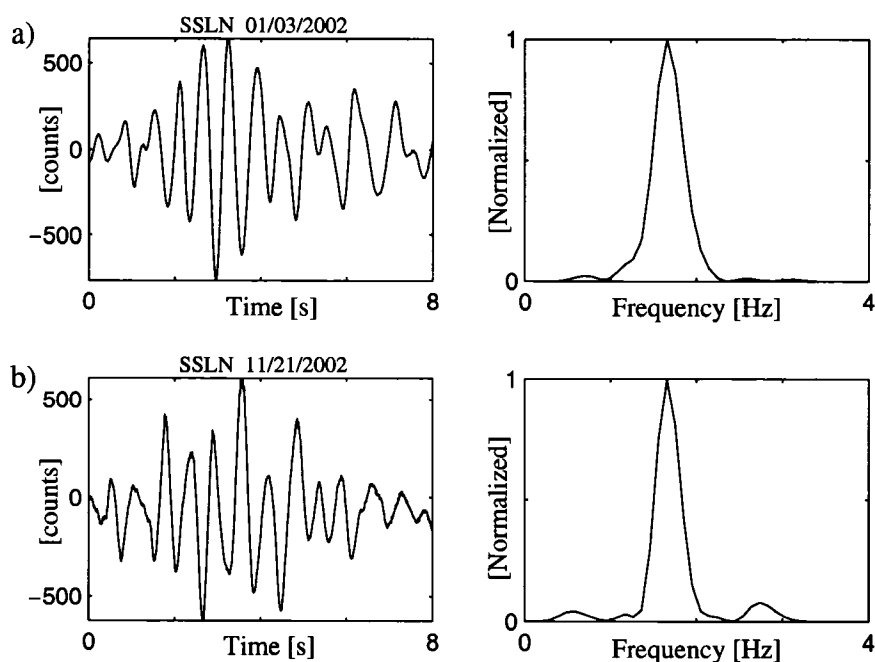


Figure 2.9. Waveforms and normalized power spectra of reference events recorded at station SSLN on a) 3 January 2002 and b) 21 November 2002. The spectral-coherence between the two reference events is 0.66. Each reference event represents a family of repeating events.

hypocentral locations are not available for the LP events, preliminary locations obtained by using HYPOELLIPSE [Lahr, 1999] indicate that they are located beneath the summit at shallow (0–3 km) depths (Figure 2.10) [Dixon *et al.*, 2002, 2003, 2004]. We only selected events with HYPOELLIPSE quality factors A and B, indicating 68% confidence levels for horizontal and vertical location errors of < 2.67 km [Lahr, 1999]. These shallow locations are supported by acoustic data recorded by the pressure sensor [Petersen *et al.*, 2004]. Nearly every seismic event is accompanied by an infrasonic signal; which suggests that the source is located within the conduit system at very shallow depths.

In order to improve signal-to-noise ratios and thus to allow more precise arrival time picks, repeating events were aligned by cross-correlation and stacked at each station. The stacked events were located using HYPOELLIPSE. The location places a cluster of repeating events (recorded on 3 January 2002) about 1 km west of the summit at shallow depth (~ 2

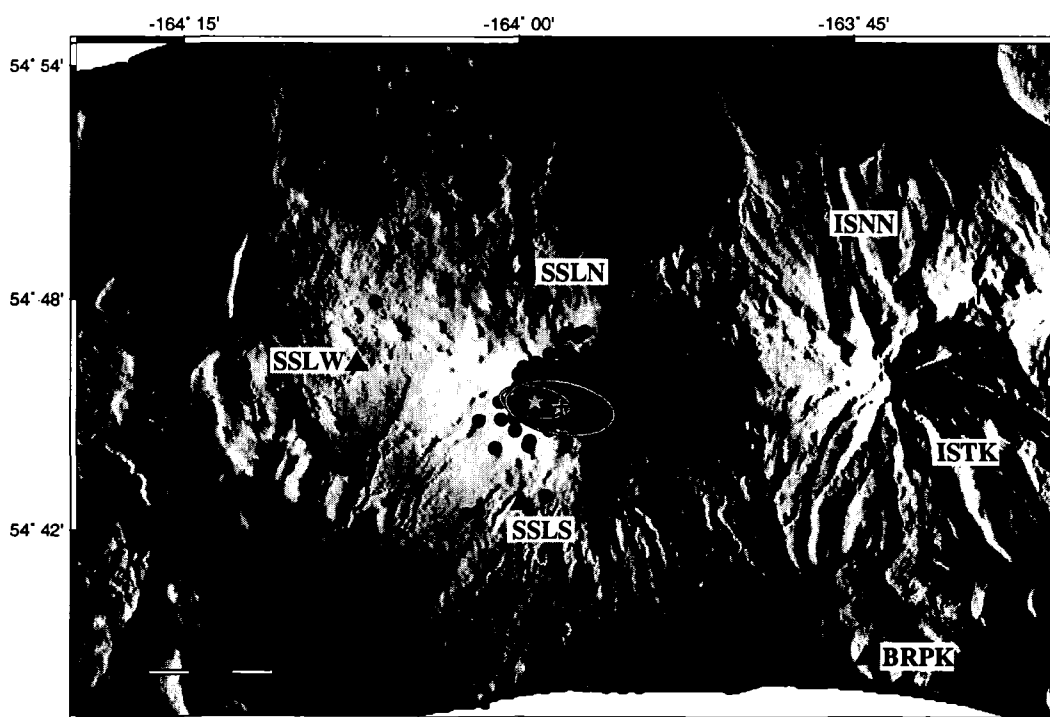


Figure 2.10. Epicenters for LP and coupled events at Shishaldin since 1997 [Dixon *et al.*, 2002, 2003, 2004], located with 68% confidence levels for horizontal and vertical locations of < 2.67 km [Lahr, 1999]. The vast majority originate beneath Shishaldin's summit (black cross) at depths of 0–3 km. Magnitudes vary between 0.4 and 1.8. Epicentral locations (star) and error ellipsoids (68% confidence) for stacked repeating events from 3 January 2002 and 20 November 2002 are marked.

km below summit). Although standard errors calculated by HYPOELLIPSE indicate that these hypocentral depths are well constrained, uncertainties in the velocity model and the lack of S-waves suggest that in fact there is a large degree of uncertainty in earthquake depth. A second cluster of repeating events (recorded on 21 November 2003) is located directly beneath the summit. The depth for this cluster is poorly resolved. The epicentral locations for the two clusters are shown in Figure 2.10. The locations of these two clusters confirm that the bulk of LP events most likely originate beneath Shishaldin's summit area.

Although hypocentral depths at Shishaldin are poorly constrained using standard location algorithm, other techniques may be used to confirm that a shallow depth is reasonable.

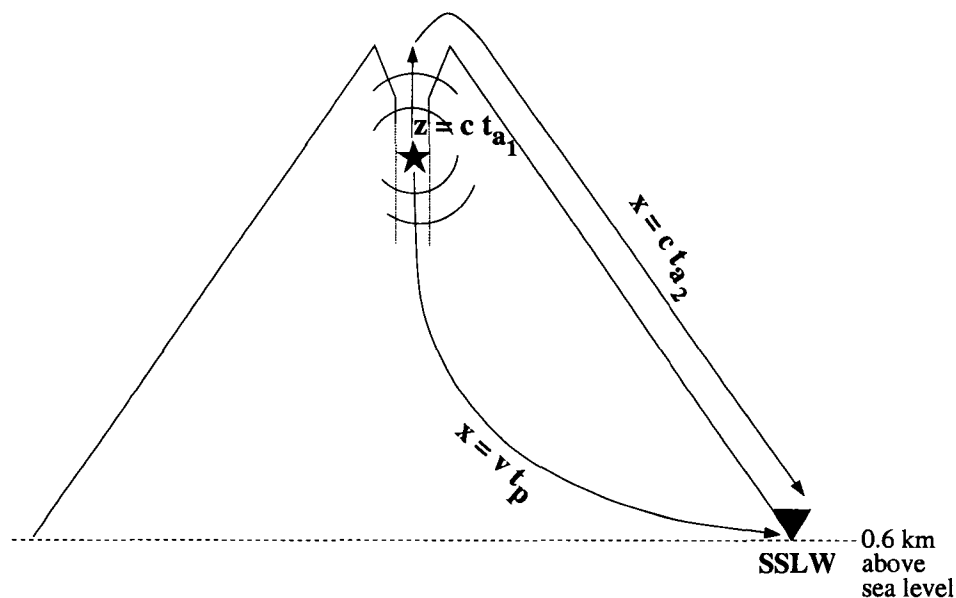


Figure 2.11. Illustration of how the depth of explosion events can be estimated by using the time difference ($\Delta t = 26.1$ s) between P-wave arrival (t_p) and airwave arrival ($t_a = t_{a_1} + t_{a_2}$) measured for an earthquake with a ground-coupled airwave phase recorded at station SSLW at a distance of $x = 10.1$ km from the summit. Assuming an acoustic velocity (c) of 0.331 km/s and a seismic velocity (v) of 2.0 km/s, the source is located at a depth (z) of about 0.2 km.

For events with associated airwaves, depths can be constrained by using the difference in arrival time between the P-wave and airwave. We selected a representative explosion event with a good signal-to-noise ratio recorded at station SSLN and SSLW on April 30, 2004 (18:20:10 UTC), and picked arrival times with a 0.1-s uncertainty for SSLW and 0.2 s for SSLN. For station SSLW (9.8 km horizontal and 2.2 km vertical distance from summit), the arrival time difference (Δt) is 26.1 s (Figure 2.11). The arrival time difference for station SSLN (6.3 km horizontal and 2.1 km vertical distance from summit) is 17.2 s. We assume the simplest model for which the airwave from the summit to the seismic station and the seismic wave are assumed to travel the same distance [Hagerty *et al.*, 2000]. This assumption is reasonable for cases in which the station-summit distance is much greater than the depth (z) [Hagerty *et al.*, 2000]. The depth $z = c(\Delta t - [1/c - 1/v]x)$ of the source can be

estimated by using reasonable values for the acoustic velocity (c) and the seismic velocity (v). Assuming an acoustic velocity of 0.331 km/s (speed of sound through air at 0°C) and a seismic velocity of 3.05 km/s (P-wave velocity for upper 3 km of Pavlof volcano [McNutt and Jacob, 1986]), the source would be spuriously located outside the volcano. A value of $v = 2.0$ km/s results in a depth of about 0.2 km. Although we note that these values are only approximate, the calculations confirm that the source is likely located at very shallow depth.

2.11 Constraints on allowable source models

There are two general trends for models explaining the generation of LP events related to the presence of gas within fluid bodies; one is based on bubble coalescence and the other on conduit oscillation induced directly by fluid transfer. The sudden coalescence of gas bubbles, accumulating below a structural barrier, into a single gas bubble has been studied in laboratory experiments [Jaupart and Vergnolle, 1988, 1989] and has been used to explain the source of low-frequency events at Stromboli volcano [Ripepe and Gordeev, 1999]. The other trend of models is based on pressure fluctuations promoting crack or conduit oscillation induced by fluid transfer through a magmatic or hydrothermal conduit system (e.g. Chouet *et al.* [1994]; Chouet [1996]). A similar fluid dynamic process is used to explain seismic tremor but with a different excitation mechanism producing a sustained signal rather than the discrete signal observed for LP events [Chouet, 1996]. Hellweg [2000] considers turbulent flow conditions as the generator for conduit oscillation. Hellweg [2000] describes how eddies are able to develop on the downstream side of an object and that they produce density variations that propagate through the conduit system as sound and seismic waves. An alternate consideration is presented by Zimanowski [1998] who suggests that a phreatomagmatic explosion caused by a near surface interaction between ground-water and magmatic melt may trigger a seismic low-frequency event. A phreatic explosion resulting from the pressurization of a hydrothermal system may have the same effect.

Possible constraints on trigger mechanisms for LP events observed at Shishaldin include

that the process must be capable of producing at least one LP event every 0.5–5 minutes. The system generates almost exclusively discrete seismic events instead of releasing energy in the form of tremor. The later was dominant during the 1999 eruption, but has been rarely observed since late 1999. The trigger mechanism must be capable of generating events that exhibit varying amplitudes, at a relatively constant rate. The similarity of waveforms within certain clusters of repeating events requires a source mechanism stationary within only a few hundreds of meters ($1/4$ of a wavelength); the source is acting repeatedly and, therefore, is non-destructive. The lack of VT events indicates that the conduit represents an open system through which gas can constantly escape without causing brittle failure of surrounding volcanic rocks. The system produced a puffing volcanic plume, even during 1997 and 1998 [*P. Stelling, personal communication, 2004*] when Shishaldin was seismically quiet.

All of the source models described in the above paragraph may satisfy these criteria. The last condition is the most complex one, because it requires an explanation of how the system changed from gas release without major seismic activity to gas release accompanied by LP events. A possible scenario may be that during 1997 and 1998 the volcanic system was degassing in the form of free gas bubble nucleation, also called a *soda bottle* system and described by *Ripepe and Gordeev* [1999] and *Hellweg* [2000]. The amount of gas released from the magma through the conduit may have been too small to form seismic signals large enough to be recorded. During the 1999 eruption the conduit system may have been modified. Since then the gas released from the magma column at greater depths in the volcanic system, has to pass obstacles in the conduit such as fallback deposits. In late 1999 the system recovered from the eruption and pressurized again. The velocity of the gas flow increased within the narrowed conduit and past the obstacle produces turbulent flow features, similar to the eddies described by *Hellweg* [2000]. However, these are assumptions solely based on the criteria for possible source models described above; the underlying processes causing Shishaldin's LP events are still poorly understood and remain a matter of future work. A denser seismic network is needed to get more precise locations in order

to constrain allowable source models.

2.12 Discussion and conclusions

The continuous high level of LP seismicity beneath Shishaldin's summit has only been observed starting in late 1999, which suggests that the 1999 eruption itself and/or the associated M_L 5.2 earthquake changed the nature of the conduit system and started a new regime of seismic activity at Shishaldin. The overall increase in seismicity since July 2001 may indicate another regime. The potential ~ 3 cm shallow inflation northwest of the cone based on InSAR data described by *Mann* [2002] occurred sometime between October 2000 and July 2001. The inflation is unconfirmed due to the lack of additional data, but assuming the InSAR signal truly results from the volcano, the inflation may have preceded the change in seismic activity. Magma accumulation is a likely source for inflation. However, since late 1999, the nature of seismic activity has changed through time via the evolution of systematic differences in event waveforms [*Petersen et al.*, 2002]. Time periods of a few days to several months during which repeating LP events occur have been observed. The event appearance varying between different temporal clusters of repeating events probably reflects subtle differences in locations and processes. The event sizes vary over time, but the rates remain roughly constant. The processes causing the variation in event sizes may be related to changes in gas and/or heat flux. The LP source is located within the conduit system; the source processes involving fluid and gas are still poorly understood. However, the conduit system is capable of releasing a large amount of seismic energy without significant stress changes or explosive eruptions. As indicated by the lack of VT events, it represents an open system allowing the release of gas and energy without the opening of new cracks. The level of degassing seems to vary somewhat but is steady enough to produce the almost continuous high background level of LP events observed at Shishaldin. Because the system is open, the high level of seismicity may not indicate a hazardous state. Persistent tremor combined with thermal anomalies in the satellite imagery would indicate rapid degassing with an increased gas flux and a heat source that has moved to shallow parts of the volcano.

In any case, sealing of the conduit leading to an extreme increase in gas pressure would be a major concern. Therefore, a change in seismicity such as a conversion from LP to VT seismicity, suggesting a sealed system or the occurrence of volcanic tremor together with thermal anomalies would raise the alert level for a possible eruption. In fact, in May 2004, AVO went from Level of Concern Color Code green to yellow for Shishaldin, because of continuous tremor and thermal anomalies observed in the satellite data.

Shishaldin is unusual among volcanoes in its long-lasting high level of LP seismicity without preceding or accompanying eruptive activity. For example, at Popocatepetl Volcano, a high rate of LP seismicity lasted from 1994 to 2000 [Arciniega-Ceballos *et al.*, 2003], but it accompanied eruptive activity including explosions with ash plume heights of up to 12 km and lava dome growth. At Unzen Volcano, a maximum of ~ 110 summit earthquakes ($M \geq 0$) per day were observed during the initial phase of the vigorous endogenous growth of the lava dome (November 1993–January 1994) [Nakada *et al.*, 1999]. A swarm of more than 4000 LP events directly preceded the 1989–1990 eruption of Redoubt Volcano, but only lasted for 23 hours [Power *et al.*, 1994; Benoit and McNutt, 1996]. Benoit and McNutt [1996] studied 136 earthquake swarm durations that are not associated with eruptive activity. The mean duration for these swarms is 3.5 days and only three of these swarms had durations exceeding 1 year: Rabaul exhibited a swarm of shallow VT earthquakes that lasted 630 days and was accompanied by a caldera floor uplift of 10 cm/year; at Adagdak, a swarm of VT events located at ~ 5 km depth lasted 865 days; and at Long-Valley, a migrating swarm of VT events lasted 570 days [Benoit and McNutt, 1996]. Usu Volcano presented a swarm of similar duration as Shishaldin. The swarm lasted 4 years and 7 months, but Usus strongest activity accompanied the eruption and included mostly VT earthquakes [Okada *et al.*, 1981; Benoit and McNutt, 1996]. On Montserrat, LP events usually occur in swarms starting at a rate of about one event every 1–2 minutes, but the events occasionally merge into tremor and the swarms last only for a few hours to several days [Neuberg *et al.*, 2000]. Thus, the conjunction between a high rate of LP seismicity, extended swarm duration, lack of VT events beneath the summit area and absence of volcanic tremor and eruptive activity

is a rarely observed occurrence. This behavior at Shishaldin stands out from many other volcanoes anywhere in the world.

2.13 Acknowledgements

We thank our colleagues at the Alaska Volcano Observatory for helpful comments regarding Shishaldin seismicity. We are especially grateful to AVO analyst Scott Stihler for locating Shishaldin earthquakes and to Guy Tytgat for installing and maintaining the Shishaldin monitoring network. We also thank Dave Hill and Randy White of the U.S.G.S. for helpful suggestions that improved the manuscript. Hiroyuki Kumagai and an anonymous reviewer provided thorough and valuable reviews. Several figures were produced using the Generic Mapping Tools software by *Wessel and Smith* [1998].

References

- Almendros, J., B. Chouet and P. Dawson (2001), Spatial extent of a hydrothermal system at Kilauea Volcano, Hawaii, determined from array analyses of shallow long-period seismicity: 2. Results, *J. Geophys. Res.*, *106*(7), 13581–13597.
- Arciniega-Ceballos A., B. Chouet and P. Dawson (2003), Long-period events and tremor at Popocatepetl volcano (1994–2000) and their broadband characteristics, *Bull. Volcanol.*, *65*, 124–135.
- Beget, J., C. Nye and P. Stelling (1998), Postglacial collapse and regrowth of Shishaldin Volcano, Alaska, requires high eruption rates, *EOS Trans. Am. Geophys. Union*, *70*, S359.
- Benoit, J. P. and S. R. McNutt (1996), Global Volcanic Earthquake Swarm Database 1979–1989, *U.S. Geological Survey Open-File Report*, *96–69*, 334 pages.
- Caplan-Auerbach, J. and T. Petersen (2005), Repeating coupled earthquakes at Shishaldin Volcano, Alaska, *J. Volcanol. Geotherm. Res.*, *145*, 151–172.
- Chouet, B. A. (1996), Long-period volcano seismicity: Its source and use in eruption forecasting, *Nature*, *380*, 309–316.
- Chouet, B. A., R. A. Page, C. D. Stephens, J. C. Lahr and J. A. Power (1994), Precursory swarms of long-period events at Redoubt Volcano (1989–1990), Alaska: Their origin and use as a forecasting tool, *J. Volcanol. Geotherm. Res.*, *62*, 95–135.
- Chouet, B. A. (1985), Excitation of a buried magmatic pipe: A seismic source model for volcanic tremor, *J. Volcanol. Geotherm. Res.*, *90*, 1881–1893.
- Dixon, J. P., S. D. Stihler, J. A. Power, G. Tytgat, S. C. Moran, J. J. Sanchez, S. R. McNutt, S. Estes and J. Paskievitch (2004), Catalog of earthquake hypocenters at Alaskan volcanoes: January 1 through December 31, 2003, *U.S. Geological Survey Open-File Report*, *04–1234*, 69 pp.

- Dixon, J. P., S. D. Stihler, J. A. Power, G. Tytgat, S. Estes, S. C. Moran, J. Paskievitch, J. J. Sanchez and S. R. McNutt (2003), Catalog of earthquake hypocenters at Alaskan volcanoes: January 1, 2002 through December 31, 2002, *U.S. Geological Survey Open-File Report, 03-0267*, 58 pp.
- Dixon, J. P., S. D. Stihler, J. A. Power, G. Tytgat, S. Estes, S. C. Moran, J. Paskievitch and S. R. McNutt (2002), Catalog of earthquake hypocenters at Alaskan volcanoes: January 1, 2000 through December 31, 2001, *U.S. Geological Survey Open-File Report, 02-0342*, 56 pp.
- Fehler, M. (1983), Observations of volcanic tremor at Mount St. Helens Volcano, *J. Geophys. Res.*, *88*, 3476–3484.
- Geller, R. J. and C. S. Mueller (1980), Four similar earthquakes in central California, *Geophys. Res. Lett.*, *7*(10), 821–824.
- Gil Cruz, F. and B. A. Chouet (1997), Long-period events, the most characteristic seismicity accompanying the emplacement and extrusion of a lava dome in Galeras Volcano, Colombia, in 1991, *J. Volcanol. Geotherm. Res.*, *77*, 121–158.
- Gutenberg, B. and C. F. Richter (1956), Magnitude and energy of earthquakes, *Annali di Geofisica*, *9*, 1–15.
- Hagerty, M. T., S. Y. Schwartz, M. A. Garcés and M. Protti (2000), Analysis of seismic and acoustic observations at Arenal Volcano, Costa Rica, 1995–1997, *J. Volcanol. Geotherm. Res.*, *101*, 27–65.
- Harlow, D. H., J. A. Power, E. Laguerta, G. Ambubuyog, R. A. White and R. P. Hoblitt (1997), Precursory Seismicity and forecasting of the June 15, 1991 eruption of Mount Pinatubo, Philippines, in *Fire and Mud*, edited by C. Newhall and R. Punongbuyan, University of Washington Press, 285–304.

- Havskov, J., S. De la Cruz-Reyna, S. K. Singh, F. Medina and C. Gutierrez (1983), Seismic activity related to the March–April, 1982 eruptions of El Chichon Volcano, Chiapas, Mexico, *Geophys. Res. Lett.*, *10*, 293–296.
- Hellweg, M. (2000), Physical models for the source for Lascars harmonic tremor, *J. Volcanol. Geotherm. Res.*, *101*, 183–198.
- Jaupart, C. and S. Vergnolle (1989), The generation and collapse of a foam layer at the roof of a basaltic magma chamber, *J. Fluid Mech.*, *203*, 347–380.
- Jaupart, C. and S. Vergnolle (1988), Laboratory models of Hawaiian and Strombolian eruptions, *Nature*, *331*, 58–60.
- Julian, B. (1994), Volcanic tremor: Nonlinear excitation by fluid flow, *J. Geophys. Res.*, *99*(6), 11859–11877.
- Lahr, J. C. (1999), HYPOELLIPSE: A computer program for determining local earthquake hypocentral parameters, magnitude, and first motion pattern (Y2K compliant version), *U.S. Geological Survey Open-File Report*, *99-023*, 112 pp.
- Lahr, J. C., B. A. Chouet, C. D. Stephens, J. A. Power and R. A. (1994), Earthquake classification, location, and error analysis in a volcanic environment: implications for the magmatic system of the 1989–1990 eruption at Redoubt Volcano, Alaska, *J. Volcanol. Geotherm. Res.*, *62*, 137–151.
- Lu, Z., T. Masterlark, C. Jr. Wicks, W. Thatcher, D. Dzurisin and J. Power (2003), Interferometric Synthetic Aperture Radar studies of Alaska volcanoes, *Earth Observation Magazine*, *12*(3), 8–18.
- Malone, S. D. (1983), Volcanic earthquakes: Examples from Mount St. Helens, in *Earthquakes: Observations, Theory and Interpretation*, edited by H. Kanamori and E. Boshi, Elsevier, Amsterdam, 436–455.

- Mann, D. (2002), Deformation of Alaskan volcanoes measured using SAR interferometry and GPS, *PhD thesis*, University of Alaska Fairbanks, August 2002, 122 pages.
- McNutt, S. R., J. Dehn and J. Gardner (2000), Phreatic explosions at Shishaldin Volcano, Alaska, September 1999 to August 2000, *EOS Trans. Am. Geophys. Union*, 81(48), Fall Meet. Suppl., Abstract V22B-12.
- McNutt, S. R. (1992), Volcanic Tremor, in *Encyclopedia of Earth System Science*, edited by W. A. Nierenberg, Academic Press, San Diego, CA, 417-425.
- McNutt, S. R. and K. H. Jacob (1986), Determination of large-scale velocity structure of the crust and upper mantle in the vicinity of Pavlof volcano, Alaska, *J. Geophys. Res.*, 91(5), 5013-5022.
- Miller, T. P., R. G. McGimsey, D. H. Richter, J. R. Riehle, C. J. Nye, M. E. Yount and J. A. Dumoulin (1998), Catalog of the historically active volcanoes of Alaska – Shishaldin Volcano, *U.S. Geological Survey Open-File Report*, 98-482, 104 pp.
- Moran, S. C., S. D. Stihler and J. A. Power (2002), A tectonic earthquake sequence preceding the April-May 1999 eruption of Shishaldin Volcano, Alaska, *Bull. Volcanol.*, 64, 520-524.
- Mori, J., H. Patia, C. McKee, I. Itikarai, P. Lowenstein, P. De Saint Ours and B. Talai (1989), Seismicity associated with eruptive activity at Langila Volcano, Papua New Guinea, *J. Volcanol. Geotherm. Res.*, 38, 243-255.
- Nakada, S., H. Shimizu and K. Ohta (1999), Overview of the 1990-1950 eruption at Unzen Volcano, *J. Volcanol. Geotherm. Res.*, 89, 1-22.
- Neuberg, J., R. Luckett, B. Baptie and K. Olsen (2000), Models of tremor and low-frequency earthquake swarms on Montserrat, *J. Volcanol. Geotherm. Res.*, 101, 83-104.
- Neuberg, J., B. Baptie, R. Luckett and R. Stewart (1998), Results from the broadband seismic network on Montserrat, *Geophys. Res. Lett.*, 25, 3661-3664.

- Nye, C. T., T. Keith, J. C. Eichelberger, T. P. Miller, S. R. McNutt, S. C. Moran, D. J. Schneider, J. Dehn and J. R. Schaefer (2002), The 1999 eruptions of Shishaldin Volcano Alaska: monitoring a distant eruption, *Bull. Volcanol.*, *64*, 507–519.
- Okada, H., H. Watanabe, H. Yamashita and I. Yokoyama (1981), Seismological significance of the 1977–1978 eruptions and the magma intrusion process of Usu Volcano, Hokkaido, *J. Volcanol. Geotherm. Res.*, *9*, 311–334.
- Petersen, T., J. Caplan-Auerbach and S. R. McNutt (2004), The continuously high level of long-period seismicity at Shishaldin Volcano, Unimak Island, Alaska, 1999 to 2004, *IAVCEI General Assembly*, Pucón, Chile, November 2004, Abstract s08d–pf–136.
- Petersen, T., J. Caplan-Auerbach and S. R. McNutt (2002), Temporal distribution and rates of repetitive low-frequency earthquakes at Shishaldin Volcano, Alaska, *EOS Trans. Am. Geophys. Union*, *83*(47), Fall Meet. Suppl., Abstract V21A–1173.
- Power, J. A., S. D. Stihler, R. A. White and S. C. Moran (2002), Observations of deep long-period (DLP) seismic events beneath Aleutian Arc volcanoes, 1989 to 2002, *EOS Trans. Am. Geophys. Union*, *83*(47), Fall Meet. Suppl., Abstract S11D–11.
- Power, J. A., J. C. Lahr, R. A. Page, B. A. Chouet, C. D. Stephens, D. H. Harlow, T. L. Murray and J. N. Davies (1994), Seismic evolution of the 1989–1990 eruption sequence of Redoubt Volcano, Alaska, *J. Volcanol. Geotherm. Res.*, *62*, 69–94.
- Richter, C. F. (1935), An instrumental earthquake magnitude scale, *Bull. Seismol. Soc. Am.*, *25*, 1–32.
- Ripepe, M., S. Ciliberto and M. Schiava Della (2001), Time constraints for modeling source dynamics of volcanic explosions at Stromboli, *J. Geophys. Res.*, *106*(5), 8713–8727.
- Ripepe, M. and E. Gordeev (1999), Gas bubble dynamics model for shallow volcanic tremor at Stromboli, *J. Geophys. Res.*, *104*, 10639–10654.

- Ripepe, M., P. Poggi, T. Braun and E. Gordeev (1996), Infrasonic waves and volcanic tremor at Stromboli, *Geophys. Res. Lett.*, *23*(2), 181–184.
- Stelling, P., J. Beget, C. Nye, J. Gardner, J. D. Devine and R. M. M. George (2002), Geology and petrology of ejecta from the 1999 eruption of Shishaldin Volcano, Alaska, *Bull. Volcanol.*, *64*, 548–561.
- Thompson, G., S. R. McNutt and G. Tytgat (2002), Three distinct regimes of volcanic tremor associated with the eruption of Shishaldin Volcano, Alaska, *Bull. Volcanol.*, *64*, 535–547.
- Wessel, P. and W. H. F. Smith (1998), New, improved version of the Generic Mapping Tools released, *EOS Trans. Am. Geophys. Union*, *79*, 579.
- Zimanowski, B. (1998), Phreatomagmatic Explosions, in *From Magma to Tephra: modelling physical processes of explosive volcanic eruptions*, edited by A. Freund and M. Rosi, Elsevier, 25–53.

Chapter 3

Seismo-acoustic signals associated with degassing explosions recorded at Shishaldin Volcano, Alaska, 2003–2004¹

3.1 Abstract

In summer 2003, a Chaparral Model 2 microphone was deployed at Shishaldin Volcano, Aleutian Islands, Alaska. The pressure sensor was co-located with a short-period seismometer on the volcano's north flank at a distance of 6.62 km from the active summit vent. The seismo-acoustic data exhibit a correlation between impulsive acoustic signals (1–2 Pa) and long-period (LP; 1–2 Hz) earthquakes. Since it last erupted in 1999, Shishaldin has been characterized by sustained seismicity consisting of many hundreds to two thousand LP events per day. The activity is accompanied by up to ~200 m high discrete gas puffs exiting the small summit vent, but no significant eruptive activity has been confirmed. The acoustic waveforms possess similarity throughout the data set (July 2003–November 2004) indicating a repetitive source mechanism. The simplicity of the acoustic waveforms, the impulsive onsets with relatively short (~10–20 s) gradually decaying codas and the waveform similarities suggest that the acoustic pulses are generated at the fluid-air interface within an open-vent system. SO₂ measurements have revealed a low SO₂ flux, suggesting a hydrothermal system with magmatic gases leaking through. This hypothesis is supported by the steady-state nature of Shishaldin's volcanic system since 1999. Time delays between the seismic LP and infrasound onsets were acquired from a representative day of seismo-acoustic data. A simple model was used to estimate source depths. The short seismo-acoustic delay times have revealed that the seismic and acoustic sources are co-located at a depth of 240 ± 200 m below the crater rim. This shallow depth is confirmed by resonance of the upper portion of the open conduit, which produces standing waves with $f = 0.3$ Hz in the acoustic waveform codas. The infrasound data has allowed us to relate Shishaldin's LP earthquakes to degassing explosions, created by gas volume ruptures from a fluid-air interface.

¹Published under the same title with authors T. Petersen and S. R. McNutt in *Bulletin of Volcanology*, doi:10.1007/s00445-006-0088-z, 2006.

3.2 Introduction

Seismicity at Shishaldin Volcano, Alaska, is characterized by the sustained generation of long-period (LP) earthquakes at a rate of about one event every 0.5–5 minutes [Petersen *et al.*, 2006]. The LP seismicity has been persistent since Shishaldin last erupted in 1999 and is accompanied by small, ~200 m high, discrete steam plumes exiting the summit crater.

Shishaldin is a 2857 m high stratovolcano located near the center of Unimak Island, the easternmost of the Aleutian Islands, Alaska (Figure 3.1). The highly symmetrical cone is

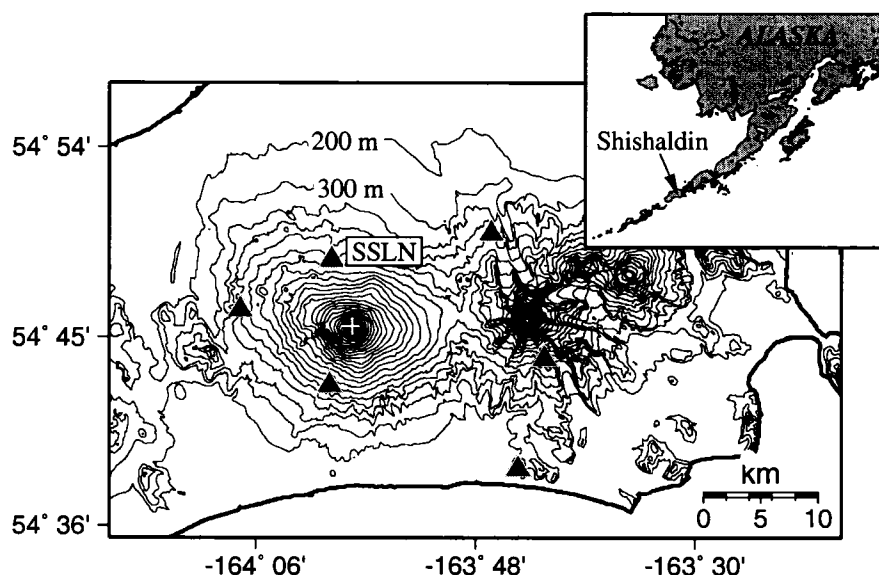


Figure 3.1. Alaska Volcano Observatory (AVO) monitoring network around Shishaldin Volcano located on Unimak Island, easternmost island in the Aleutian Arc, Alaska. The seismic network, installed in 1997, consists of six short-period seismometers (marked by triangles). Five stations have L-4 vertical component 1 Hz instruments. The station south of the summit has a 3-component L-22 seismometer with a natural frequency of 2 Hz. Broadband instruments have never been deployed around Shishaldin. The distances of the stations to the summit (2857 m above sea-level; marked by cross) are between 5.3 and 19 km. The microphone deployed in July 2003, is co-located with a L-4 seismometer at station SSLN, 6.6 km (6.3 km horizontal and 2.1 km vertical distance) from the vent. The base map was produced using Generic Mapping Tools (GMT) and 15-min Digital Elevation Model (DEM) data from the U.S.G.S.

primarily composed of basalt and basaltic andesite. Shishaldin is among the most active volcanoes in Alaska [Miller *et al.*, 1998]. The most recent eruption, in April–May 1999, exhibited both Strombolian bubble and ash bursts and Subplinian behavior with a 16-km eruption column. Acoustic waves recorded during the eruption were used to model the Strombolian explosions by the vibration of a large overpressurized bubble prior to its bursting at the top of a magma column [Vergnolle *et al.*, 2004]. Studies on thermal anomalies in satellite imagery observed during the 1999 eruption have confirmed a magma column reaching the summit at the time of Strombolian activity [Dehn *et al.*, 2002]. Since September 1999, Shishaldin has exhibited an almost continuous and extremely high level of background seismicity consisting of many hundreds to two thousand LP earthquakes per day [Petersen *et al.*, 2006]. The timing of the LP seismic events is similar to that of puffs in the omnipresent gas plume, suggesting that the sustained generation of LP events is directly related to steady-state degassing processes in an open-vent volcanic system [Petersen *et al.*, 2006]. Caplan-Auerbach and Petersen [2005] suggest that Shishaldin LPs are generated by bubble coalescence within the edifice. However, the mechanisms responsible for the continuous high level of seismicity are still poorly understood [Petersen *et al.*, 2006]. The source depths, computed using seismic data alone, are poorly constrained between 0–3 km beneath the summit [Dixon *et al.*, 2003, 2004; Petersen *et al.*, 2006; Caplan-Auerbach and Petersen, 2005].

In recent years, infrasound data recorded at active volcanoes including Arenal [Hagerty *et al.*, 2000], Stromboli [Vergnolle *et al.*, 1996], Erebus [Rowe *et al.*, 2000], Karymsky [Johnson and Lees, 2000; Johnson *et al.*, 1998], Villarica [Johnson *et al.*, 2004], Fuego [Johnson *et al.*, 2004], Sakurajima [Garcés *et al.*, 1999] and many other volcanoes around the world, have revealed a variety of different styles of gas exhalation. Volcanic degassing explosions typical for strombolian-type eruptions at volcanoes like Shishaldin commonly generate impulsive pressure pulses in the infrasonic frequency range (< 20 Hz) together with low-frequency (1–2 Hz) seismic signals (e.g. Johnson *et al.* [2003]). The infrasonic wave travels through the atmosphere, while the seismic wave propagates through the ground, i.e.,

the complex structure of a volcanic system. Thus infrasonic waves are far less affected by their travel paths than seismic waves and therefore offer relatively unfiltered representations of source processes [Johnson, 2005]. Combined studies of seismic and infrasonic data provide an important tool to further the understanding of source dynamics, for example, seismo-acoustic data recorded at Stromboli [Ripepe *et al.*, 2001b], Etna [Ripepe *et al.*, 2001a; Gresta *et al.*, 2004] and Arenal [Hagerty *et al.*, 2000] were used to place constraints on source positions.

The model most commonly used to describe Strombolian activity and the associated seismicity is based on the coalescence of small gas bubbles into a gas slug that rises through liquid (magma) to the free surface. Small gas bubbles released from the magma grow by decompression while moving upward in the fluid [Sparks, 1978] and generate a foam layer at a physical boundary within the conduit [Jaupart and Vergnolle, 1988]. Such a boundary at which rising gas bubbles are collected might be provided by a conduit constriction [Jaupart and Vergnolle, 1989] or an increase in fluid viscosity [Thomas *et al.*, 1993]. When the foam layer reaches a critical thickness it is forced to collapse and creates a gas slug that rises to the liquid-air interface where it causes a Strombolian explosion [Jaupart and Vergnolle, 1989]. A seismic signal may be induced by the coalescence into a large gas bubble [Braun and Ripepe, 1993; Ripepe and Braun, 1994; Ripepe and Gordeev, 1999; Ripepe *et al.*, 2001b] and/or by the oscillation of the rising bubble before it reaches the fluid-air interface, whereas the bubble burst itself, i.e. the connection of volcanic gas to the atmosphere, does not appear on the seismogram due to the lack of coupling between source (oscillation in air) and conduit walls [Vergnolle *et al.*, 1996]. Infrasound signals of specific waveforms have been modeled for Strombolian explosions. Vergnolle *et al.* [1996] suggest that the most energetic part of infrasonic waves associated with Strombolian activity is generated by the vibration of the overpressurized bubble just before bursting at the fluid-air interface.

Previous studies on Shishaldin's activity since the 1999 eruption focused on the analyses of seismic data [Caplan-Auerbach and Petersen, 2005; Petersen *et al.*, 2006]. In this paper we present infrasound data associated with Shishaldin's continuously high level of LP seismicity.

We combine seismic and acoustic data to improve the understanding of Shishaldin's conduit processes and degassing mechanisms. Because source depths acquired solely from seismic data are poorly constrained between 0–3 km beneath the summit, we use the seismo-acoustic data to estimate depth of source processes responsible for Shishaldin's sustained degassing and seismic behavior.

3.3 Seismo-acoustic data

In July 2003, the 6-station seismic monitoring network around Shishaldin operated by the Alaska Volcano Observatory (AVO) was supplemented with a Chaparral Model 2 microphone (Figure 3.1) [Petersen *et al.*, 2006]. The pressure sensor replaced a Setra 239 microphone (~ 0.2 mV/Pa sensitivity) that stopped functioning in late 1999 and is co-located with seismic station SSLN at a distance of 6.62 km from the summit on the volcano's north flank (Figure 3.1). The current pressure sensor set up, the Chaparral microphone plus a Voltage Controlled Oscillator (VCO), has a flat response at frequencies ≥ 0.1 Hz and a sensitivity of 0.14 V/Pa. The system is able to record signals up to 17 Pa before saturating. A 15 m long conventional soaker hose running perpendicular to the volcano's slope is attached to the microphone and covered by a porous layer of cinder and rocks. The design was deployed to spatially filter out incoherent wind noise, although the exact noise reduction benefits are unknown.

The seismic instrument at station SSLN is a vertical-component Mark Products L-4 seismometer with a natural frequency of 1 Hz. All network instruments provide real-time analog data telemetered to AVO and digitized at 100 Hz with 12-bit resolution.

During periods of low wind noise virtually all LP seismic signals recorded between July 2003 and November 2004 are associated with an acoustic signal (Figure 3.2). The infrasonic waveforms consist of a single impulsive onset, that is always compressional, followed by a ~ 10 – 20 s lower-amplitude very monochromatic coda that is gradually decaying. The frequency content of the entire signal is confined between 0.15 and 1.9 Hz (Figure 3.3) with dominant energy at ~ 0.6 Hz. The coda has a frequency of ~ 0.3 Hz. The majority of in-

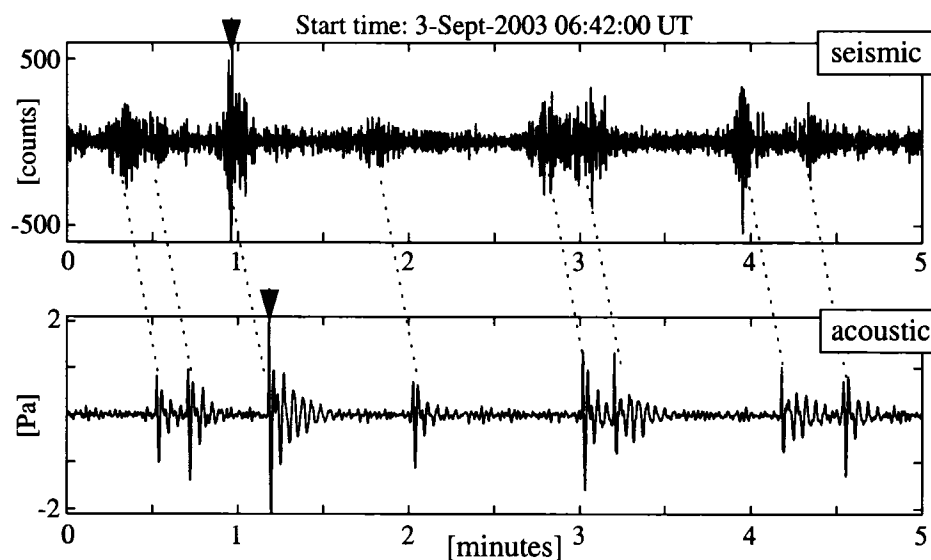


Figure 3.2. Example of seismo-acoustic data recorded at station SSLN during a time period of low wind noise (September 3, 2003 06:42:00–06:47:00 UTC). Every seismic signal is followed by an acoustic signal with a delay time of ~ 17 s. Arrows indicate the seismo-acoustic event pair shown in Figure 3.3. The data are bandpass filtered (seismic: 0.5–3 Hz, acoustic: 0.02–2 Hz).

frasound pulses have a maximum zero-to-peak amplitude of 1–2 Pa, which results in excess pressures of about 7–14 Pa at 1 km from the vent assuming an inverse pressure decrease with radial distance from the vent [Kinsler and Frey, 1962]. Acoustic pulses normalized to 1 km, produced by explosive activity at some other volcanoes with infrasound studies, range from 10–200 Pa [Johnson *et al.*, 2004]; for example, discrete Strombolian explosions at Karymsky [Johnson and Lees, 2000], Sangay [Johnson *et al.*, 2003] and Stromboli [Ripepe and Marchetti, 2002] have exhibited typical values of 10–25 Pa [Johnson *et al.*, 2004]; Strombolian and Vulcanian activity at Arenal [Hagerty *et al.*, 2000] exhibited values of 100 Pa and infrequent large bubble bursts at Erebus [Rowe *et al.*, 2000] produced values of 200 Pa. The acoustic waveforms observed at Shishaldin possess similarity throughout the data set. The simplicity of Shishaldin acoustic waveforms, the impulsive compressional onsets, the waveform similarity, and explosive signals observed at other volcanoes support our

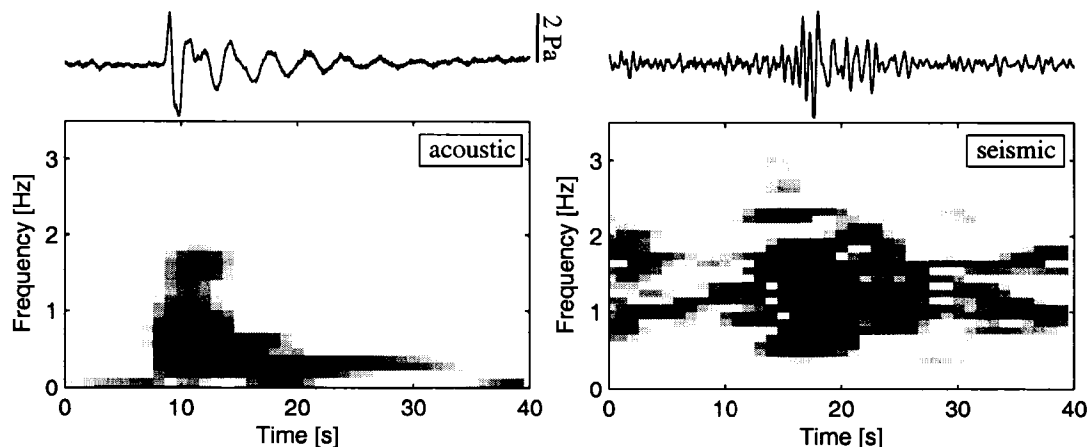


Figure 3.3. Acoustic and seismic traces with corresponding spectrograms characteristic for Shishaldin's sustained seismicity. The signals were recorded at station SSLN on September 3, 2003 (see Figure 3.2). Note that the signals are centered in each panel; the acoustic wave arrives ~ 17 s after the seismic P-wave.

inference that the acoustic signal is generated at the fluid-air interface at shallow depth within the conduit, i.e. it travels solely through the less complex atmosphere. Infrasonic pulses recorded at Stromboli, Erebus and Villarrica are directly associated with visually observed gas bubbles bursting from the free surface at the top of the conduit (*Ripepe et al. [1996]; Rowe et al. [2000]; Johnson et al. [2004]* respectively). These waveforms resemble Shishaldin's infrasound in their simple, short-duration, quasi-sinusoidal nature. The spectral peaks at Stromboli (3–8 Hz; *Ripepe et al. [1996]*) and Erebus (3 Hz; *Rowe et al. [2000]*) are significantly higher than those observed at Shishaldin (0.6 Hz). In comparison, Villarrica exhibits frequencies that resemble Shishaldin infrasound; the sharp onset is followed by a 5–10 s coda with spectral peaks at ~ 0.5 Hz [*Johnson et al., 2004*]. Villarrica infrasound is associated with a sustained sequence of bursting bubbles; the degassing is more persistent than at Erebus [*Johnson et al., 2004*].

The acoustic waveforms associated with strong Strombolian explosions recorded during the Shishaldin 1999 eruption [*Thompson et al., 2002; Caplan-Auerbach and McNutt, 2003; Vergnolle et al., 2004*] also differ from the infrasound data recorded in 2003–2004. The

signals recorded in 1999 occurred at a higher rate (several pulses per minute), were shorter in duration (1–2 s), had a broader frequency spectrum (~ 1.3 Hz onset, followed by a 2–4 Hz coda), and were significantly larger, with zero-to-peak amplitudes of up to 50 Pa at a distance of 6.62 km (~ 330 Pa normalized to 1 km).

Shishaldin's 2003–2004 LP seismic events are discrete signals with dominant spectral amplitudes between 1–2 Hz, fairly monochromatic waveforms and ~ 15 s long codas (Figure 3.3). Some of the LP events are preceded by a lower-amplitude signal with a short-period (SP; 4–7 Hz) phase (Figure 3.4). These two-phased events are termed *coupled events*, emphasizing a trigger relationship between the two discrete events [Caplan-Auerbach and Petersen, 2005]. In the model for Shishaldin's coupled events proposed by Caplan-Auerbach and Petersen [2005] the SP phase results from a pressure transient within the fluid caused by turbulent flow around an obstacle at a depth of < 4 km, and acts as a trigger for the LP event.

During a time period of increased seismic activity in May 2004, LP events with a ground-coupled airwave phase were recorded on the 3 seismic stations closest to the vent. These airwaves exhibited peak pressures up to 7 Pa on the SSLN microphone. The increase in activity was accompanied by volcanic tremor, thermal anomalies in satellite imagery, and more vigorous plume activity than usual. Ash was observed on Shishaldin's flanks, but there is no evidence for whether juvenile or crater wall material was ejected from the volcano. In November 2004, the infrasound pulses fell below detection threshold, while the seismicity continued without significant changes.

Visual observations of Shishaldin's volcanic activity in 2003 have shown that the puffs in the omnipresent summit gas plume occur at a rate similar to that of the LP seismic events [Petersen *et al.*, 2006]. Video images acquired in July 2004 confirm these results. The similarity between the timing of plume puffs and the rate at which seismo-acoustic events are generated suggests that the seismo-acoustic pulses are related to degassing activity in the form of discrete puffs. The relative contribution of meteoric and magmatic gas is unknown, but magmatic gases seem to be at least partly involved in the plume activity

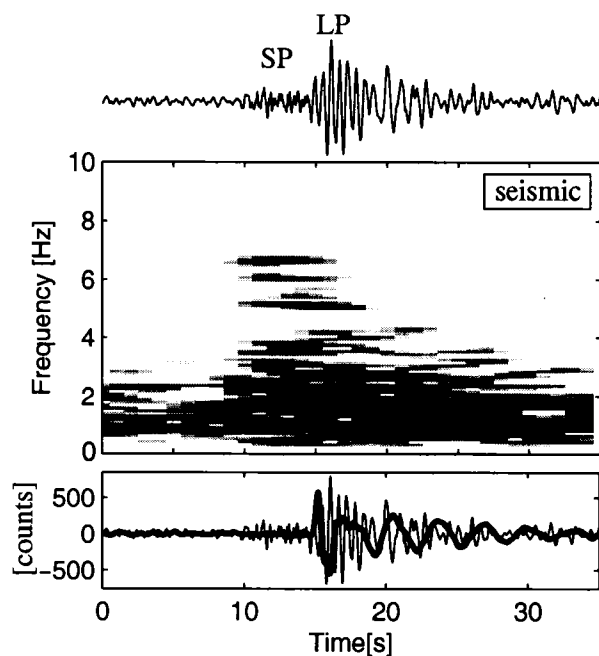


Figure 3.4. Example of a Shishaldin coupled earthquake (SSLN; September 2, 2003 16:10:50 UTC). The SP (4–7 Hz) phase precedes the LP phase by ~ 5 s. The bottom panel shows the acoustic pulse corresponding to the LP event plotted on top of seismic trace (offset by 16.43 s). The absence of an acoustic signal directly related to the SP phase suggests that the precursor signal is located at greater depth within the two-phase fluid.

because of the presence of SO_2 indicated by a blue haze [Petersen *et al.*, 2006] and detected using satellite imagery [Kearney *et al.*, 2004]. The presence of ash has only been observed on rare occasions. Measurements of surface degassing at Shishaldin on July 31, 2004, revealed a SO_2 mass flux of 58 tons/day [Kearney, 2005]. This value is very low compared to SO_2 detected at volcanoes with active magmatic systems. At Stromboli, for example, a mean flux of 280 tons/day was observed during its typical state of open-vent degassing [McGonigle *et al.*, 2003]. At Etna an SO_2 output of 940 tons/day was measured during times of strong open-vent degassing from the top of magmatic conduits [McGonigle *et al.*, 2003]. The hydrothermal activity at Poás Volcano exhibits comparably low SO_2 fluxes of 50–160 tons/day [Andres *et al.*, 1992].

Wind noise is a persistent problem in the seismo-acoustic data set; only a small per-

centage ($\ll 10\%$) of the combined data is available for analysis due to infrasound data degraded by wind in the vicinity of the recording site. Although the acoustic propagation is far less complex than the travel path of seismic waves, the influence of time varying atmospheric wind and temperature profiles have to be considered [Johnson and Lees, 2000]. Data from only a single pressure sensor limit our ability to evaluate these influences on Shishaldin's acoustic amplitudes. A weather recorder at station SSLN would provide more detailed information on the effects of wind on the acoustic data. Unfortunately, the nearest weather station is located over 90 km from Shishaldin at Cold Bay. Consequently, the only indications of local wind conditions are given by the highly sensitive pressure sensor itself. Because the difference between a windy and a calm day is clearly visible in the acoustic data, we can easily exclude from our dataset times in which wind was a significant factor.

An additional limitation to our data set is the relatively large distance between the active vent and pressure sensor. The acoustic signal strength is more likely affected by the travel path than infrasound recorded at volcanoes with stations closer to the vent [Johnson, 2003]. Even though the acoustic amplitudes have to be treated with high caution, the authenticity of the waveforms themselves is supported by a high degree of similarity.

3.4 Depth constraints using seismo-acoustic data

In order to constrain the source depths of Shishaldin explosions, a representative day of seismo-acoustic data with a good signal-to-noise ratio has been selected. About 1900 seismo-acoustic events were recorded that day (September 2, 2003). The onsets of acoustic signals are so impulsive that the arrival times can be determined with an accuracy of ≤ 0.1 s. In contrast, it is very difficult to identify the onsets of the emergent LP events in seismic traces. It has not been possible to line up the seismic waveforms corresponding to acoustic signals by using a constant delay time, because arrival time differences between seismic and acoustic events vary (Figure 3.5). We used waveform cross-correlation (correlation coefficient ≥ 0.75) with an 8 s long seismic master event to select a subset of similar waveforms for further analysis. We extracted 153 seismic events and their corresponding acoustic signals. Cross-

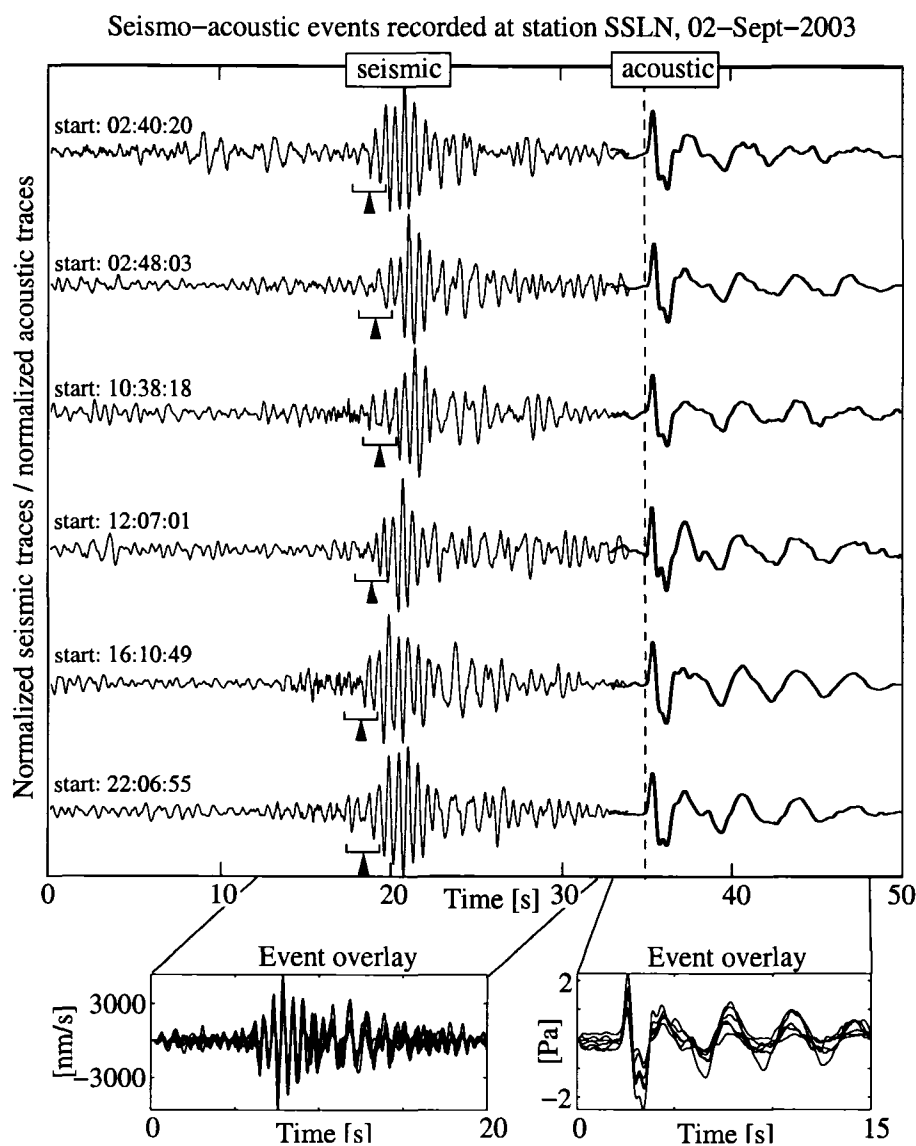


Figure 3.5. Shishaldin explosion examples selected from a subset of 153 seismo-acoustic event pairs extracted for further analysis. Seismic traces are high-pass filtered (above 0.8 Hz), acoustic traces are bandpass filtered (0.02–3 Hz). The seismic and acoustic waveforms are plotted on the same time-axis aligned with the acoustic onsets. Note that some of the LP events exhibit a short-period (SP) precursor signal. The onset of the LP phase corresponding to the acoustic signal is marked by an arrow for each seismic event. A stack of the seismic events was used to identify these onsets. The bars indicate the standard deviation (± 0.57 s) of individual events from the mean seismo-acoustic delay time $\Delta t = 16.87$ s. The errors in arrival time picks (≤ 0.44 s) are well within this range. The bottom two panels show an overlay of the 6 events. The LP events have a mean cross-correlation coefficient of 0.8, while the acoustic events have a value of 0.9.

correlating the ~ 15 s long acoustic signals with each other results in a mean correlation coefficient of 0.85. Although the degree of similarity between acoustic events fluctuates throughout the data set (July 2003–November 2004), the events recorded on the selected day are extremely similar, which indicates a highly repetitive source mechanism. The extracted seismic events exhibit similarity between the ~ 8 s long LP phases with a mean cross-correlation coefficient of 0.70. Figure 3.5 shows examples of seismo-acoustic waveform pairs and arrival time picks of Shishaldin explosions recorded at station SSLN. Arrival times were picked for 104 of the seismo-acoustic events with a precision of ≤ 0.44 s. The events are distributed over the whole day. The mean seismo-acoustic delay time for the subset of events is $\Delta t = t_a - t_s = 16.87$ s. The delay times of individual seismo-acoustic events deviate from this value by up to ± 0.57 s. The variation in delay times shows no specific trend that would indicate the influence of changing atmospheric conditions through the day. As mentioned above, we chose a particularly calm day for our analysis and selected only low wind noise acoustic events in order to exclude the effect of wind fields on acoustic wave propagation. Instead of being caused by changing atmospheric conditions the observed variation in delay times may reflect small changes in source locations. Source locations that vary within $1/4$ of the dominant wavelength of events would create a spectrum of travel times without altering the similar appearance of waveforms [Geller and Mueller, 1980]. The seismo-acoustic travel time variations observed at Shishaldin are within a quarter of a wavelength of the dominant periods of the signal, which are 0.41 s for acoustic signals (dominant spectral peak at $f = 0.6$ Hz) and 0.16 s for seismic signals ($f = 1.6$ Hz). However, the various other factors that may cause fluctuations in delay times also have to be considered. Changes in acoustic velocity within the conduit (e.g. due to thermal fluctuations), changes in seismic velocity and/or variations in the seismo-acoustic source time function may influence seismo-acoustic travel times.

Figure 3.6a shows seismo-acoustic amplitude ratios for the selected subset of events. The relation between seismic and acoustic signal strength varies greatly. In contrast to Erebus, which displays a linear relationship between seismic and acoustic amplitudes [Johnson *et*

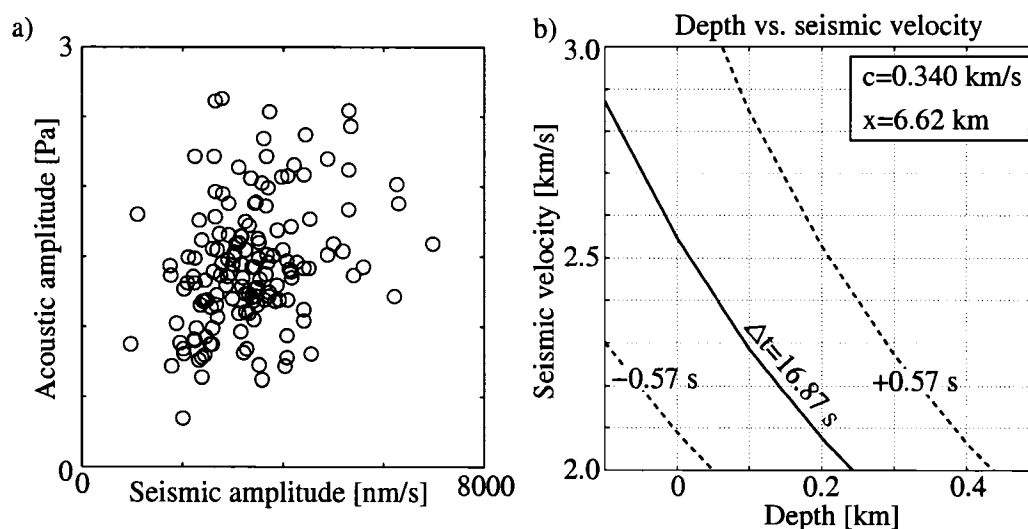


Figure 3.6. a) Seismo-acoustic amplitude ratios for the subset of 153 events. The correlation between intensity of seismic and infrasound amplitudes is very low (correlation coefficient ~ 0.3). b) Depth vs. seismic velocity for a delay time $\Delta t = 16.87 \pm 0.57$ s. The maximum depth of the seismo-acoustic source is 240 ± 200 m.

al., 2003], scatter in seismo-acoustic energy partitioning has also been observed at other volcanoes, e.g., Karymsky [Johnson *et al.*, 2003] and Arenal [Hagerty *et al.*, 2000]. Johnson *et al.* [2003] attribute the variations in seismo-acoustic amplitude ratios observed at Karymsky to changes in source locations within the conduit and/or muffling of the infrasonic pulse due to overlying material. Garcés *et al.* [1998] attribute these variations to changing acoustic properties within the conduit such as time-varying void fraction. At Shishaldin the variations in seismo-acoustic amplitude ratios may correspond to small changes in conduit conditions on a short time scale. The amount of debris in the conduit, changed by individual explosions and during the course of more vigorous degassing, could influence the partitioning of seismo-acoustic energy, e.g. a higher solid component increases the fluid-air acoustic impedance contrast allowing significantly less energy to radiate into the atmosphere than into the ground.

The estimation of explosion source depth is based on a number of assumptions. First we assume the simplest model in which the seismic and acoustic first arrivals share a common

source located at shallow depth z (Figure 3.7a). The direct distance between summit and station SSLN is $x = 6620$ m. For $x \gg z$ we can assume that the acoustic waves from summit to station and the seismic waves travel the same distance x [Hagerty *et al.*, 2000]. The delay time between the seismic and acoustic first arrivals can thus be written as $\Delta t = z/c_c + [1/c_a - 1/v]x$, in which z is the distance between the free surface within the conduit and the crater rim, c_c is the speed of sound within the conduit, c_a is the acoustic velocity in the atmosphere and v is the apparent seismic velocity. The apparent acoustic velocity $c = c_c = c_a = 340$ m/s, calculated from the move-out between ground-coupled airwaves recorded on three seismic stations in May 2004, provides a reasonable value. The seismic velocity structure around Shishaldin is poorly constrained [Petersen *et al.*, 2006]. The P-wave velocity of 3.05 km/s used by AVO for the upper 3 km of the Shishaldin velocity model was based on a model originally constructed for Pavlof volcano [McNutt and Jacob, 1986], which is nearby and has similar size and composition. We therefore assume a homogeneous seismic velocity structure v with values between 2.0 and 3.0 km/s for the upper 2 km (elevation difference between summit and station SSLN) of the volcano. Using the observed mean delay time $\Delta t = 16.87 \pm 0.57$ s, the maximum depth of the seismo-acoustic source is 240 ± 200 m below the crater rim (Figure 3.6b). The summit crater itself is about 60 m deep; we therefore assume a minimum depth of 60 m for the seismo-acoustic source. These source depth calculations are burdened with many unknowns, but provide superior resolution to locations gained by using solely seismic data.

The estimated depth of the seismo-acoustic source can be supported by assuming that the monochromatic coda on the acoustic signals is due to resonance of the air within the top portion of the conduit (portion above source A/S in Figure 3.7a). Assuming that the top of the conduit resonates like an organ pipe with one open end and one closed end, hence with a fundamental frequency of $f = c_c/(4L)$, the conduit length L can be estimated. This assumes that the crater rim (or just below) is an *open end* and the fluid free surface at depth z within the conduit provides the *closed end*, which gives the required boundary conditions. The coda frequency is $f = 0.3$ Hz; the strong coda similarity observed on the

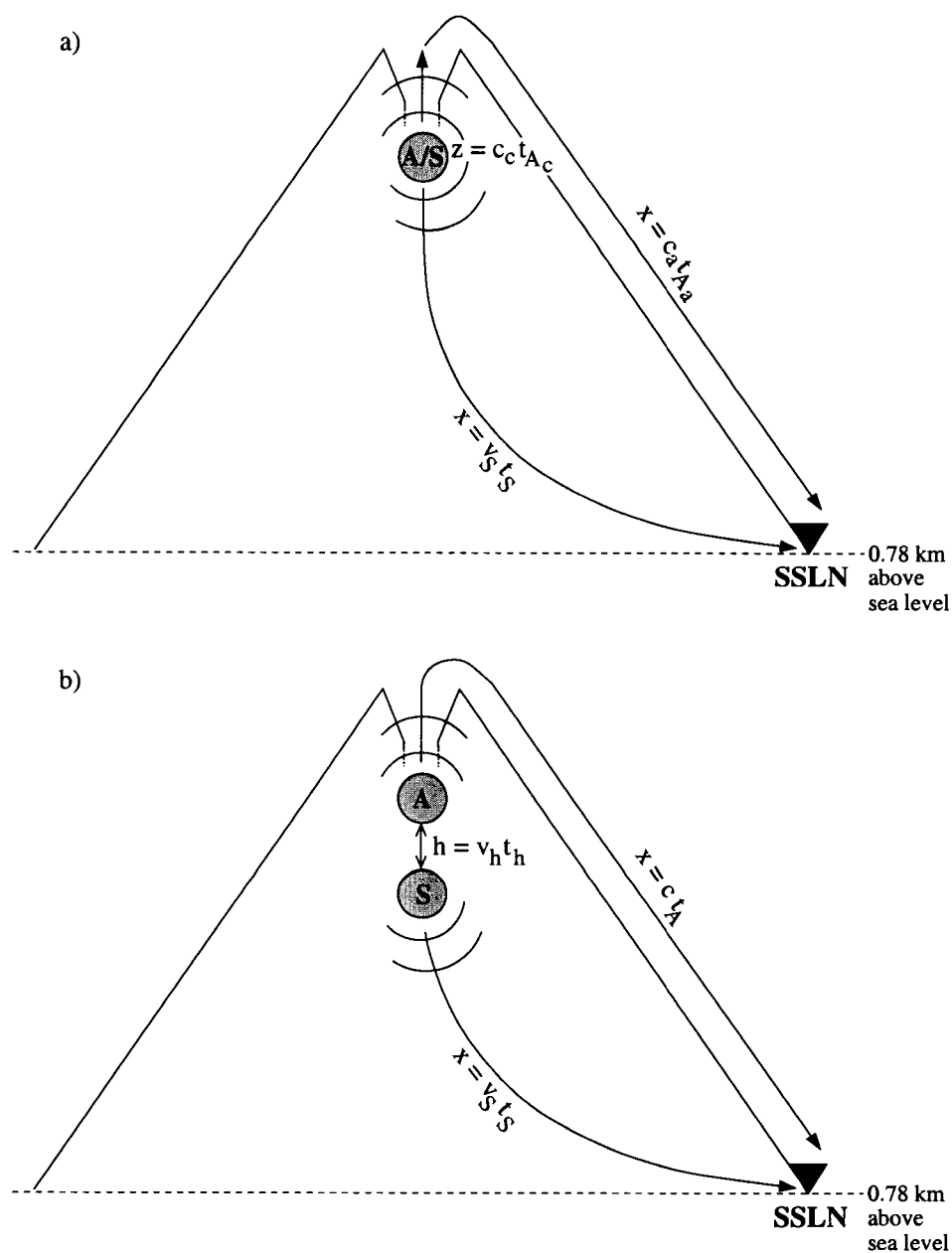


Figure 3.7. Schematic diagram of Shishaldin Volcano showing relation of LP part of seismic signal (S) and acoustic source (A). Vertical scale is exaggerated. a) Common seismo-acoustic source located at depth z beneath the crater rim. The measured delay time between seismic and acoustic arrivals is $\Delta t = t_{Ac} + t_{Aa} - t_s$, in which $t_{Ac} + t_{Aa}$ is the traveltime of the acoustic wave through the conduit and atmosphere, and t_s is the seismic traveltime. b) Acoustic and seismic source separated by distance h . v_h and t_h are the velocity and traveltime of the trigger mechanism between the two sources.

day selected for this analyses implies that the physical conditions in the top of the conduit do not change significantly. If we use a value of 340 m/s for the speed of sound c_c inside the conduit, the explosion source would be located at a depth of 280 m, which is consistent with source depth range of 240 ± 200 m previously estimated from travel times. This is very strong evidence that the source depth is indeed located at shallow depths at the bottom of the open conduit. Note that previous investigators (e.g. [Garcés and McNutt, 1997]) have often used the organ pipe model for a magma-filled conduit inside the volcano. In contrast, here we are invoking the organ pipe model with clear boundary conditions for the air-filled portion of the conduit.

In order to verify our assumption that the seismic and acoustic sources are co-located, we now consider the possibility that seismic and infrasonic waves are part of the same explosive degassing process but may be generated in two different places along the conduit separated by a vertical distance h (Figure 3.7b). The delay times calculated for the assumed seismic velocity and depth ranges are between 16.34 s (for $z = 60$ m, $v = 2000$ m/s) and 18.56 s (for $z = 440$ m, $v = 3000$ m/s). The difference between observed and calculated delay times is directly related to the ratio h/v_h , where v_h is the apparent velocity of a trigger mechanism between the two sources. In general, such a mechanism could be provided by a seismic pressure wave ascending through the conduit [Ishihara, 1985] or could be a mechanical trigger like a rising gas slug. Since we assume that the acoustic signal is associated with a bubble explosion we prefer the latter mechanism. A seismic trigger would require a highly-pressurized gas pocket waiting to be detonated just beneath the free surface, which we consider to be unlikely. However, the velocity expected for a gas slug rising through the upper part of the conduit is 2–10 m/s [Vergnolle and Brandeis, 1996]. The maximum vertical distance h is obtained when the smallest theoretical delay time (16.34 s; $z = 60$ m, $v = 2000$ m/s) and the largest velocity of the rising gas slug (10 m/s) are assumed. Considering the size of the delay time fluctuation, the acoustic and seismic sources would be separated by about 5 ± 6 m. This value seems too small compared to the errors involved to have any physical meaning. The short seismo-acoustic delay times do not leave enough

room for a significant depth separation between the source of seismic and acoustic arrivals, such as the signals observed at Sakurajima [Ishihara, 1985], suggesting that the seismic and acoustic sources at Shishaldin are co-located.

3.5 Discussion and concluding remarks

The timing between LP seismic events and acoustic phases observed at Shishaldin in 2003–2004 reveal that the explosions occur at shallow depths beneath the summit and that the LP seismic and acoustic sources are virtually coincident. Based on analyses of all available data, we infer that the infrasonic signals are caused by the explosive outflux of volatiles at the top of a fluid-filled conduit into an open conduit system about 240 m in length. The impulsive acceleration of steam/gas into the atmosphere, also known as *jetting*, produces a compressional wave that excites the conduit into acoustic resonance triggering an LP earthquake.

The persistent degassing activity requires an efficient supply of gas to the upper conduit. It is unknown whether or not magmatic fluids are involved. However, there is no evidence for shallow magma and the low SO₂ flux observed at Shishaldin suggests that magmatic emissions are filtered through a hydrothermal system. This supports our inference that a hydrothermal source filled with bubbly water is responsible for the sustained explosive activity observed at Shishaldin since it last erupted in 1999.

The frequency range of acoustic waveforms recorded at Shishaldin in 2003–2004 (0.15–1.9 Hz with dominant energy at ~0.6 Hz) is much lower than those observed at Stromboli or at Shishaldin in 1999. The Strombolian activity at Shishaldin in 1999 that has been explained by the vibration of a large bubble (radius ~5 m) prior to bursting at a shallow magma-air interface, displays infrasound with dominant frequencies of ~1 Hz [Vergnolle *et al.*, 2004] and very short codas. These frequencies are significantly lower than those expected for bubble oscillation modes (~9 Hz), based on the studies by Vergnolle and Brandeis [1996] and Vergnolle *et al.* [1996], and lower than infrasound recorded at Stromboli (3 Hz; Ripepe *et al.* [1996]). In the case of Stromboli the explosions were recorded at a distance of 150 m

from the vent, and infrasonic and seismic signals share the same spectral content [Ripepe *et al.*, 1996]. In the Shishaldin case the distance between the active vent and the station is much larger (6.62 km vs. 0.15 km at Stromboli); similar to infrasound recorded at Tungurahua volcano (source-station distance ~ 9 km; Johnson *et al.* [2003]), the higher frequency acoustic energy is attenuated during the relative long propagation. In contrast, the large difference in frequency content between the acoustic signals recorded at Shishaldin in 2003–2004 (0.15–1.9 Hz) and in 1999 (1.3–4 Hz) has to be explained by changes in parameters closer to the source and/or by changes in source processes; the acoustic propagation through the atmosphere remains more or less the same. Because the 2003–2004 acoustic signals are already located at a shallow depth within the conduit the significant difference in frequencies cannot be simply explained by a difference in source location (shallower in 1999 vs. deeper in 2003–2004). Instead, we suggest that the condition of the conduit has changed. At times of Strombolian activity in 1999 the vent had just been cleared of solid debris by a Sub-Plinian phase, and was filled with fluid magma. We expect that the conduit has evolved into a more complex system since then. A cooler conduit with rough walls and filled with a mixture of fluid, gas and a small amount of solid volcanic material would be more likely to dampen higher frequency infrasound. However, the degassing explosions at Shishaldin since the eruption in 1999 cannot be explained simply by bubbles bursting at the top of a magma column, especially because there is no evidence for shallow magma in 2003–2004. This suggests that a more complex gas discharge process, such as jetting, takes place.

In this paper we have presented the characteristics of Shishaldin seismo-acoustic signals recorded at a distance of 6.62 km from the active summit vent. The study of seismo-acoustic delay times has reduced the uncertainty in estimating source depths. The infrasound data has allowed us to relate Shishaldin's LP earthquakes to degassing explosions, created by gas volume ruptures from a fluid-air interface located at shallow depth (240 ± 200 m). This depth is confirmed if we assume that resonance of the upper open part of the conduit forms the 0.3 Hz acoustic coda. The gas volume discharge appears to be more complex than the pure bubble bursts associated with the 1999 eruption of Shishaldin; the conduit has changed

to a hydrothermal system with magmatic gases leaking through it, and to being a less open system altered by solid components within the fluid-gas mixture. This realization allows a more complete picture of the dynamics behind Shishaldin's sustained LP activity.

3.6 Acknowledgements

We thank our colleagues at the Alaska Volcano Observatory, notably Silvio De Angelis, for helpful discussions regarding Shishaldin infrasound data, and Jackie Caplan-Auerbach who provided helpful comments that greatly improved the manuscript. We would like to express special thanks to Dan Osborne and Jay Helmericks who provided us with a well calibrated pressure sensor, and to Guy Tytgat for installing the instrument at Shishaldin. We are also grateful to Courtney Kearney for providing us with the SO₂ data, and to Dave Schneider who acquired video images of Shishaldin. We thank Jonathan Lees and an anonymous reviewer for their careful reviews that helped to improve and clarify the manuscript.

References

- Andres, R. J., J. Barquero and W. I. Rose (1992), New measurements of SO₂ flux at Poás Volcano, Costa Rica, *J. Volcanol. Geotherm. Res.*, *49*, 175–177.
- Braun, T. and M. Ripepe (1993), Interaction of seismic and air waves recorded at Stromboli Volcano, *Geoph. Res. Lett.*, *20*, 65–68.
- Caplan-Auerbach, J. and T. Petersen (2005), Repeating coupled earthquakes at Shishaldin Volcano, Alaska, *J. Volcanol. Geotherm. Res.*, *145*, 151–172.
- Caplan-Auerbach, J. and S. R. McNutt (2003), New insights into the 1999 eruption of Shishaldin Volcano, Alaska, based on acoustic data, *Bull. Volcanol.*, *65*, 405–417.
- Dehn, J., K. G. Dean, K. Engle and P. Izbekov (2002), Thermal precursors in satellite images of the 1999 eruption of Shishaldin Volcano, *Bull. Volcanol.*, *64*(8), 525–534.
- Dixon, J. P., S. D. Stihler, J. A. Power, G. Tytgat, S. C. Moran, J. J. Sanchez, S. R. McNutt, S. Estes and J. Paskievitch (2004), Catalog of earthquake hypocenters at Alaskan volcanoes: January 1 through December 31, 2003, *U.S. Geological Survey Open-File Report*, *04-1234*, 69 pp.
- Dixon, J. P., S. D. Stihler, J. A. Power, G. Tytgat, S. Estes, S. C. Moran, J. Paskievitch, J. J. Sanchez and S. R. McNutt (2003), Catalog of earthquake hypocenters at Alaskan volcanoes: January 1, 2002 through December 31, 2002, *U.S. Geological Survey Open-File Report*, *03-0267*, 58 pp.
- Garcés, M. A., M. Iguchi, K. Ishihara, M. Morrissey, Y. Sudo, T. Tsutsui (1999), Infrasonic precursors to a Vulcanian eruption at Sakurajima Volcano, Japan, *Geophys. Res. Lett.*, *26*(16), 2537–2540.
- Garcés, M. A., T. Hagerty and S. Y. Schwartz (1998), Magma acoustics and time-varying melt properties at Arenal Volcano, Costa Rica, *Geophys. Res. Lett.*, *25*(13), 2293–2296.

- Garcs, M. A. and S. R. McNutt (1997), Theory of the airborne sound field generated in a resonant magma conduit, *J. Volcanol. Geotherm. Res.*, *78*, 155–178.
- Geller, R. J. and C. S. Mueller (1980), Four similar earthquakes in central California, *Geophys. Res. Lett.*, *7*(10), 821–824.
- Gresta, S., M. Ripepe, E. Marchetti, S. D'Amico, M. Coltelli, A. J. L. Harris and E. Privitera (2004), Seismoacoustic measurements during the July–August 2001 eruption of Mt. Etna volcano, Italy, *J. Volcanol. Geotherm. Res.*, *137*, 219–230.
- Hagerty, M. T., S. Y. Schwartz, M. A. Garcés and M. Protti (2000), Analysis of seismic and acoustic observations at Arenal Volcano, Costa Rica, 1995–1997, *J. Volcanol. Geotherm. Res.*, *101*, 27–65.
- Ishihara, K. (1985), Dynamical analysis of volcanic explosion, *J. Geodynamics*, *3*, 327–349.
- Jaupart, C. and S. Vergnolle (1989), The generation and collapse of a foam layer at the roof of a basaltic magma chamber, *J. Fluid Mech.*, *203*, 347–380.
- Jaupart, C. and S. Vergnolle (1988), Laboratory models of Hawaiian and Strombolian eruptions, *Nature*, *331*, 58–60.
- Johnson, J. B. (2005), Source location variability and volcanic vent mapping with a small-aperture infrasound array at Stromboli Volcano, Italy, *Bull. Volcanol.*, *67*, 1–14.
- Johnson, J. B., R. C. Aster RC and P. R. Kyle (2004), Volcanic eruptions observed with infrasound, *Geophys. Res. Lett.*, *31*, L14604, doi:10.1029/2004GL020020.
- Johnson, J. B., R. C. Aster, M. C. Ruiz, S. D. Malone, P. J. McChesney, J. M. Lees and P. R. Kyle (2003), Interpretation and utility of infrasonic records from erupting volcanoes, *J. Volcanol. Geotherm. Res.*, *121*, 15–63.
- Johnson, J. B. (2003), Generation and propagation of infrasonic airwaves from volcanic explosions, *J. Volcanol. Geotherm. Res.*, *121*, 1–14.

- Johnson, J. B. and J. M. Lees (2000), Plugs and chugs – seismic and acoustic observations of degassing explosions at Karymsky, Russia and Sangay, Ecuador, *J. Volcanol. Geotherm. Res.*, *101*, 67–82.
- Johnson, J. B., J. M. Lees and E. I. Gordeev (1998), Degassing explosions at Karymsky Volcano, Kamchatka, *Geophys. Res. Lett.*, *25*(21), 3999–4002.
- Kearney, C., J. Dehn and K. G. Dean (2004), Space-based TIR Detection of Volcanic SO₂ in the North Pacific using ASTER and MODIS, *EOS Trans. Am. Geophys. Union*, *85*(47), Fall Meet. Suppl., Abstract V33C–1477.
- Kearney, C. (2005), Detection of Volcanic SO₂ in the North Pacific Region Using ASTER and MODIS, *MS thesis*, University of Alaska Fairbanks, 1–92.
- Kinsler, L. E. and A. R. Frey (1962), *Fundamentals of acoustics*, John Wiley and sons, New York, 2nd edition, 160 pp.
- McGonigle, A. J. S., C. Oppenheimer, A. R. Hayes, B. Galle, M. Edmonds, T. Caltabiano, G. Salerno, M. Burton and T. A. Mather (2003), Sulphur dioxide fluxes from Mount Etna, Vulcano, and Stromboli measured with an automated scanning ultraviolet spectrometer, *J. Geophys. Res.*, *108*(B9), doi:10.1029/2002JB002261.
- McNutt, S. R. and K. H. Jacob (1986), Determination of large-scale velocity structure of the crust and upper mantle in the vicinity of Pavlof volcano, Alaska, *J. Geophys. Res.*, *91*(5), 5013–5022.
- Miller, T. P., R. G. McGimsey, D. H. Richter, J. R. Riehle, C. J. Nye, M. E. Yount and J. A. Dumoulin (1998), Catalog of the historically active volcanoes of Alaska – Shishaldin Volcano, *U.S. Geological Survey Open-File Report*, 98–482, 104 pp.
- Petersen, T., J. Caplan-Auerbach and S. R. McNutt (2006), Sustained long-period seismicity at Shishaldin Volcano, Alaska, *J. Volcanol. Geotherm. Res.*, *151*, 365–381.

- Ripepe, M. and E. Marchetti (2002), Array tracking of infrasonic sources at Stromboli volcano, *Geophys. Res. Lett.*, *29*(22), L2076, doi:10.1029/2002GL015452.
- Ripepe, M., M. Coltelli, E. Privitera, S. Gresta, M. Moretti and D. Piccinini (2001a), Seismic and infrasonic evidences for an impulsive source of the shallow volcanic tremor at Mt. Etna, Italy, *Geophys. Res. Lett.*, *28*(6), 1071–1074.
- Ripepe, M., S. Ciliberto and M. Schiava Della (2001b), Time constraints for modeling source dynamics of volcanic explosions at Stromboli, *J. Geophys. Res.*, *106*(5), 8713–8727.
- Ripepe, M. and E. Gordeev (1999), Gas bubble dynamics model for shallow volcanic tremor at Stromboli, *J. Geophys. Res.*, *104*, 10639–10654.
- Ripepe, M., P. Poggi, T. Braun and E. Gordeev (1996), Infrasonic waves and volcanic tremor at Stromboli, *Geophys. Res. Lett.*, *23*(2), 181–184.
- Ripepe, M. and T. Braun (1994), Air-wave phases in Strombolian explosion-quakes seismograms: a possible indicator for the magma level? *Acta Vulcanol.*, *5*, 201–206.
- Rowe, C. A., R. C. Aster, P. R. Kyle, R. R. Dibble and J. W. Schlue (2000), Seismic and acoustic observations at Mount Erebus Volcano, Ross Island, Antarctica, 1994–1998, *J. Volcanol. Geotherm. Res.*, *101*, 105–128.
- Sparks, R. S. J. (1978), The dynamics of bubble formation and growth in magmas: A review and analysis, *J. Volcanol. Geotherm. Res.*, *3*, 1–37.
- Thomas, N., S. Tait and T. Koyaguchi (1993), Mixing of stratified liquids by the motion of gas bubbles: application to magma mixing, *Earth Planet. Sci. Lett.* *115*, 161–175.
- Thompson, G., S. R. McNutt and G. Tytgat (2002), Three distinct regimes of volcanic tremor associated with the eruption of Shishaldin Volcano, Alaska, *Bull. Volcanol.*, *64*, 535–547.

Vergnolle, S., M. Boichu and J. Caplan-Auerbach (2004), Acoustic measurements of the 1999 basaltic eruption of Shishaldin volcano, Alaska: 1. Origin of Strombolian activity , *J. Volcanol. Geotherm. Res.*, 137(1-3), 109-134.

Vergnolle, S. and G. Brandeis (1996), Strombolian explosions: 1. A large bubble breaking at the surface of a lava column as a source of sound, *J. Geophys. Res.*, 101, 20433-20447.

Vergnolle, S., G. Brandeis and J.-C. Mareschal (1996), Strombolian explosions: 2. Eruption dynamics determined from acoustic measurements, *J. Geophys. Res.*, 101(B9), 20449-20466.

Chapter 4

Swarms of repeating long-period earthquakes at Shishaldin Volcano, Alaska, 2001–2004

4.1 Abstract

During 2001–2004, a series of four periods of elevated long-period seismic activity, each lasting about 1–2 months, occurred at Shishaldin Volcano, Aleutian Islands, Alaska. The time periods are termed swarms of repeating events, reflecting an abundance of earthquakes with highly similar waveforms that indicate stable, non-destructive sources. These swarms are characterized by increased earthquake amplitudes, although the seismicity rate of one event every 0.5–5 minutes has remained more or less constant since Shishaldin last erupted in 1999. A method based on waveform cross-correlation is used to identify highly repetitive events, suggestive of spatially distinct source locations. The waveform analysis shows that several different families of similar events co-exist during a given swarm day, but generally only one large family dominates. A network of hydrothermal fractures may explain the events that do not belong to a dominant repeating event group, i.e. multiple sources at different locations exist next to a dominant source. The dominant waveforms exhibit systematic changes throughout each swarm, but some of these waveforms do reappear over the course of 4 years indicating repeatedly activated source locations. The choked flow model provides a plausible trigger mechanism for the repeating events observed at Shishaldin, explaining the gradual changes in waveforms over time by changes in pressure gradient across a constriction within the uppermost part of the conduit. The sustained generation of Shishaldin's long-period events may be attributed to complex dynamics of a multi-fractured hydrothermal system: the pressure gradient within the main conduit may be regulated by temporarily sealing and reopening of parallel flow pathways, by the amount of debris within the main conduit and/or by changing gas influx into the hydrothermal system. The observations suggest that Shishaldin's swarms of repeating events represent time periods during which a dominant source is activated.

4.2 Introduction

Low-frequency earthquakes associated with volcanic activity have been widely observed and are frequently associated with volcanic unrest and eruptions [Chouet, 1996]. Low-frequency events can be classified into two event types according to the frequency content of their onsets: *long-period* (LP) events and *hybrid* events. The waveforms of LP events are characterized by emergent onsets and a low frequency content of 0.2–5 Hz with one or more sharply defined spectral peaks between 0.5 and 2.0 Hz followed by a superposition of simple decaying sinusoids. Hybrid events are very similar to LP events but are characterized by an additional high-frequency (> 5 Hz) component in their sometimes impulsive onsets [Neuberg *et al.*, 2000]; the amount of high frequency energy reaching the seismic instruments is highly dependent on the effects of attenuation. Initial definitions of hybrid events require a variety of first motions resulting from brittle failure [Lahr *et al.*, 1994]. However, Neuberg *et al.* [2000] suggest that hybrid and LP events are part of a continuum of seismic waves that share common source processes but differ in the amount of high-frequency energy attenuated within their travel path.

A number of different theoretical models have been proposed for the generation of LP waveforms at volcanoes, mostly focused on the idea that the low frequency energy is a manifestation of pressure-induced vibrations of fluid-filled resonators in magmatic and hydrothermal systems [Chouet, 1996]. The low-frequency waveforms are generated by the radiation of energy trapped along the boundary of a fluid-filled container embedded in an elastic solid [Chouet, 1988; Neuberg *et al.*, 2000]. Various crack and conduit geometries have been proposed for the sources of LP events (e.g. Chouet [1996]; Neuberg *et al.* [2000]). In order to create LP earthquakes an initial release of seismic energy is required within or close to the resonating body, such that energy can be trapped at the fluid-solid interface by the impedance contrast between the fluid and the surrounding solid (e.g., Chouet [1988]). The mechanism that triggers the oscillation of the conduit walls may be provided by pressure transients induced by the flux of hot volcanic gases from depth (e.g., Chouet *et al.* [1994]). Alternative trigger mechanisms include small phreato-magmatic explosions at depth that

result from magma-water interactions [Wohletz, 1986, 2002; Buttner and Zimanowski, 1998]; a mechanism analogous to a pressure-cooker in which gas periodically escapes through fractures in a solid plug [Johnson and Lees, 2000]; magma flow instabilities caused by conduit constrictions [Julian, 1994; Morrissey and Chouet, 1997]; the sudden coalescence of foam into a single gas slug [Jaupart and Vergnolle, 1988, 1989]; the oscillation of a gas slug at the top of the fluid prior to bursting [Vergnolle and Brandeis, 1994, 1996; Gil Cruz and Chouet, 1997; Vergnolle et al., 2004]; and turbulent flow conditions that regularly form behind an obstacle, inducing conduit vibration [Hellweg, 2000].

Low-frequency events often occur in swarms, with typical durations of hours to months [Benoit and McNutt, 1996]. At Redoubt Volcano, for example, the LP swarm that directly preceded the 1989–1990 eruption lasted 23 hours at a rate of about one event every 20 s [Power et al., 1994]. A high degree of similarity between low-frequency waveforms within swarms has been observed at many volcanoes (e.g., Mt. Redoubt [Stephens and Chouet, 2001]; Unzen [Umakoshi et al., 2003]; Soufrière Hills [White et al., 1998]; Shishaldin [Petersen et al., 2006]). These *repeating events* or *multiplets* represent seismic waves that have similar source processes and travel along an identical path to the seismometer indicating a common event source location. At Soufrière Hills Volcano multiplets that correlate with observed tilt signals associated with dome deformation cycles were observed indicating the pressurization and depressurization of the volcanic system [Neuberg et al., 2006]. Neuberg et al. [2006] suggest that these events are the consequence of brittle failure of melt that activates resonators within the upper conduit. Mount St. Helens exhibited highly repetitive low-frequency events, termed *drumbeats*, which accompanied a lava-dome-building eruption; the events occur in about 30-s intervals and are thought to be caused by stick-slip motion between the upward moving dome and the surrounding rocks (e.g., Malone et al. [2005]; [W. Thelen, written communication, 2006]). At Mt. Augustine a swarm of low-frequency multiplets that lasted ~90 minutes accompanied eruptive activity on January 12, 2006 [M. Gardine, written communication, 2006]. Mt. Erebus has exhibited repeating low-frequency events produced by impulsive explosions of large gas bubbles from the surface of a long-lived,

actively convecting lava lake (e.g., *Grêt et al.* [2005]). At Mt. Redoubt, a slow evolution of repeating LP waveforms occurred within an 18-hour swarm preceding a major eruption, suggesting a migrating or physically changing source [*Stephens and Chouet*, 2001]. Similar evolving waveforms were also observed at Mt. Unzen over a time period of 2 months of active dome growth [*Umakoshi et al.*, 2003]. *Arciniaga et al.* [2005] observed repetitive LP events at Popocatepetl exhibiting changes in waveforms that correlate with changes in eruptive activity from degassing to lava dome formation.

Repeating events often can be classified into waveform families or groups. *Green and Neuberg* [2006] analyzed a 6-day period of multiplets recorded at Soufrière Hills Volcano, Montserrat, and observed nine families containing more than 45 events each by comparing 8-s sections of low-frequency events and using a correlation threshold of $\psi \geq 0.7$. *Stephens and Chouet* [2001] found that the majority of LP events for an 18-hour swarm at Redoubt Volcano, Alaska, belonged to one waveform family ($\psi \geq 0.68$ for 10-s waveform sections). *Umakoshi et al.* [2003] classified high-frequency earthquakes recorded at Unzen Volcano, Japan, into over 70 families ($\psi \geq 0.9$ for a 5.5-s correlation window; [*K. Umakoshi, written communication*, 2006]) with more than 100 events each over a time period of 2 months.

Repeating waveforms in general also have been observed for earthquakes that are not associated with volcanic activity. Repeating tectonic earthquakes at plate boundaries, such as the Northeastern Japan subduction zone boundary [*Igarashi et al.*, 2003] and the San Andreas Fault [*Nadeau and Johnson*, 1998] are caused by slip of small asperities surrounded by stable sliding areas on the plate boundary. Although these similar waveforms are generated by repetitive source processes they occur in significantly smaller rates and numbers than repeating low-frequency events observed at volcanoes; e.g., *Igarashi et al.* [2003] identified about 800 repeating earthquakes recorded over a time period of 8 years.

In this study, I investigate the nature of highly repetitive LP earthquakes recorded during several periods of elevated seismic activity at Shishaldin Volcano, Aleutian Arc, Alaska. The time periods during which these repeating events are abundant are characterized by an increase in earthquake amplitudes. These time periods are referred to in this study as

swarms of repeating events, or simply *swarms*. A series of four swarms occurred during 2001–2004 (Figure 4.1; *Swarms A, B, C and D*). Each of these swarms lasted about 1–2 months. Shishaldin exhibits seismicity rates that peaked at several thousands of LP events per day recorded at a distance of ~ 6 km from their source located beneath the summit vent [Petersen *et al.*, 2006]. The seismicity during the time between the individual swarms is characterized by LP events with decreased amplitudes, compared to the swarms. The event rate of one event every 0.5–5 minutes has remained more or less constant between a few months after it last erupted in 1999 and May 2004 [Petersen *et al.*, 2006] and then again from December 2004 until August 2006 [AVO unpublished data]. Although swarms of LP earthquakes elsewhere are commonly seen as indicators of volcanic unrest and often precede and/or accompany eruptive activity [Lahr *et al.*, 1994; Chouet, 1996], at Shishaldin no eruption has occurred since 1999 and the volcano appears to be in a steady state mode of seismic energy release [Petersen *et al.*, 2006].

This study reports a type of volcanic behavior less commonly observed and discusses the implications of Shishaldin's swarms of LP events that exhibit highly similar waveforms. The prolonged nature of Shishaldin's seismic activity and the observations of repeating low-frequency events at other volcanoes provide motivation for analyzing Shishaldin repeating LP events. Do several dominant waveforms that represent different sources co-exist during swarms, e.g. as observed at Soufrière Hills Volcano [Green and Neuberg, 2006]? Or is only one source process dominant at a time, e.g. as observed at Mt. Redoubt [Stephens and Chouet, 2001]? Does a dominant waveform gradually change over time within a swarm, e.g. the waveforms analyzed at Mt. Unzen [Umakoshi *et al.*, 2003], or does it abruptly stop, e.g. like the families of multiplets at Soufrière Hills Volcano [Green and Neuberg, 2006]? I apply waveform cross-correlation methods to identify systematic changes of dominant waveforms within the swarms, and use these changes to quantify the driving force behind the generation of Shishaldin LP seismicity.

4.3 Methodology

4.3.1 Data selection

The main challenge in analyzing Shishaldin's LP events is the large number of events that occurred every day for a time period of many years [Petersen *et al.*, 2006]. The first step in approaching the problem of using such a large data set is to focus on certain time periods. Because swarms of LP events observed at many other volcanoes are often associated with eruptive activity, the periods of elevated seismicity at Shishaldin may be of special interest. Also the Shishaldin swarms are characterized by an abundance of large amplitude events; hence they provide data with good signal-to-noise ratios. Figure 4.1 shows the daily number

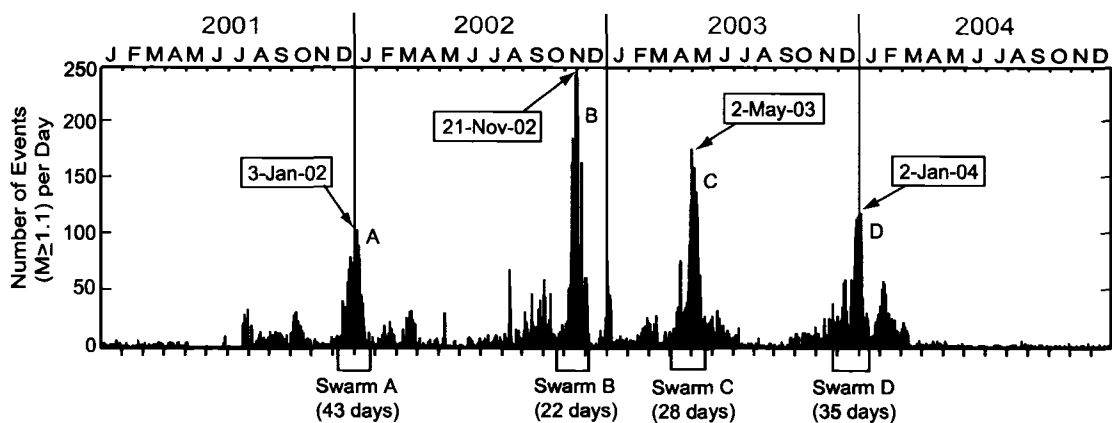


Figure 4.1. Daily number of earthquakes with magnitudes $M \geq 1.1$, termed *pseudohelicorder counts* (see text), recorded from January 2001 through December 2004. Four main periods of increased seismicity (A, B, C and D) occurred during those 4 years of sustained seismic activity. The interval between tick marks on the time axis (top) represents one month. The time periods analyzed in this chapter and the days used as representatives for each swarm are indicated. A swarm is defined by a gradual increase in number of events included in the counts, which leads up to a $\geq 100\%$ increase from background level (about one event with $M \geq 1.1$ per day). Note that the vast majority of Shishaldin LP events are too small to be included in the pseudohelicorder counts.

of events that are included in a counting method, introduced by Petersen *et al.* [2006] as *pseudohelicorder counts* or simply *counts*, which uses an amplitude threshold value that is equivalent to a magnitude $M = 1.1$. It is important to note that the counts only include

large earthquakes and that the vast majority of Shishaldin's LP events have magnitudes < 1.0 , which are neglected by this counting method. However, for this study the counts provide an adequate way to select swarm periods (Figure 4.1). Each swarm exhibits a gradual increase in number of events included in the counts, lasting up to one month. A swarm reaches peak values in the counts for a few days, followed by a more rapid decrease in the number of large ($M \geq 1.1$) events. In order to investigate patterns and systematic changes in the thousands of low-frequency earthquakes that occur within each swarm, it is necessary to classify such events into smaller and more manageable groups. A method based on waveform cross-correlation is used to identify highly similar events.

The seismic data that are analyzed were recorded at station SSLN with a sampling frequency of 100 Hz. SSLN is part of a 6-station short-period monitoring network operated by AVO that is distributed around Shishaldin's summit at distances between 5.3 and 19 km. Station SSLN has a vertical component L-4C instrument with 1 Hz natural frequency located at a horizontal distance of 6.3 km from Shishaldin's summit vent. The station provides the best quality continuous data in the Shishaldin seismic network; the other stations are generally noisy because of local site conditions and/or larger distances from the source region, which is located at shallow depth beneath the summit [Caplan-Auerbach and Petersen, 2005; Petersen *et al.*, 2006].

4.3.2 Event extraction

The input catalog for the waveform analysis was established by using a short-term-average to long-term-average (STA/LTA) algorithm, adopted from Hawthorne and West [2005], to extract events from continuous seismic data recorded at station SSLN. The program performs a Hilbert transform on the raw input data to create an envelope and computes STA and LTA values using window lengths of 0.8 s and 7 s, respectively, and a STA/LTA ratio of 2.5 is required for event triggering. These values were empirically chosen by Hawthorne and West [2005] as default parameters accounting for data from several volcanoes monitored by the Alaska Volcano Observatory (AVO). In this study, the threshold $\text{STA/LTA} > 2.5$

is sufficient for extracting events from data with higher noise levels, but causes a large number of low amplitude waveforms to be selected during times of low background noise. In order to create a more uniform dataset, a peak amplitude threshold that is approximately equivalent to a signal-to-noise (S/N) ratio > 3 for low noise data was used as an additional event selection criterion. The events selected are referred to as *extracted events*. Each extracted event is 20 s long including the entire LP waveform. The number of extracted events per day during swarms reaches values of up to 2200.

4.3.3 Event classification

The similarities between the extracted events can be quantified by using waveform cross-correlation. Because of the huge dimensions of the data set the extracted events are reduced to more manageable groups by applying cross-correlation to only one day at a time. Within these daily data sets each event is cross-correlated with all other events. The data are not pre-filtered in order to preserve the original waveforms. The entire waveform of the 20-s long extracted events is cross-correlated, but the maximum correlation coefficient is calculated using only an empirically selected 8-s window surrounding the highest amplitude part of the LP waveform to avoid interference with adjacent events. For each day, a maximum correlation coefficient matrix, termed *similarity matrix*, is created indicating the degree of waveform similarities between events (Figure 4.2). Theoretically, identical waveforms result in a maximum correlation coefficient of 1; two time-series with no correlation produce a coefficient of 0.

Now that a similarity matrix is created a classification scheme is required to isolate the events that exhibit highly repetitive waveforms. First, a master event representing the waveform that is dominant during a given day is selected. In order to perform this in a systematic way, the mean correlation value of the calculated maximum correlation coefficients is determined for each event within a matrix (i.e. the mean of the values within a row is calculated for all rows). The event with the highest mean correlation value is selected as *master event*. A scheme based on event size was also tried, but was rejected due

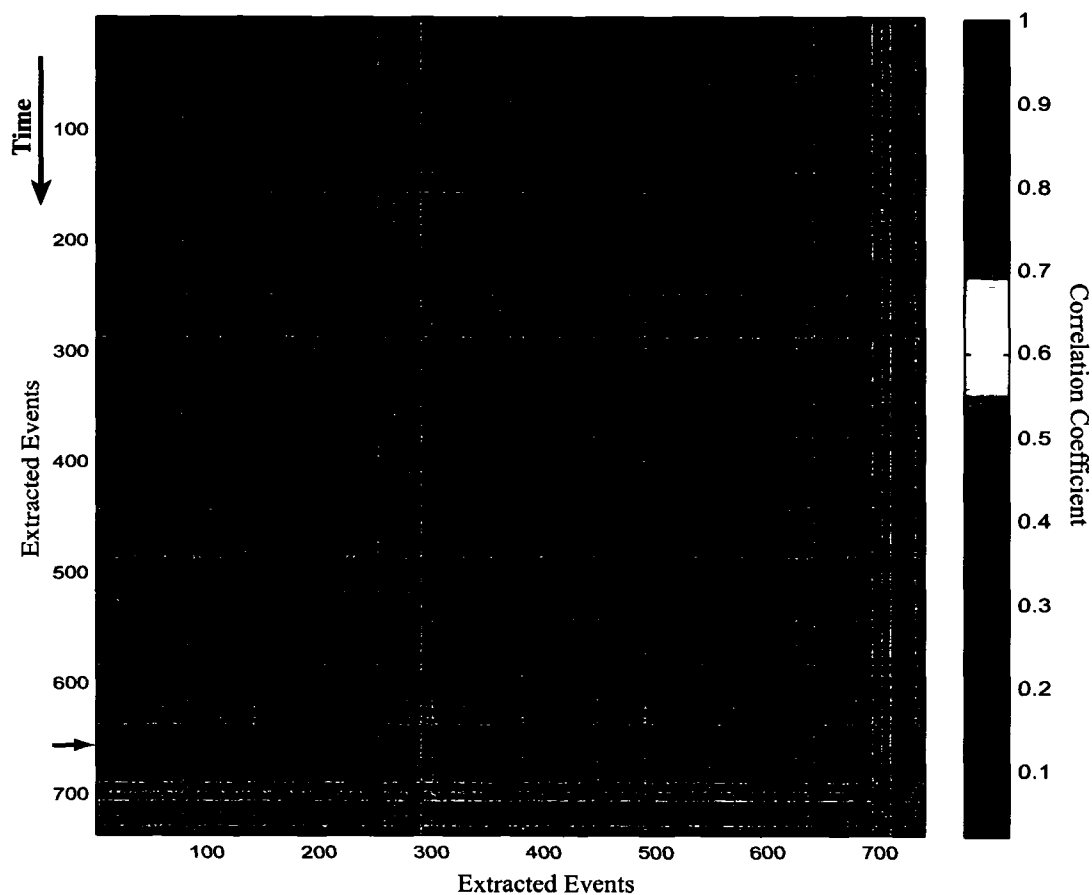


Figure 4.2. Similarity matrix of 738 extracted events recorded at station SSLN on January 3, 2002. The extracted events represent 60% of all events with $S/N \geq 2$ (1237 events; manually selected). The events are more or less evenly distributed across the whole day. Values on the diagonal represent the auto-correlation between an event and itself; points close to the diagonal represent events that occur closely spaced in time; points further away from the diagonal are separated by longer time periods. The mean correlation value calculated for the entire matrix is 0.75 indicating that all events are very similar to each other. The master event is indicated by a red arrow.

to ambiguous results. However, now that we have a master event (Figure 4.3) a threshold correlation coefficient value, ψ , is required to classify the extracted events into a family of events that are highly similar to this master event. A value of $\psi \geq 0.9$ would provide almost identical waveforms; in order to be tolerant towards events with poor signal-to-noise ratios

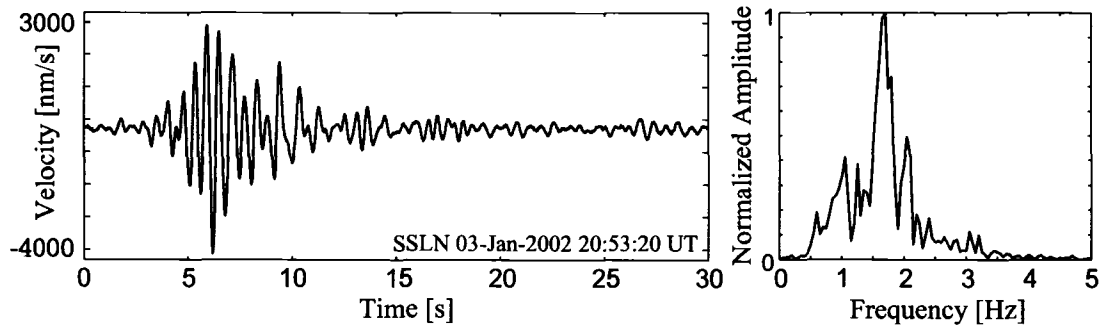


Figure 4.3. Example for a master event and the corresponding normalized power spectrum. The event was recorded at station SSLN at 20:53:20 UT, January 3, 2002 has a mean correlation value of 0.85 with all other events extracted during that day. The seismic trace is unfiltered. The dominant spectral peak is at ~ 1.6 Hz.

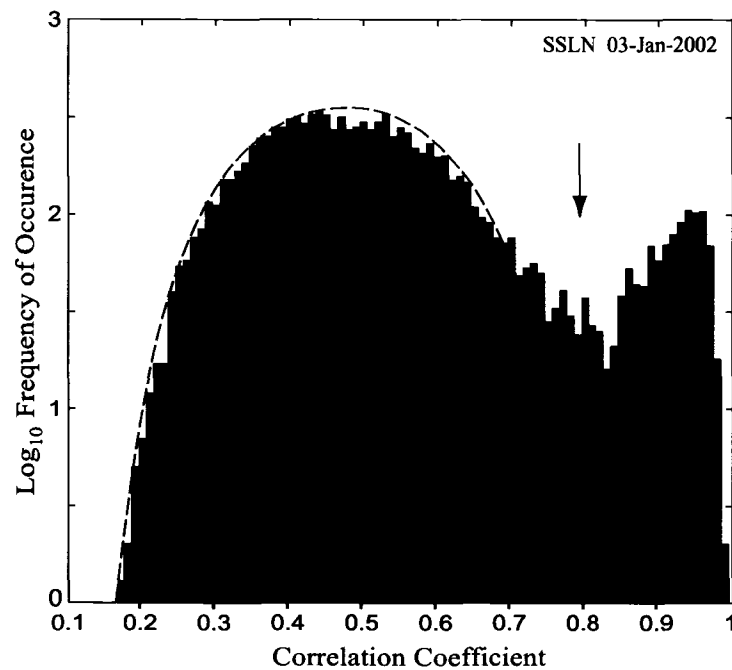


Figure 4.4. Histogram of correlation coefficients for the January 3, 2002 master event with all other events extracted that day. *Repeating events* are defined as events that have cross-correlation values above those expected from the normally distributed curve. The chosen threshold correlation coefficient is $\psi \geq 0.8$.

a threshold value of $\psi \geq 0.8$ was chosen instead. The events with a correlation coefficient > 0.8 with respect to the master event are selected as *repeating events* representing the dominant waveform family of the day. The distribution of coefficients resulting from cross-correlating the master event with all other events recorded that day justifies the chosen selection criterion (Figure 4.4): the repeating events have cross-correlation values above the normally distributed curve that would be expected for the random correlations between signals and noise [Green and Neuberg, 2006].

In order to test whether or not the waveform similarity is due to site effects specific for station SSLN, the waveforms recorded at other stations that correspond to the selected repeating events are cross-correlated using the same parameters as for SSLN (20-s correlation window; coefficients calculated within 8-s window). Figure 4.5 shows the similarity matrix

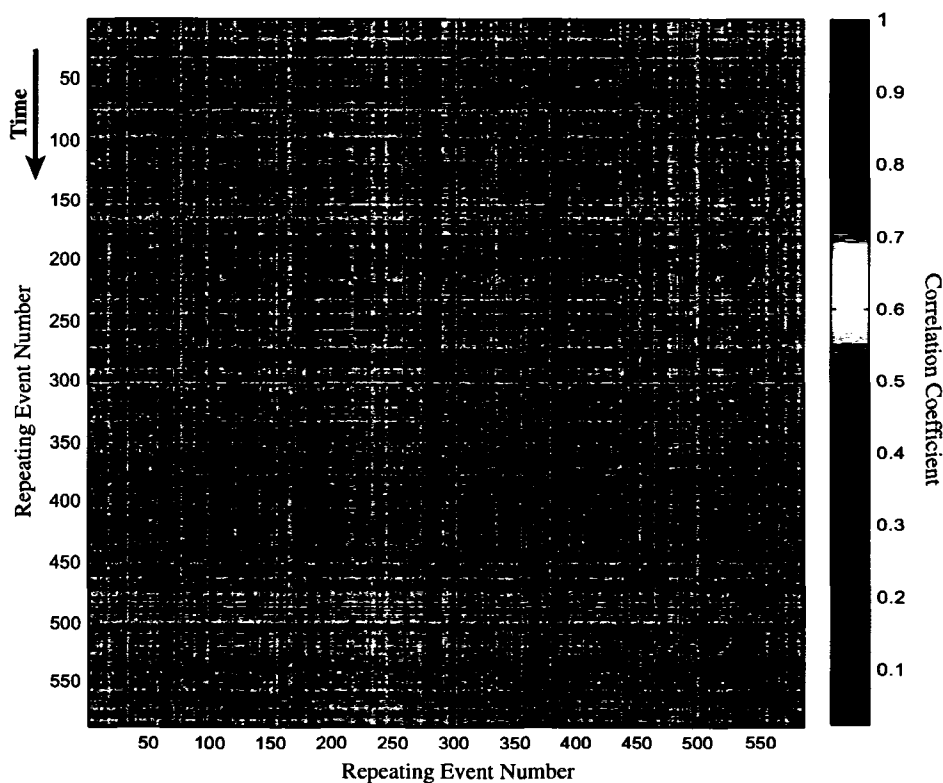


Figure 4.5. Similarity matrix of the repeating events selected on January 3, 2002 recorded on station SSLW. The matrix has a mean correlation value of 0.7.

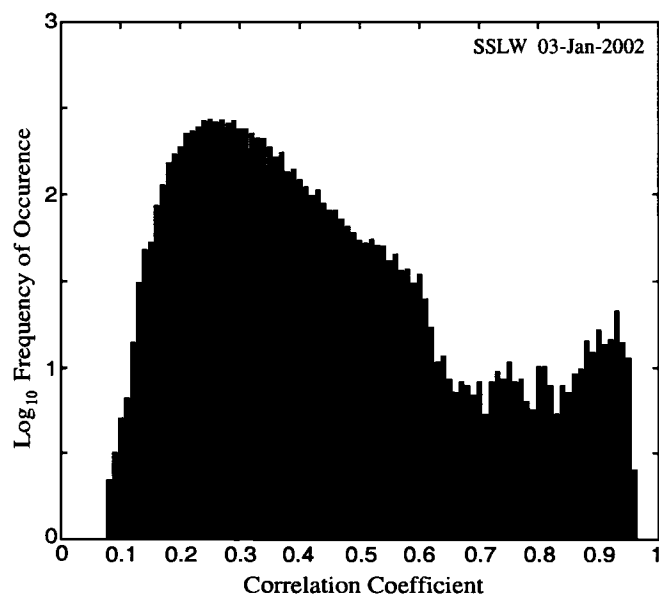


Figure 4.6. Histogram of correlation coefficients for events recorded on January 3, 2002 at station SSLW. The distribution of coefficients results from cross-correlating all events with the master event selected for this station. The threshold correlation coefficient, ψ , is around 0.7.

for station SSLW that is located at about 10 km west of the summit and exhibits a lower signal-to-noise ratio than SSLN; the mean correlation value calculated for the entire matrix is 0.70. Because waveform similarity depends not only on the source similarity but also on attenuation between the source and the station and signal-to-noise ratio, this lower value would be expected for station SSLW as indicated by the distribution of coefficients shown in Figure 4.6. Although events recorded at this station have smaller amplitudes and are affected by a higher noise level they still exhibit a relatively high degree of similarity.

The correlation function only measures the similarity of the waveform shape and not the amplitudes of the events. Thus, the amplitudes may vary for events with similar waveforms, i.e. the events traveled along a nearly identical path, but were not necessarily produced by a source with a constant strength. Figure 4.7 displays an example for the distribution of maximum amplitudes typical for Shishaldin's repeating events. The largest amplitude that can be measured is 4000 nm/s; amplitudes above this value are clipped. The abundance of

amplitudes equal to 4000 nm/s is generally higher around swarm peak times, but overall the amplitudes of repeating events are more or less evenly distributed between this value and the threshold of 1000 nm/s provided by the $S/N > 3$ criterion. This means that the repeating events appear in all sizes.

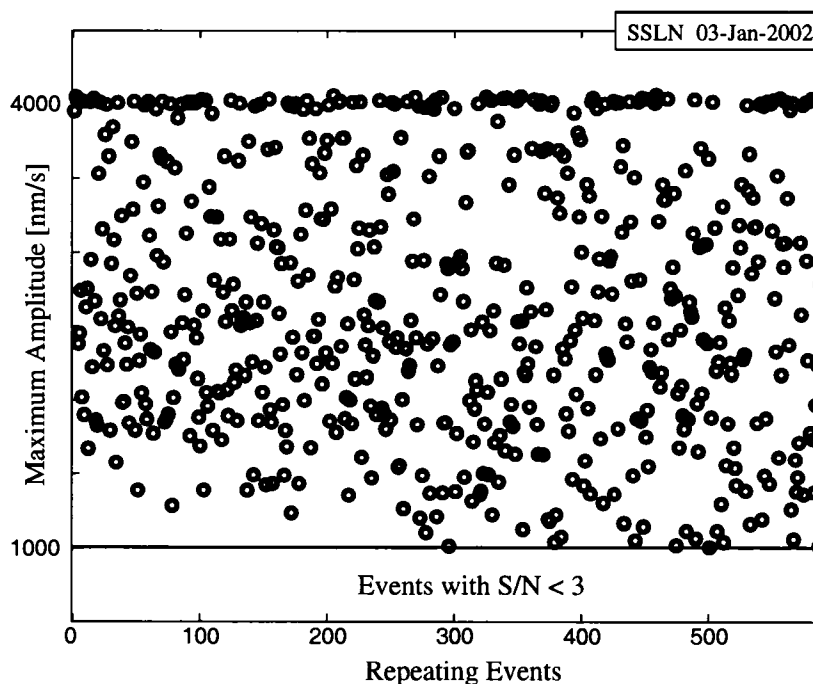


Figure 4.7. Distribution of maximum amplitudes of repeating events recorded at station SSLN on January 3, 2002. Events with amplitudes < 1000 nm/s were removed during the event extraction by the $S/N > 3$ criterion. The remaining amplitudes are more or less evenly distributed, i.e. repeating events come in all sizes. Note that the apparent cluster at 4000 nm/s is due to clipping of waveforms such that this value actually represents all events of 4000 nm/s and above.

4.3.4 Family detection

The high number of LP events recorded at Shishaldin every day over time periods of many years makes a detailed family classification rather challenging. In order to test whether or not only one large waveform family exists on a given day during swarm periods, a day with a good signal-to-noise ratio and a large number of higher-amplitude events was selected for

each swarm (Figure 4.1). All the previously classified repeating events, i.e. events that are well correlated ($\psi \geq 0.8$) with the master event are removed from the similarity matrix as the family dominant that day (*family 1*). The remaining events are cross-correlated and the second dominant family (*family 2*) is determined following the same procedure and using the same correlation threshold. The results are shown in Table 4.1. For example, on

Table 4.1. Family classification for representative days within each swarm. The table shows the percent of all extracted events that fall within a given family.

Swarm	Day	Number of Extracted Events	Family 1	Family 2
A	03-Jan-2002	738	80%	< 1%
B	21-Nov-2002	731	58%	< 5%
C	02-May-2003	1623	31%	6%
D	02-Jan-2004	1742	43%	1%

3-Jan-2002 (Swarm A) family 1 accounts for 80% of the extracted data and only < 1% of the total number of events used belong to family 2. The events that do not belong to family 1 or family 2 are classified into a large number of even smaller families. This suggests that at any given day during swarms several different families of similar events co-exist but that generally only one large family dominates. The days in between swarms exhibit a continuum of different LP events rather than being dominated by a certain waveform; these events may be interpreted as signals originating from different non-stationary sources. This lack of large dominant families may also be due to the generally smaller event sizes in between swarms, so that the S/N ratio is too poor for a positive classification to be made.

In order to investigate how the dominant waveforms evolve throughout each swarm the repeating events are lined up with the master event to create a *daily stack* that represents an average waveform dominant on a specific day (Figure 4.8). The results are presented in the following section.

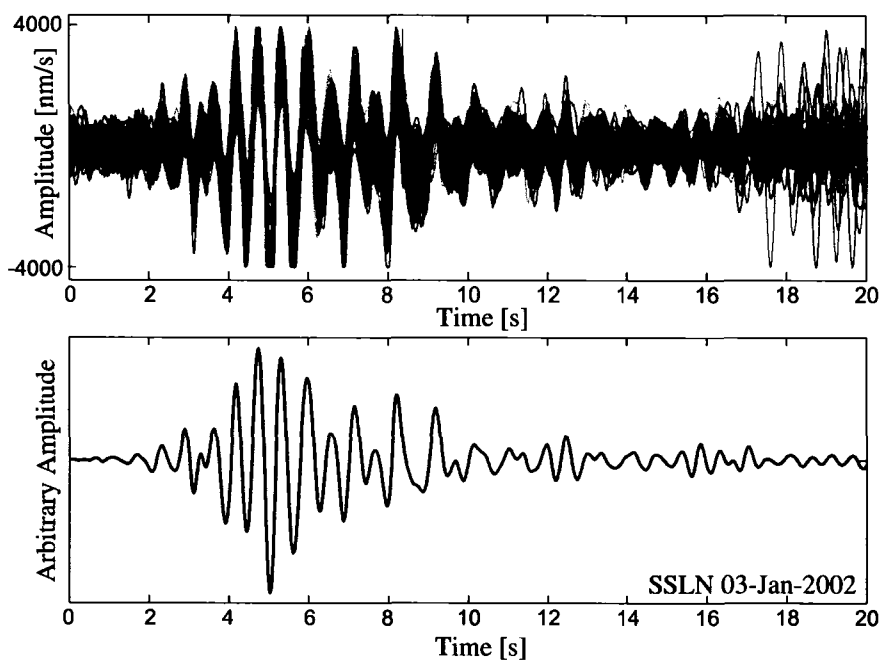


Figure 4.8. Overlay of the 588 repeating events recorded on January 3, 2002 (top) and the corresponding daily stack (bottom).

4.4 Results

Daily stacks were created for each of the four swarms (Figures 4.9, 4.12, 4.16 and 4.18); days with a high noise level were excluded from the analysis. A total number of 106,097 events were extracted of which 31,310 events are included in the 97 daily stacks, i.e. 30% of the extracted events are grouped into repeating events (Swarm A: 45% are repeating events; Swarm B: 44% are repeating events; Swarm C: 19% are repeating events; Swarm D: 25% are repeating events). The days with the largest number of high amplitude events within each swarm were chosen as the representative days (Figure 4.1).

Swarm A exhibits a dominant waveform that is stable over a time period of 30 days (14-Dec-2001 until 12-Jan-2002) and then evolves over the course of a few days into a slightly different waveform that dominates until the swarm activity ends (Figures 4.9 and 4.10). This second waveform group has a longer-period component that is particularly pronounced within the coda. Figure 4.11 displays the spectral amplitudes for each waveform stack.

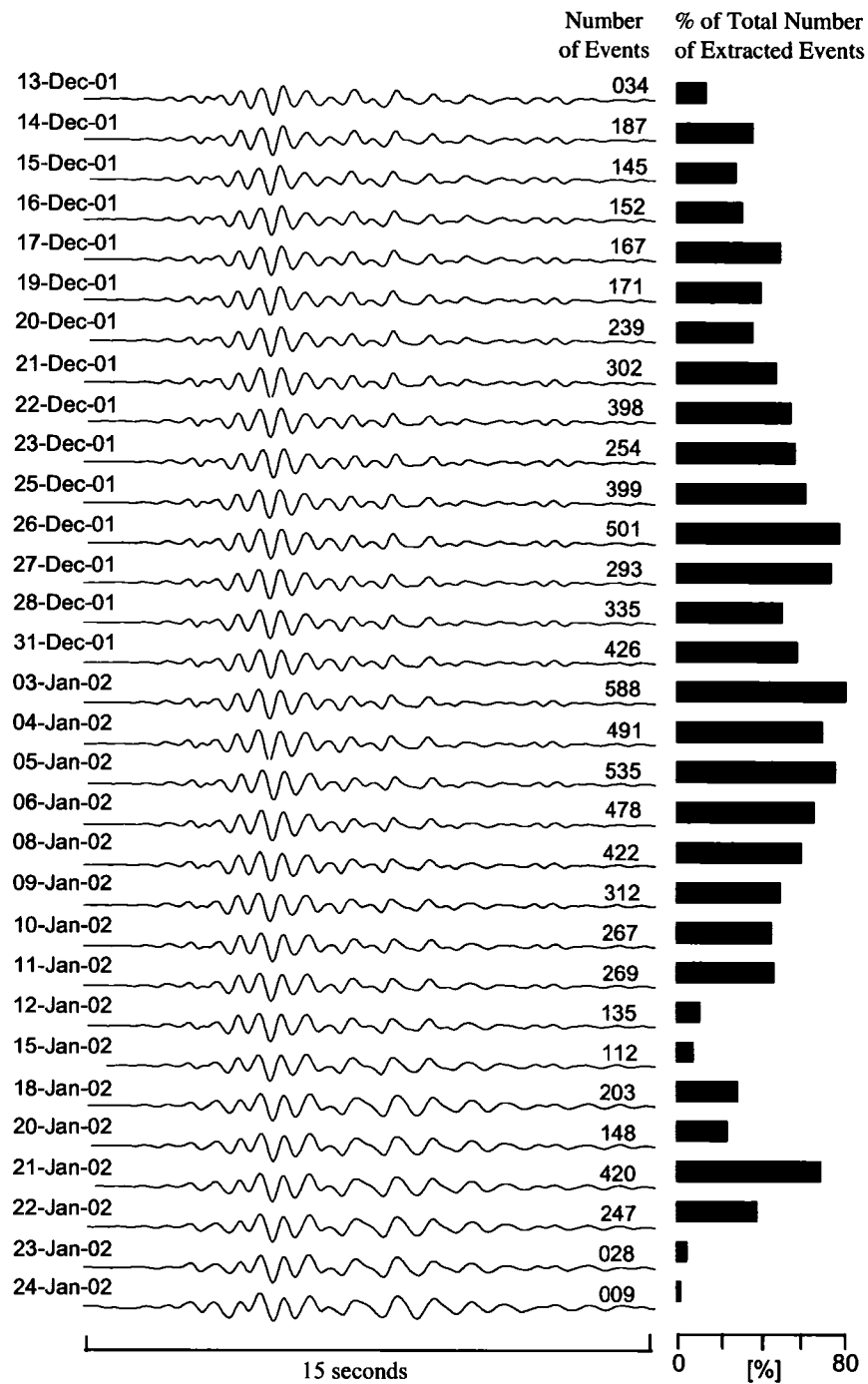


Figure 4.9. Daily stacks for Swarm A. The number of events included in the stacks ranges from 9–588. The percentages of events that were selected as repeating events from the total number of extracted events are indicated by bars. Eighty percent of the events extracted on January 3, 2002 are repeating events.

Although the waveforms exhibit common spectral peaks throughout the entire swarm, the waveform change is accompanied by a shift in energy partitioning towards lower frequencies. This pattern is representative for Swarms A, B and C; Swarm D exhibits a reversed pattern.

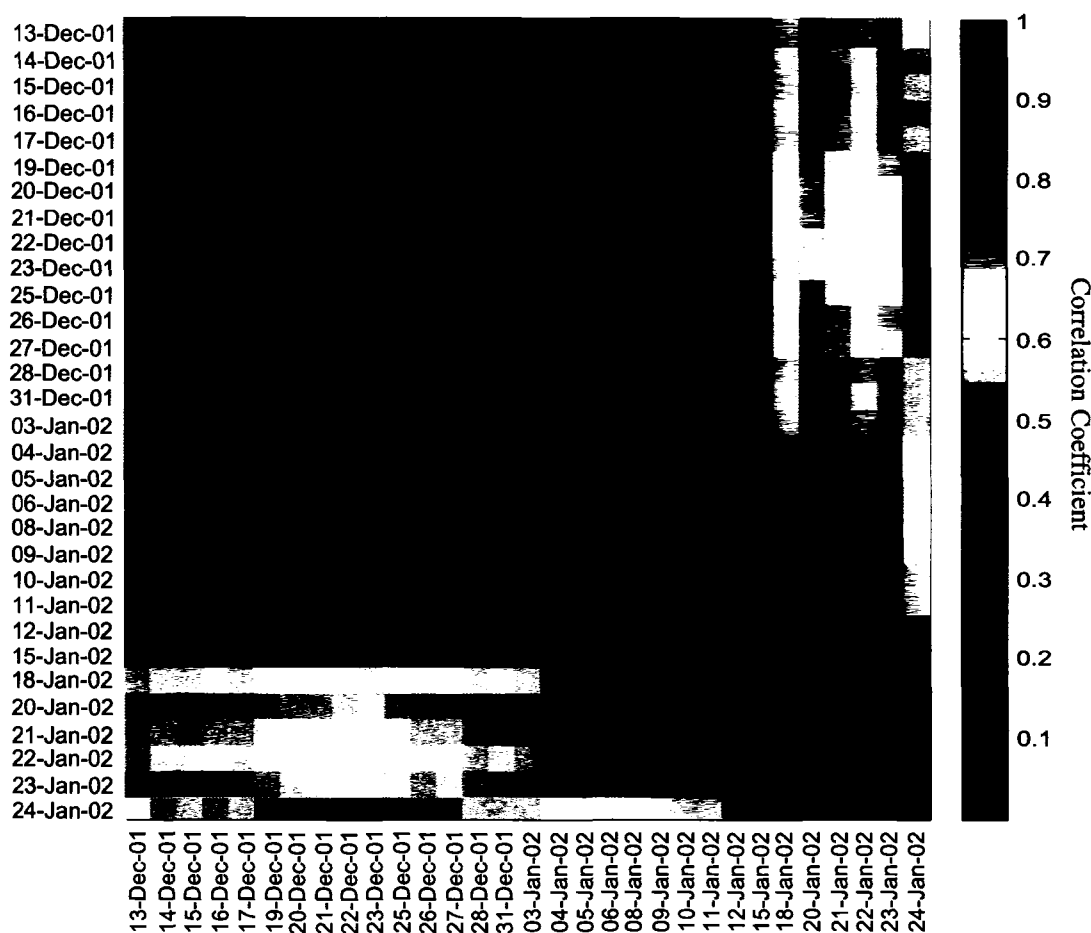


Figure 4.10. Similarity matrix for Swarm A daily stacks. The diagonal represents the auto-correlation.

During Swarm B the initial dominant waveform remains stable for 13 days until it gets replaced by a variety of relatively small families during the last 9 days of the swarm (Figures 4.12 and 4.13). Figure 4.14 shows the similarity matrix for 21-Nov-2002, the day on which the initial waveform stops being dominant. The matrix shows that the waveform

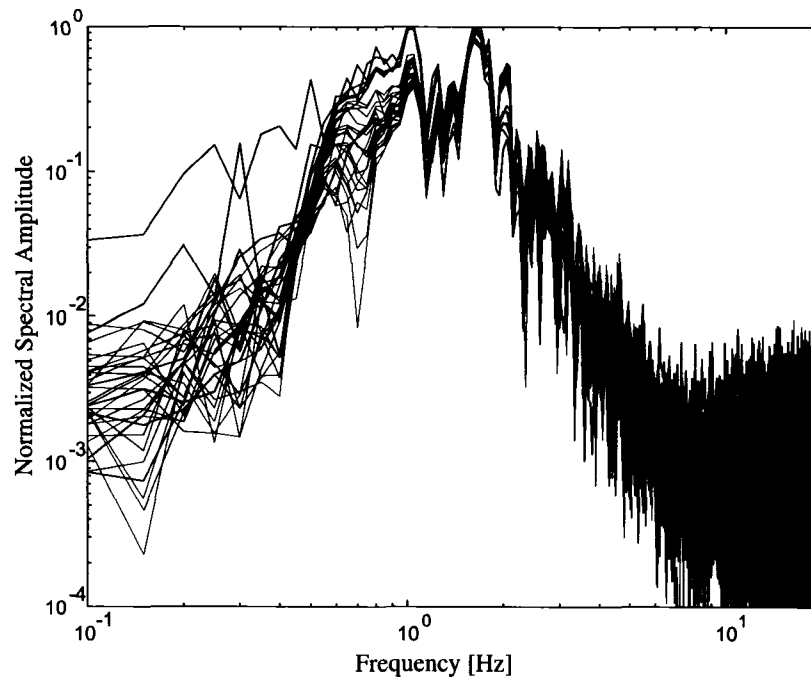


Figure 4.11. Spectral amplitudes for Swarm A daily stacks. The first group (13-Dec-2001 until 15-Jan-2002; red) exhibits maximum spectral amplitudes at 1.6 Hz and the second group (18-Jan-2002 until 24-Jan-2002; black) at 1.0 and 1.6 Hz.

similarity stops abruptly (within one minute) at about 13:24 UT with no other major family of repeating events taking its place. The last event that belongs to the dominant repeating event family was recorded at 13:07 UT; hence the transition occurred over a time period of about 17 minutes. The seismic amplitudes abruptly decreased at the same time after they had increased over the course of several days prior to the transition on November 21, 2002 (Figure 4.15). A search for the initial dominant waveform using cross-correlation of the master event with the events extracted on the following days reveals that the initial dominant waveform completely disappeared.

The initial dominant waveform in Swarm C remains stable for 17 days until it slowly, over the course of 5 days, is replaced by a different dominant waveform family (Figures 4.16 and 4.17). Swarm D exhibits the opposite pattern in which the initial dominant waveform

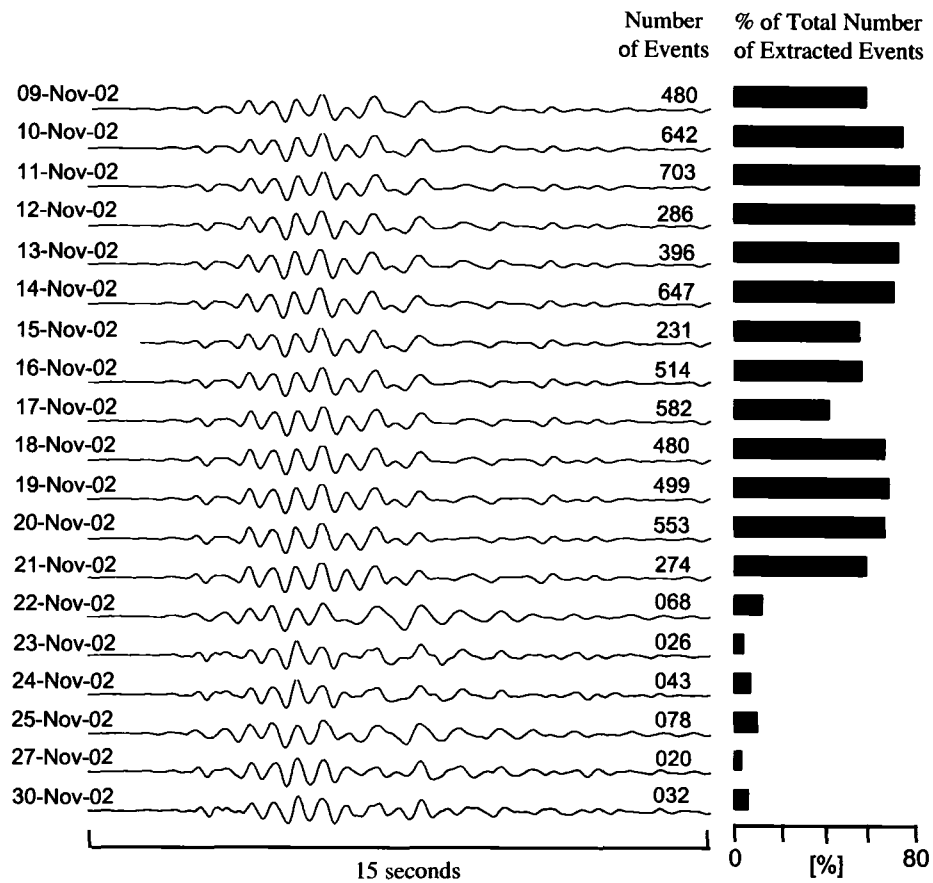


Figure 4.12. Daily stacks for Swarm B. Each stack is composed of 20 to 703 events. The bars indicate the percentage of events that were selected as repeating events from the total number of extracted events.

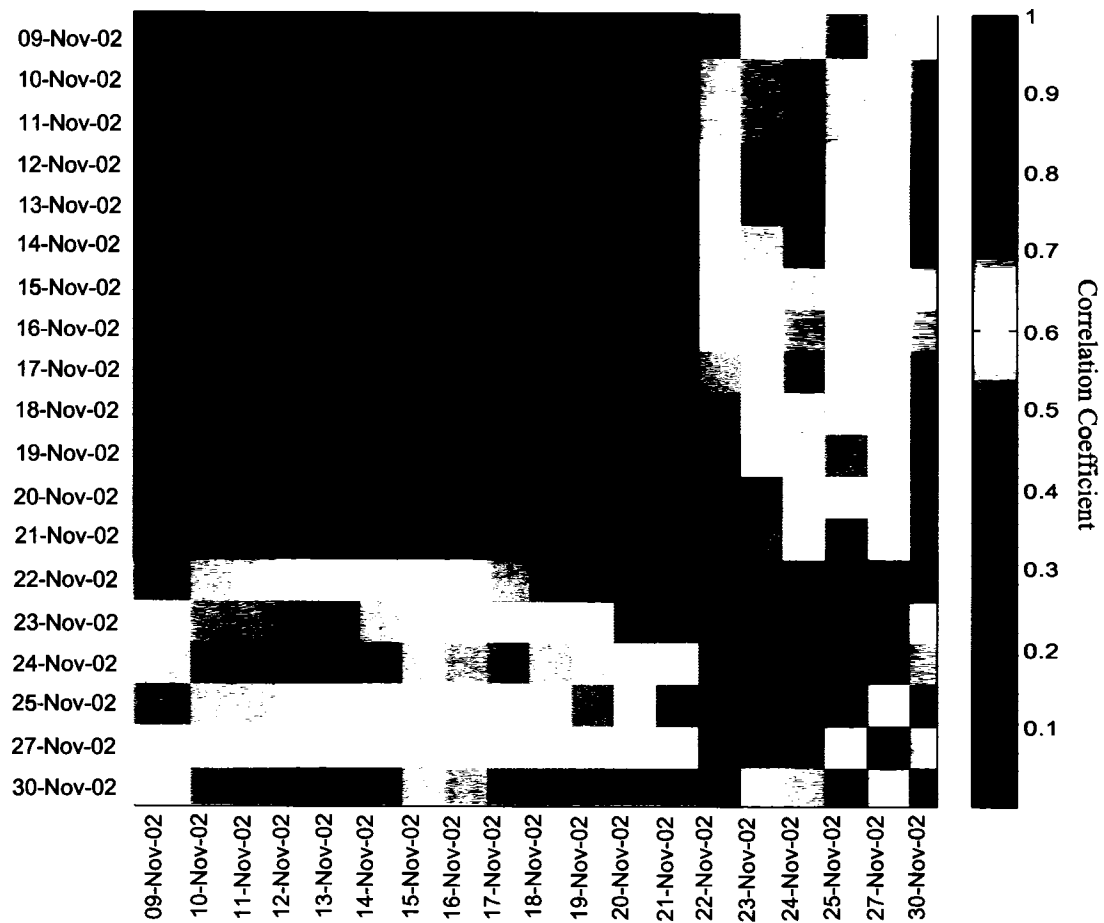


Figure 4.13. Similarity matrix for Swarm B.

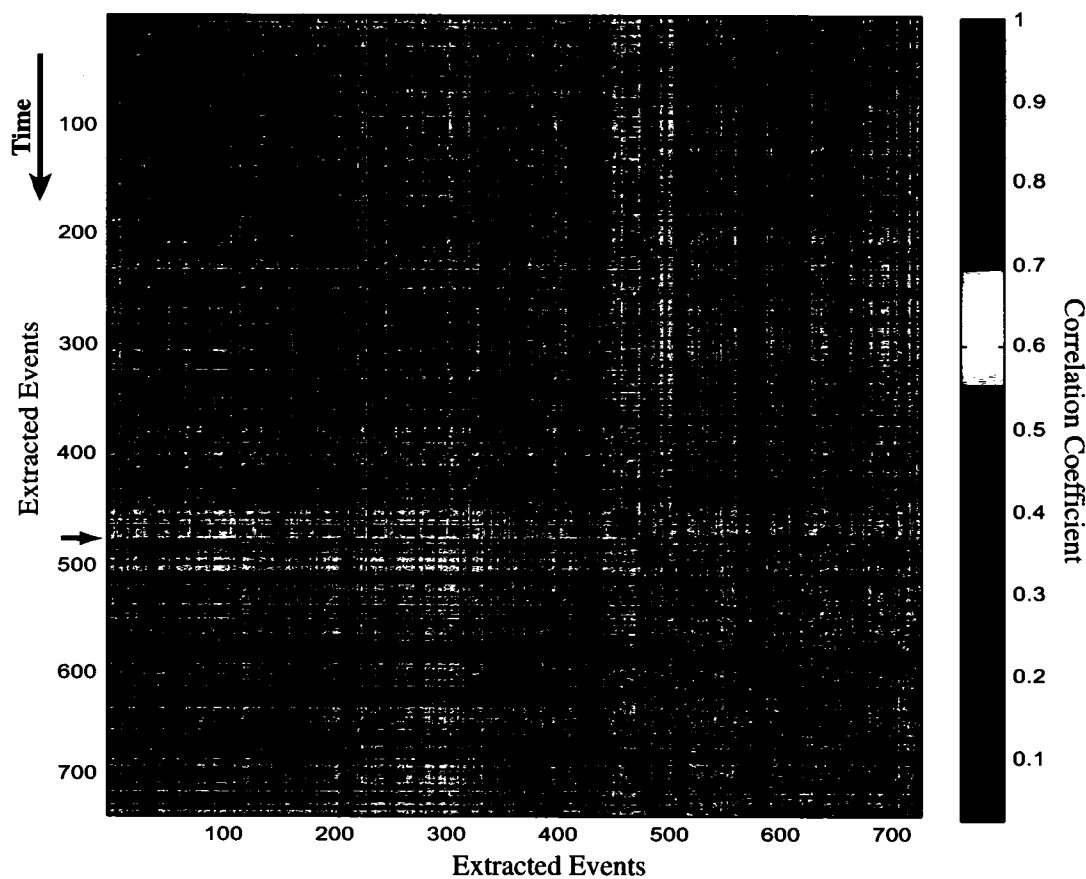


Figure 4.14. Similarity matrix for extracted events recorded on 21-Nov-2002 at station SSLN. The well correlated part of the matrix (event 1 to 480) has a mean correlation value of 0.7; the rest of the matrix has a mean value of 0.5. The events stop being similar at 13:24 UT (event 480; red arrow), and the last event classified into the dominant repeating event family was recorded at 13:07 UT (event 474).

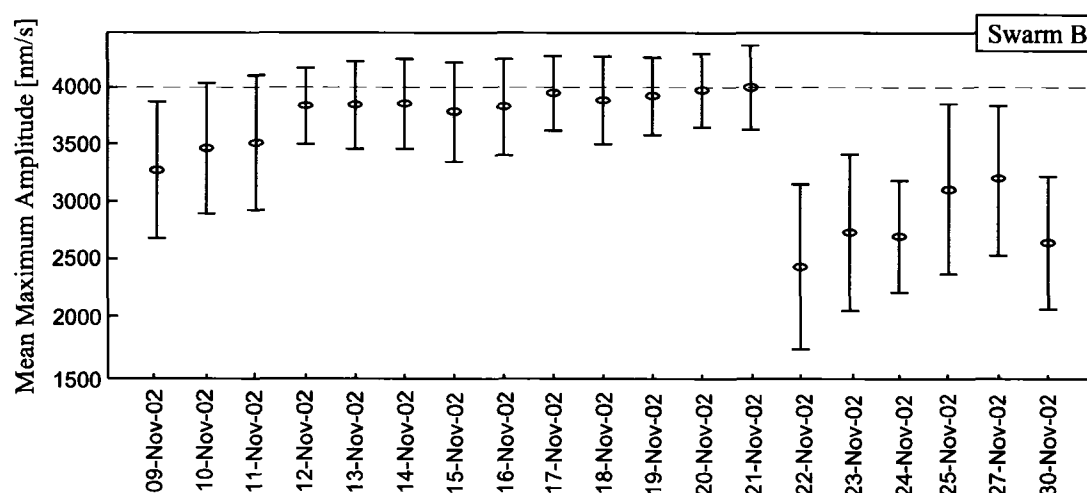


Figure 4.15. The zero-to-peak amplitude distribution of the repeating events of Swarm B. The ellipses represent the mean value and the bars indicate the standard deviation. The drop in amplitude occurred at the same time the waveform changed on 21-Nov-2002 at about 13:24 UT. Note that waveforms are clipped above 4000 nm/s.

already starts to change slowly into a different waveform after 3 days (Figures 4.18 and 4.19). The evolution takes place over a time period of 7 days, and the new dominant waveform then lasts for 25 days until the amplitudes have decreased to background level.

Figure 4.20 displays the daily stacks for the representative days in each swarm. These averaged waveforms represent the majority of similar events within each swarm. Figure 4.21 shows the corresponding spectral amplitudes. Each stack has a pronounced spectral peak at about 1.6 Hz that is evident at all three stations closest to the summit. Although these four waveforms share some similar features they are all significantly different from each other with the maximum cross-correlation coefficient between the stacked waveforms ranging between 0.4 and 0.7. Figure 4.22 provides a quantitative comparison of the 97 daily stacks by displaying the similarity matrix, which results from cross-correlating each of the stacks with all other stacks. It is evident that some of the dominant waveforms do reappear over the course of the 4 years studied; for example, the second group of repeating events in Swarm A recurs at the end of Swarm C, and as the majority of Swarm D. This provides additional evidence for the source process of the repeating events being non-destructive.

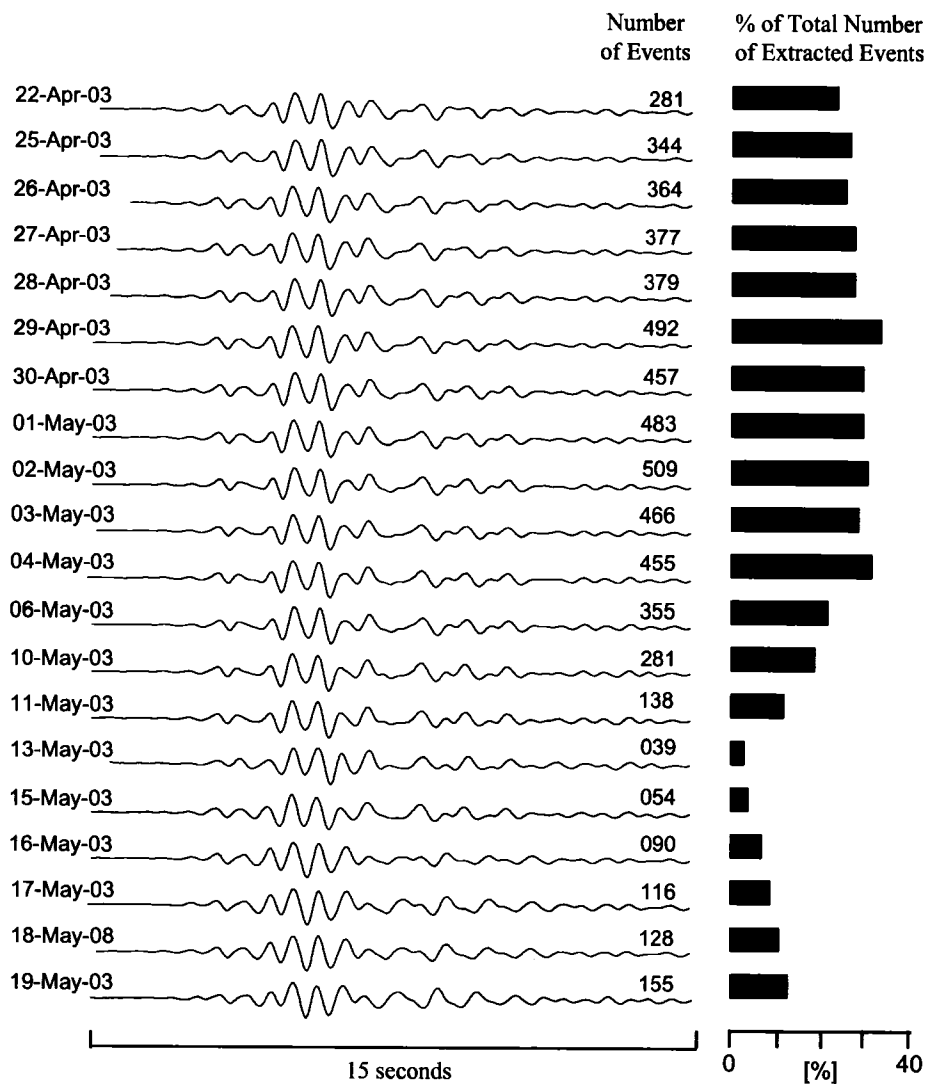


Figure 4.16. Daily stacks for Swarm C.

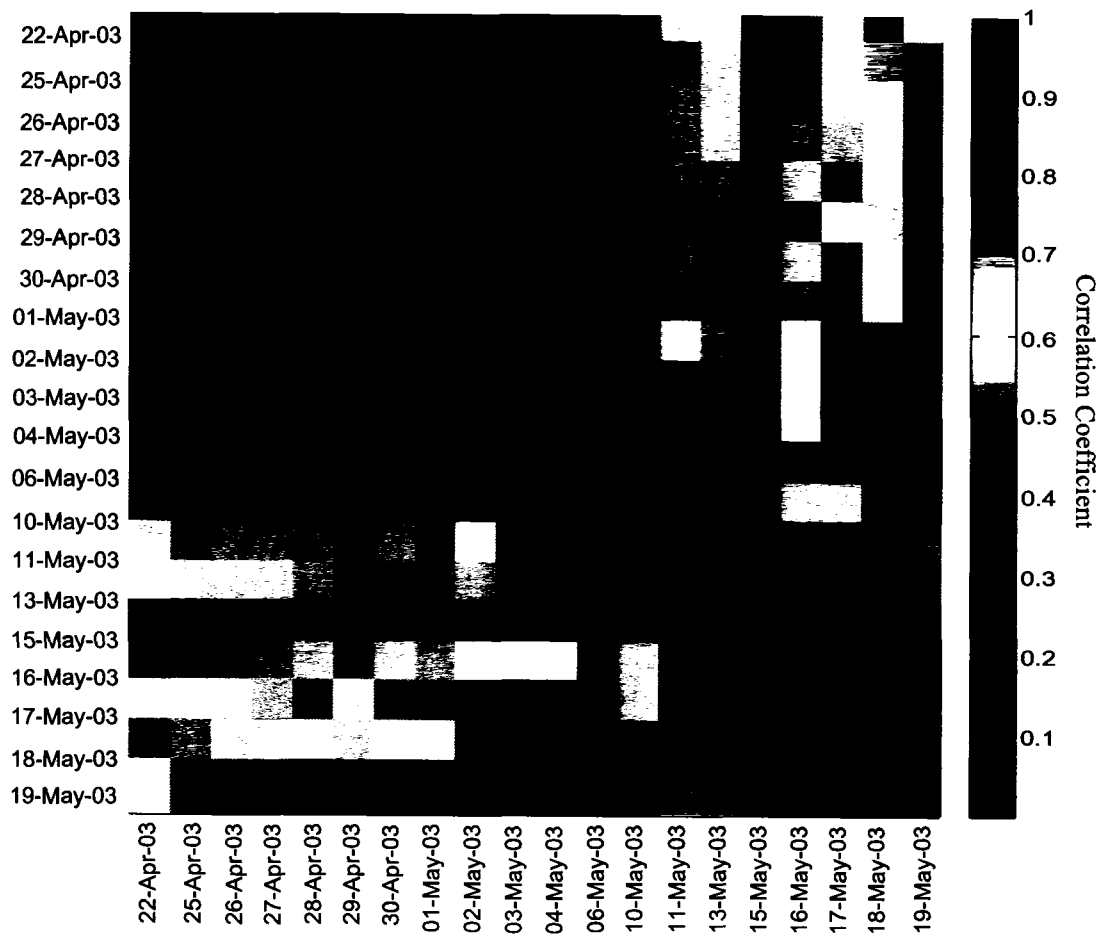


Figure 4.17. Similarity matrix for repeating events of Swarm C.

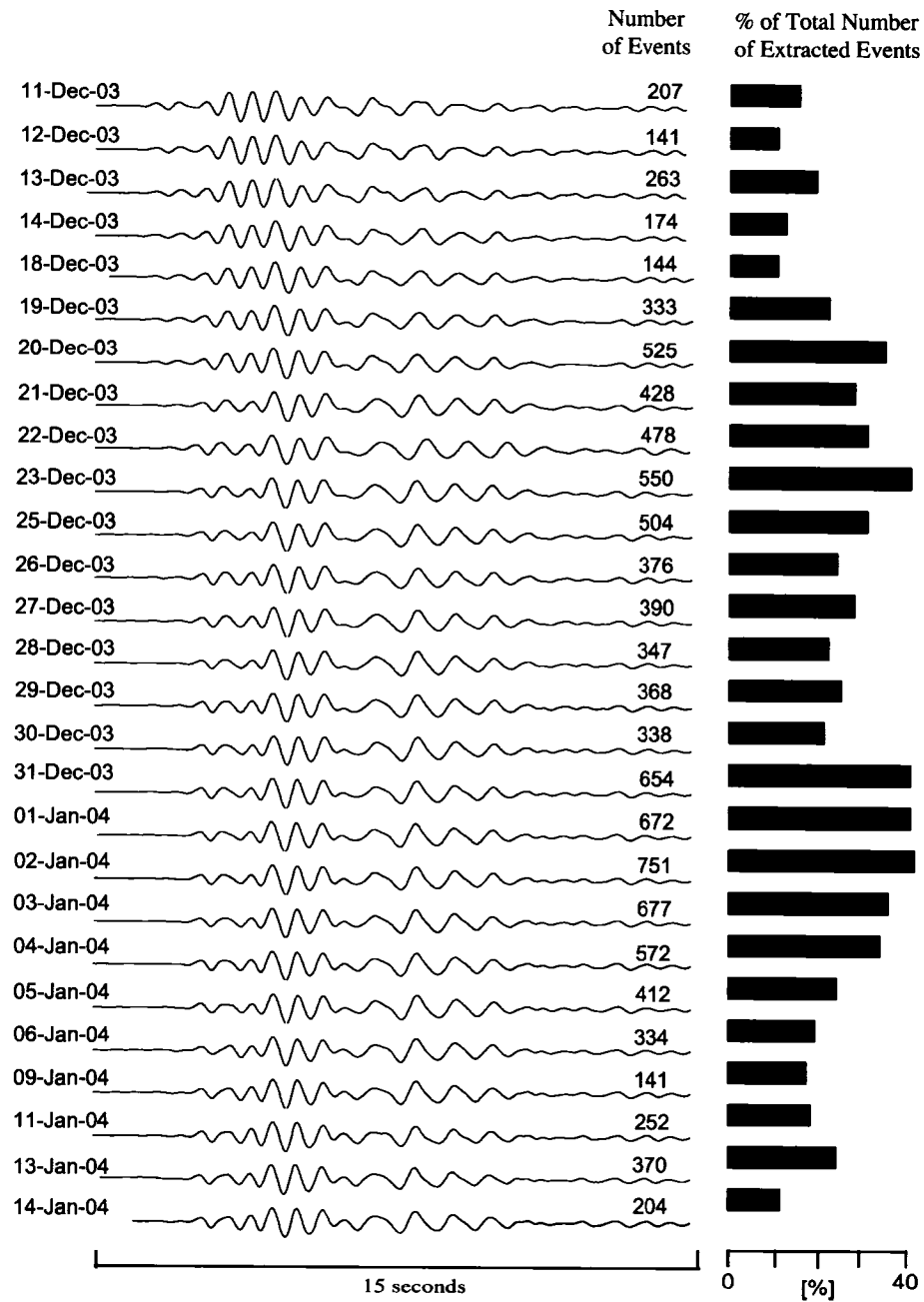


Figure 4.18. Daily stacks for Swarm D.

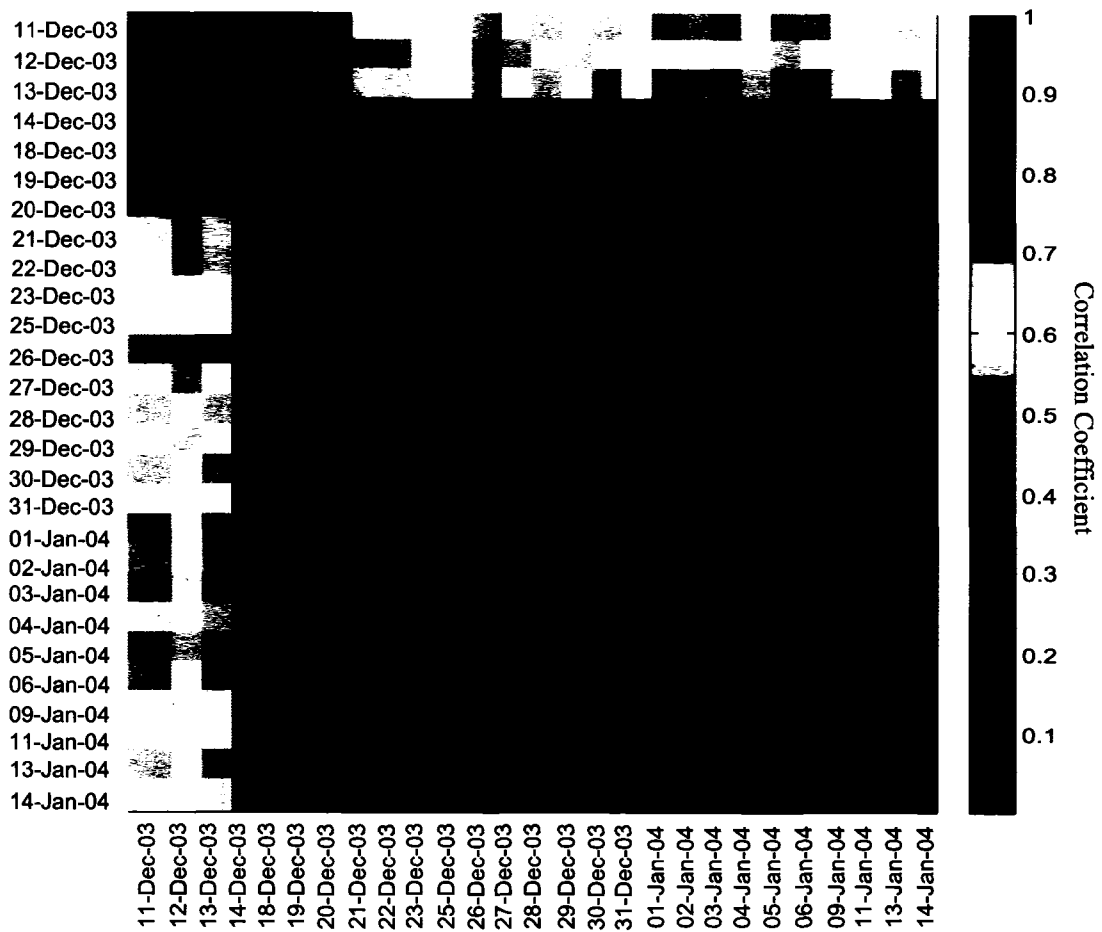


Figure 4.19. Similarity matrix for repeating events of Swarm D.

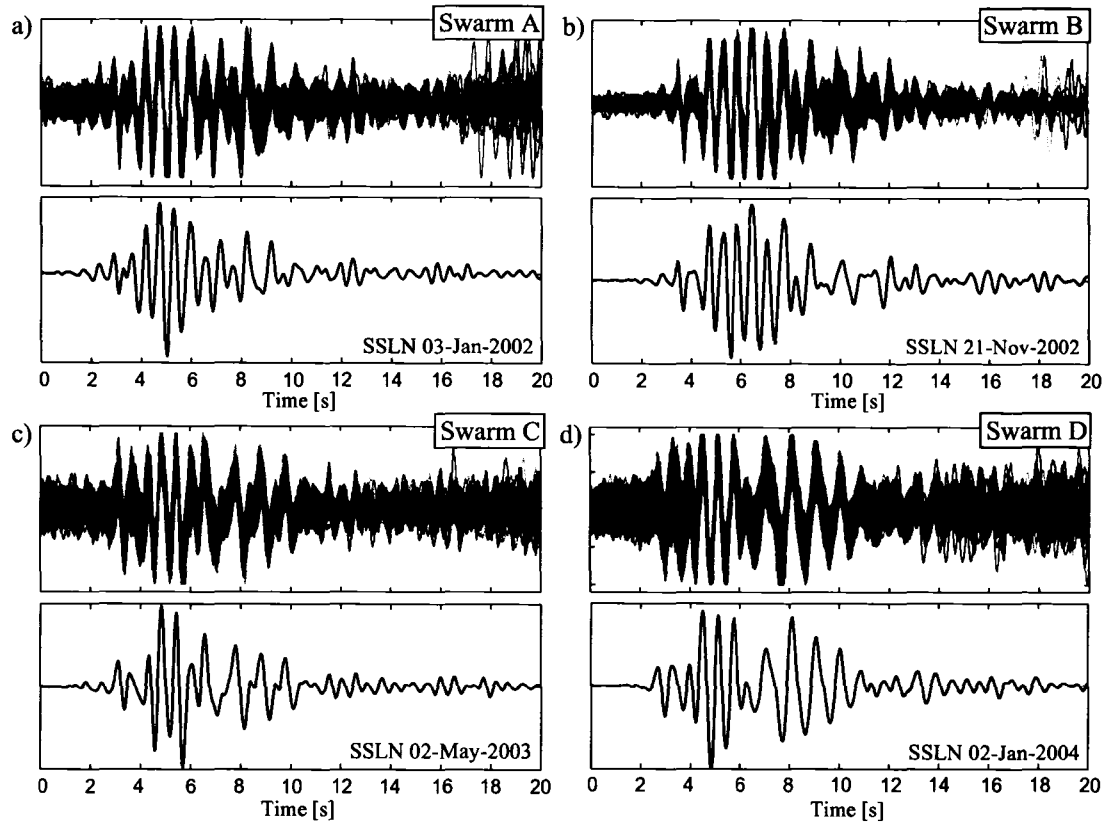


Figure 4.20. Repeating event overlays and stacks for the representative days of each swarm indicated in Figure 4.1: a) 03-Jan-2002 (588 events; Swarm A), b) 21-Nov-2002 (274 events; Swarm B), c) 02-May-2003 (509 events; Swarm C) and d) 02-Jan-2004 (751 events; Swarm D). The maximum amplitude of events ranges between 1000 and 4000 nm/s within each of the overlays. The maximum cross-correlation coefficient between the stacked waveforms in a) and b) is 0.7; a) is also similar to c) and d) with a value of 0.6. Cross-correlating c) and d) as well as b) and d) result in a value of 0.4.

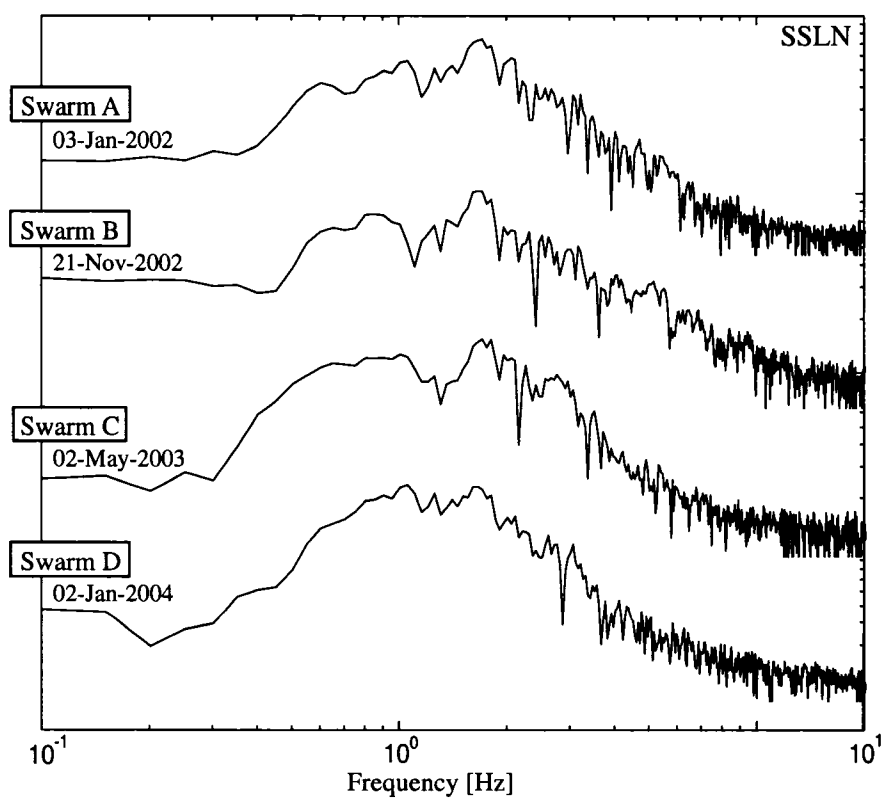


Figure 4.21. Spectral amplitudes for daily stacks of repeating events recorded on the representative day for each swarm. Note that the pronounced peak at about 1.6 Hz is clearly visible in all traces indicating the stable part of the source structure.

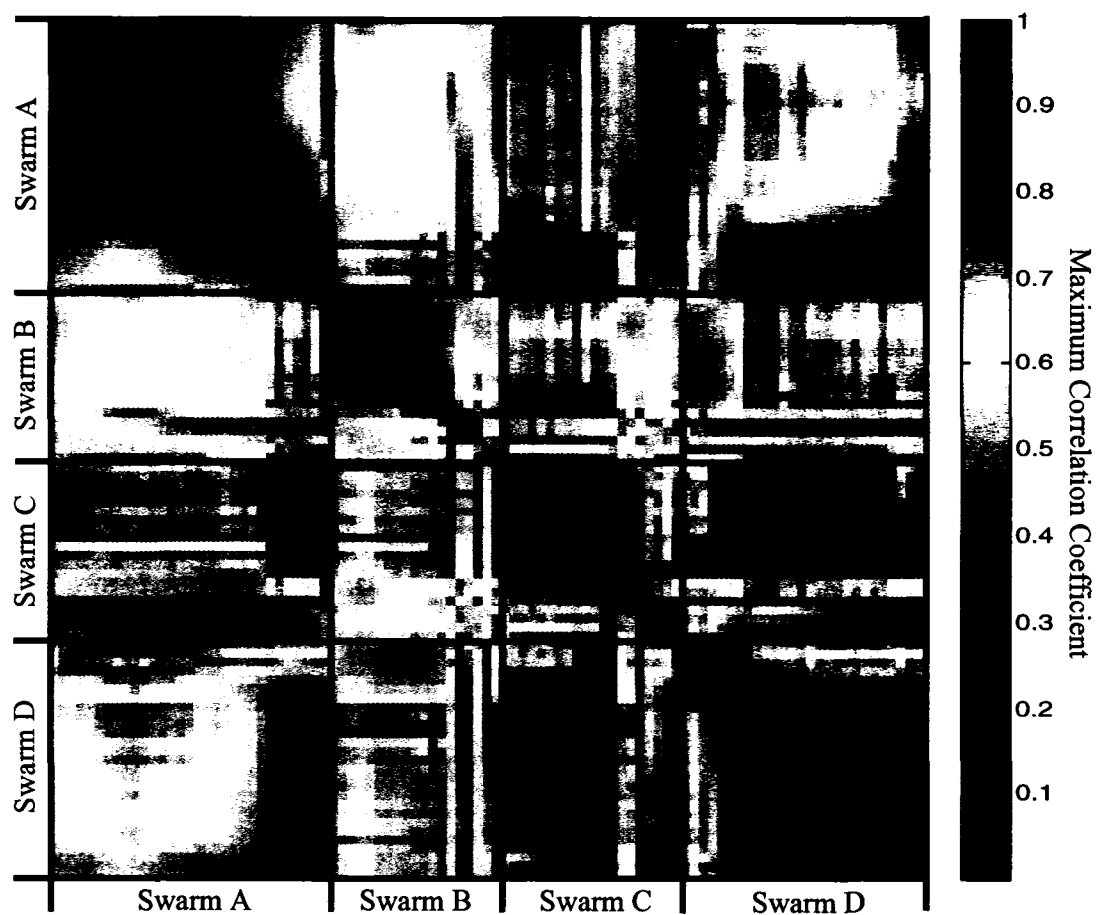


Figure 4.22. Similarity matrix for the 97 daily stacks from all swarms. Orange to red indicates highly similar waveforms (maximum correlation coefficients > 0.7). The diagonal represents the auto-correlation. Note that each swarm exhibits waveforms that are highly similar to waveforms recorded during other time periods; for example, the second group in Swarm A reappears at the end of Swarm C, and as the majority of Swarm D.

4.5 Implications and discussion

Previous studies of Shishaldin show evidence for a seismic source mechanism that allows a virtually simultaneous release of an acoustic wave into the atmosphere [*Petersen and McNutt, 2006*]. *Petersen and McNutt* [2006] infer that this seismo-acoustic source is located at shallow depth ($\leq 240 \pm 200$ m) at the interface between a fluid-filled conduit and an overlying open conduit system and that it is generated by the explosive outflux of volatiles. Based on (1) the sustained seismicity, (2) the lack of surface emissions of magma at Shishaldin since it last erupted in 1999, and (3) on the low SO₂ flux emitted by the volcano's small gas plume exiting the summit crater in discrete puffs, *Petersen and McNutt* [2006] suggest that Shishaldin's conduit system has become hydrothermal. The underlying magma storage system supplying the heat source and volcanic gases is expected to be located at shallow depths; preliminary studies on melt inclusions from recent eruptions indicate magma trapping pressures that are equivalent to depths ≤ 3 km, which is very shallow for volcanoes in the Aleutian Arc [*T. Plank, written communication, 2006*; *L. Szramek, written communication, 2006*].

A number of implications can be drawn from the observation of repeating events at Shishaldin: (1) The presence of highly similar waveforms implies a source location that is stable, so that the seismic energy travels along an identical path to the seismometer. The repeating events observed at Shishaldin must occur within a very limited source volume with a maximum radius of ~ 470 m predicted using the quarter-wavelength hypothesis of *Geller and Mueller* [1980] with a P-wave velocity in the source region of 3000 m/s and a dominant frequency of 1.6 Hz. It is noted that the quarter-wavelength hypothesis is primarily applicable for general seismic body waves; the high degree of heterogeneity in volcanic environments may require more confined source volumes in order to exhibit waveform similarity. *Neuberg et al.* [2006] performed numerical tests on low-frequency wavelets showing that in order to produce waveform similarity the source location may only vary by a significantly smaller amount (less than one tenth of a wavelength) than predicted by the quarter-wavelength hypothesis. Accordingly, Shishaldin repeating events would be lo-

cated within a distance of ~ 190 m from each other. (2) The source mechanism must be repeatable and therefore non-destructive in order to reproduce the same waveforms every few minutes over extended time periods of up to several weeks. (3) The high rate of one repeating event about every 0.25–10 minutes implies that the mechanism must be able to recharge rapidly (within ≥ 15 seconds). (4) The mechanism must be able to account for the variation of maximum amplitudes between repeating events recorded within ≥ 15 s of each other. In general, for LP events a larger peak amplitude can be generated by either a seismic signal with more initial energy, a less attenuating path or a change in impedance contrast between the fluid and solid allowing more seismic energy to escape the resonator and reach the seismometer. For LP events with highly similar waveforms the change in path is not an acceptable explanation, because this would cause shifts in waveform phases. A change in impedance contrast would change the resonance frequencies also resulting in an alteration of waveforms. Therefore, it seems most likely that the amplitude of the source trigger itself is what changes. *Petersen et al.* [2006] showed that Shishaldin LP events range from magnitude M_L 0.1–1.8, with most events having magnitudes < 1.0 .

A mechanism or mechanisms are required to trigger the initial seismic energy that then produces the waveforms characteristic for low-frequency events via resonance at a fluid-solid interface. A few different physical processes have been proposed as the trigger mechanism for low-frequency seismic energy in hydrothermal environments: (1) *Bame and Fehler* [1986] show that hydrothermal fracturing is able to generate earthquakes with a low-frequency component. However, the repeated fracturing of rock in a hydrothermal environment is a destructive process and therefore is unlikely to produce the seismic source, stable over periods of weeks, observed at Shishaldin. (2) Other hydrothermal triggers for low-frequency seismic energy are explosions resulting from magma-water interactions: the collapse of an insulating layer at the magma-water boundary causes superheated water to rapidly expand to steam forming seismic shockwaves [*Wohletz*, 1986; *Buttner and Zimanowski*, 1998]. To achieve the generation of highly similar earthquakes at the observed high rates, a rapid recharge of the hydrothermal supply to a fixed source location would be required, which

seems questionable. Also, magma-water interactions can generate instabilities at the magma surface that cause magma break-up, resulting in a phreato-magmatic eruption [Wohletz, 1986, 2002], which was not observed at Shishaldin. Finally, there is no evidence of shallow magma in the Shishaldin conduit based upon the low SO₂ flux and the lack of surface emissions of magma. Therefore, magma-water interaction does not seem a plausible source mechanism for Shishaldin. (3) Another trigger mechanism is the choked flow of gases (e.g. *Chouet et al.* [1994]; *Morrissey and Chouet* [1997]). In the choked flow model a shock wave is generated downstream of a constriction within the conduit by the acceleration of fluids to supersonic speeds. The shock wave produces a pressure transient in the flow that applies a sudden force to the conduit walls, triggering resonance of the fluid-filled crack, which produces a low-frequency earthquake. The model requires a conduit constriction with a large and steady pressure difference between the volumes above and below. *Chouet et al.* [1994] proposed this mechanism as the trigger for LP events at Redoubt Volcano that occurred at a rate of 3–5 events per minute. *Chouet et al.* [1994] suggested that superheated steam released from the top of a magma body located at 1.5 ± 0.5 km depth was forced through a crack connected to the overlying, lower pressure, hydrothermal system. This crack contained a constriction at a depth of 270–370 m below the summit, allowing choked flow to develop. *Chouet et al.* [1994] inferred that a decrease in pressure gradient across the constriction produced a decrease in seismic amplitudes.

The choked flow model presents a plausible trigger mechanism for the repeating events observed at Shishaldin. The volcano's persistent degassing activity from its summit vent indicates an efficient supply of gas to the upper conduit necessary for a fluid-flow induced source mechanism. The choked flow model fulfills the requirements for a repeatable non-destructive source mechanism at a fixed location that is able to recharge rapidly. The observed variation in amplitudes may be explained by small changes in pressure. A network of hydrothermal fractures around the main conduit (Figure 4.23) may explain the events that were not classified into a dominant repeating event group due to differences in waveform, i.e. multiple sources at different locations may exist next to a dominant source.

This may also explain the continuum of different LP events that occur in between swarms. Therefore, swarms of repeating events would represent time periods during which the main source is activated, increasing the overall amplitudes and creating larger events at a higher rate. In between swarms, the dominant source is turned off and replaced by a multi-source system that generates lower amplitude seismicity. The choked flow model explains the gradual change in waveforms observed at Shishaldin: a slowly decreasing pressure gradient is expected to move the location of the shock front upward along the wall, gradually changing the seismic waveforms (e.g. *Chouet et al. [1994]; Morrissey and Chouet [1997]*), and eventually causing the amplitudes to decline to background level. A shallower depth location of the shock front, caused by a lower pressure gradient, is likely to enhance lower frequency components within the seismic waveforms, because surface waves become more pronounced. The seismic first motion is expected to be a dilatation produced by a sudden pressure drop associated with the shock but cannot be clearly identified in the emergent onsets of the stacks (e.g. Figure 4.9).

A decrease in pressure gradient may be caused by distribution of the fluid-flow between the main conduit and parallel flow pathways or by erosion of the conduit constriction. A slowly decreasing influx of steam and/or magmatic gases into the hydrothermal system may also cause a decrease in pressure gradient [*Morrissey and Chouet, 1997*], and would explain small changes in relative excitation of the resonance frequencies [*Chouet et al., 1994*] that accompany the waveform changes within each swarm. The opening of additional pathways through which gases can escape may also decrease the pressure gradient within the main conduit, although volcano-tectonic events commonly associated with fracturing of volcanic rock have been rarely observed within Shishaldin's edifice [*Petersen et al., 2006*]. However, the most likely explanation for the abrupt disappearance of the dominant waveform on November 21, 2002 is a sudden drop in pressure gradient caused by the rapid destruction of the constriction within the conduit; this concurs with previous studies that suggest that a modification of the conduit occurred that day [*Caplan-Auerbach and Petersen, 2005*]. I speculate that the constriction then slowly, over the course of several months, was replaced

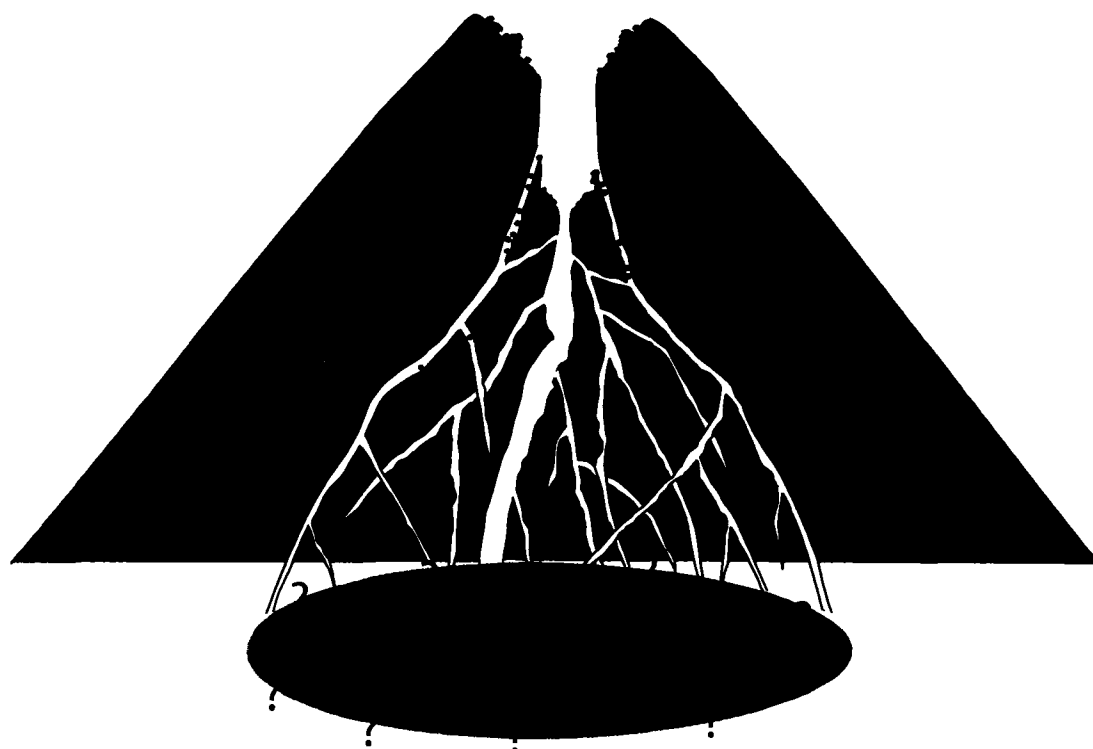


Figure 4.23. Schematic illustration of Shishaldin's multi-fractured hydrothermal system. Volcanic debris and precipitates (yellow dots) that temporarily seal fractures are indicated.

by volcanic debris falling down from the uppermost conduit walls allowing the next swarm to produce events with highly similar waveforms.

The activation of a new swarm period may be induced by temporarily sealing the network of small hydrothermal fractures with precipitates, causing the degassing activity to refocus on the main passageway. The reappearance of some of the dominant waveforms across different swarm periods indicates that sources at the same location are being activated repeatedly. This suggests that overall the geometry of the hydrothermal system remained relatively stable; the pressure gradient inside the main conduit would be regulated by changes in gas influx and the amount of volcanic debris.

4.6 Conclusions

Swarms of long-period repeating earthquakes at Shishaldin Volcano, Alaska, are time periods characterized by events with highly similar waveforms that dominate at high event rates. A scheme to classify these events into manageable groups has been developed by use of waveform cross-correlation. An average waveform representing the majority of highly similar events recorded on a given day was established for 97 days distributed over the four swarm periods that occurred during 2001–2004. Each of these dominant waveforms (daily families of repeating events) represents a spatially distinct and non-destructive source mechanism that generates seismic waves which travel along a nearly identical path to the seismometer. The waveform classification allowed systematic changes of the dominant source process to be recognized. The dominant waveforms slowly evolved over time for three of the four swarms analyzed; during one swarm the change occurred abruptly. The swarms exhibit dominant waveforms that reappear over the course of 4 years indicating repeatedly activated source locations. Among models considered, the choked flow model provides an acceptable trigger mechanism for the repeating events observed at Shishaldin. The generation of Shishaldin's LP events seems to be driven by complex dynamics within a multi-fractured hydrothermal system. Further progress in the interpretation of Shishaldin's seismicity will depend on a denser seismic network and a multidisciplinary approach including gas sampling and studies on groundwater dynamics within volcanic systems like Shishaldin.

References

- Arciniega, A., B. Chouet, and P. Dawson (2005), Families of long-period seismic signals observed in Popocatepetl Volcano, Mexico, *EOS Trans. Am. Geophys. Union*, 86(52), Fall Meet. Suppl., Abstract V21C-0609.
- Bame, D. and M. Fehler (1986), Observations of long period earthquakes accompanying hydraulic fracturing, *Geophys. Res. Lett.*, 13, 149–152.
- Benoit, J. P. and S. R. McNutt (1996), Global Volcanic Earthquake Swarm Database 1979–1989, *U.S. Geological Survey Open-File Report*, 96-69, 334 pages.
- Buttner, R. and B. Zimanowski (1998), Physics of thermohydraulic explosions, *Phys. Rev. E*, 57, 5726–5729.
- Caplan-Auerbach, J. and T. Petersen (2005), Repeating coupled earthquakes at Shishaldin Volcano, Alaska, *J. Volcanol. Geotherm. Res.*, 145, 151–172.
- Chouet, B. A. (1996), Long-period volcano seismicity: Its source and use in eruption forecasting, *Nature*, 380, 309–316.
- Chouet, B. A., R. A. Page, C. D. Stephens, J. C. Lahr and J. A. Power (1994), Precursory swarms of long-period events at Redoubt Volcano (1989–1990), Alaska: Their origin and use as a forecasting tool, *J. Volcanol. Geotherm. Res.*, 62, 95–135.
- Chouet, B. A. (1988), Resonance of a fluid-driven crack: Radiation properties and implications for the source of long-period events and harmonic tremor, *J. Geophys. Res.*, 93(B5), 4375–4400.
- Geller, R. J. and C. S. Mueller (1980), Four similar earthquakes in central California, *Geophys. Res. Lett.*, 7(10), 821–824.
- Gil Cruz, F. and B. A. Chouet (1997), Long-period events, the most characteristic seismicity accompanying the emplacement and extrusion of a lava dome in Galeras Volcano, Colombia, in 1991, *J. Volcanol. Geotherm. Res.*, 77, 121–158.

- Green, D. N. and J. Neuberg (2006), Waveform classification of volcanic low-frequency earthquake swarms and its implication at Soufrière Hills Volcano, Montserrat, *J. Volcanol. Geotherm. Res.*, *153*, 51–63.
- Grêt, A., R. Snieder, R. C. Aster and P. R. Kyle (2005), Monitoring rapid temporal change in a volcano with coda wave interferometry, *Geoph. Res. Lett.*, *32*, L06304, doi:10.1029/2004GL021143.
- Hawthorne, J. and M. West (2005), Toward the systematic counting of small volcanic seismic events, *EOS Trans. Am. Geophys. Union*, *86*(52), Fall Meet. Suppl., Abstract S11B–0171.
- Hellweg, M. (2000), Physical models for the source of Lascars harmonic tremor, *J. Volcanol. Geotherm. Res.* *101*, 183–198.
- Igarashi, T., T. Matsuzawa and A. Hasegawa (2003), Repeating earthquakes and interpolate aseismic slip in the northeastern Japan subduction zone, *J. Geophys. Res.*, *108*(B5), L2249, doi:10.1029/2002JB001920.
- Jaupart, C. and S. Vergnolle (1989), The generation and collapse of a foam layer at the roof of a basaltic magma chamber, *J. Fluid Mech.*, *203*, 347–380.
- Jaupart, C. and S. Vergnolle (1988), Laboratory models of Hawaiian and Strombolian eruptions, *Nature*, *331*, 58–60.
- Johnson, J. B. and J. M. Lees (2000), Plugs and chugs – seismic and acoustic observations of degassing explosions at Karymsky, Russia and Sangay, Ecuador, *J. Volcanol. Geotherm. Res.*, *101*, 67–82.
- Julian, B. (1994), Volcanic tremor: Nonlinear excitation by fluid flow, *J. Geophys. Res.*, *99*(6), 11859–11877.
- Lahr, J. C., B. A. Chouet, C. D. Stephens, J. A. Power and R. A. (1994), Earthquake classification, location, and error analysis in a volcanic environment: implications for the

- magmatic system of the 1989–1990 eruption at Redoubt Volcano, Alaska, *J. Volcanol. Geotherm. Res.*, *62*, 137–151.
- Malone, S. D., W. A. Thelen and A. Qamar (2005), Source scaling of volcanic earthquakes at Mount St. Helens, *Cities on Volcanoes 4th Conference*, IAVCEI, Quito, Ecuador, Abstract SIVB-023-P.
- Molina, I., H. Kumagai and H. Yepes (2004), Resonances of a volcanic conduit triggered by repetitive injections of an ash-laden gas, *Geophys. Res. Lett.*, *31*, L03603, doi:10.1029/2003GL018934.
- Morrissey, M. M. and B. A. Chouet (1997), A numerical investigation of choked flow dynamics and its application to the triggering mechanism of long-period events at Redoubt Volcano, Alaska, *J. Geophys. Res.*, *102*, 7965–7983.
- Nadeau, R. M. and L. R. Johnson (1998), Seismological studies at Parkfield VI: Moment release rates and estimates of source parameters for small repeating earthquakes, *Bull. Seismol. Soc. Am.*, *88*, 790–814.
- Neuberg, J., H. Tuffen, L. Collier D. N. Green, T. Powell and D. B. Dingwell (2006), The trigger mechanism of low-frequency earthquakes on Montserrat. , *J. Volcanol. Geotherm. Res.*, *152*, doi:10.1016/j.jvolgeores.2005.08.008.
- Neuberg, J., R. Luckett, B. Baptie and K. Olsen (2000), Models of tremor and low-frequency earthquake swarms on Montserrat, *J. Volcanol. Geotherm. Res.*, *101*, 83–104.
- Petersen, T., J. Caplan-Auerbach and S. R. McNutt (2006), Sustained long-period seismicity at Shishaldin Volcano, Alaska, *J. Volcanol. Geotherm. Res.*, *151*, 365–381.
- Petersen, T. and S. R. McNutt (2006), Seismo-acoustic signals associated with degassing explosions recorded at Shishaldin Volcano, Alaska, 2003–2004, *Bull. Volcanol.*, doi:10.1007/s00445-006-0088-z.

- Power, J. A., J. C. Lahr, R. A. Page, B. A. Chouet, C. D. Stephens, D. H. Harlow, T. L. Murray and J. N. Davies (1994), Seismic evolution of the 1989–1990 eruption sequence of Redoubt Volcano, Alaska, *J. Volcanol. Geotherm. Res.*, *62*, 69–94.
- Stephens, C. D. and B. A. Chouet (2001), Evolution of the December 14, 1898 precursory long-period event swarm at Redoubt Volcano, Alaska, *J. Volcanol. Geotherm. Res.*, *109*, 133–148.
- Umakoshi, K., H. Shimizu and N. Matsuwo (2003), Seismic activity associated with the endogenous growth of lava dome at Unzen Volcano, Japan, *IUGG XXIII Meeting*, Sapporo, Japan, Abstract V10-01A-D-014.
- Vergnolle, S., M. Boichu and J. Caplan-Auerbach (2004), Acoustic measurements of the 1999 basaltic eruption of Shishaldin volcano, Alaska: 1. Origin of Strombolian activity, *J. Volcanol. Geotherm. Res.*, *137*(1–3), 109–134.
- Vergnolle, S. and G. Brandeis (1996), Strombolian explosions: 1. A large bubble breaking at the surface of a lava column as a source of sound, *J. Geophys. Res.*, *101*, 20433–20447.
- Vergnolle, S., G. Brandeis and J.-C. Mareschal (1996), Strombolian explosions: 2. Eruption dynamics determined from acoustic measurements, *J. Geophys. Res.*, *101*(B9), 20449–20466.
- Vergnolle, S. and G. Brandeis (1994), Origin of the sound generated by Strombolian explosions, *Geophys. Res. Lett.*, *21*(18), 1959–1962.
- White, R. A., A. D. Miller, L. Lynch and J. Power (1998), Observations of hybrid seismic events at Soufrière Hills volcano, Montserrat: July 1995 to September 1996, *Geophys. Res. Lett.*, *25*(19), 3657–3660.
- Wohletz, K. (1986), Explosive magma-water interactions: thermodynamics, explosion mechanisms, and field studies, *Bull. Volcanol.*, *48*, 245–264.

Wohletz, K. (2002), Water-magma interaction: some theory and experiments on peperite formation, *J. Volcanol. Geotherm. Res.*, 114, 19–35.

Chapter 5

General conclusions

This thesis presents a study of the continuously high level of seismic activity at Shishaldin Volcano, Alaska. Since a few months after it last erupted in 1999 until the time of this writing (November 2006), Shishaldin has produced hundreds to thousands of long-period (1–2 Hz) earthquakes every day. The immense extent of the seismic dataset together with the limitations given by the seismic monitoring network used to record the earthquakes presented serious challenges. However, a multi-parameter data analysis that incorporates both seismic and infrasound data and any other additional observations available allowed us to derive important conclusions about the nature of Shishaldin's sustained seismicity. The results and conclusions of the individual studies are given in detail within each of the previous chapters. In this chapter an overall conclusion is presented, along with a summary of the main contributions of this work and the remaining unknowns that should provide motivation for future studies at Shishaldin and *unusual* volcanoes in general.

I compared Shishaldin to other volcanoes that have been seismically studied and concluded that it exhibits a behavior that is unusual in its long-lasting high level of long-period seismicity without preceding or accompanying eruptive activity. Every indication is that the high rate of seismicity will continue without reflecting a hazardous state. Sealing of the conduit and/or a change in gas flux due to an injection of new magma into shallower depths, generating enough overpressure to open a pathway to the surface, would be expected to change Shishaldin's behavior. A change in behavior may occur rapidly and only shortly before an eruption, but would very likely be preceded by a conversion from long-period to volcano-tectonic seismicity; continuous volcanic tremor would be expected to accompany the transition.

In May 2004, the Alaska Volcano Observatory went from Level of Concern Color Code green to yellow for Shishaldin, because the seismic regime changed to episodes of tremor alternating with discrete long-period events. Thermal anomalies were observed in satellite data, suggestive of the surface exhalation of hot magmatic gases. Also, a sequence of

discrete pressure pulses was recorded, which was seven times stronger than the ones that had accompanied the sustained long-period seismicity, although still not nearly as strong as the infrasonic signals observed during the 1999 eruption. However, no eruption was confirmed in 2004 and the seismicity at Shishaldin went back to its background stage of one long-period event every 0.5–5 minutes soon after the tremor disappeared in October 2004. The seismic activity at Shishaldin has not changed since then, as of the time of this writing. The prolonged nature of Shishaldin's seismic activity opens up a number of non-trivial questions: What are the driving forces behind Shishaldin's unusual behavior? How long will this activity last? What do we learn from the Shishaldin case study? Why do we not see this kind of activity at many other volcanoes? The finding of answers to some of these questions is rather challenging, however, this thesis has provided significant contributions to a greater understanding of Shishaldin.

Previously, the location of Shishaldin's long-period earthquakes was poorly constrained between depths of 0–3 km beneath the summit. Combining seismic and infrasound data revealed that the seismic and acoustic sources are co-located at a depth of 240 ± 200 m below the crater rim. The infrasound data also allowed us, together with visual observations of the gas plume emitted from the summit vent, to relate the long-period earthquakes to degassing explosions, created by complex gas volume ruptures from a fluid-air interface, known as *jetting*. The inclusion of SO_2 flux measurements strengthened our hypothesis that, after the 1999 eruption, Shishaldin's conduit changed to a hydrothermal system with magmatic gases leaking through. A hydrothermal instead of a magmatic system being responsible for the sustained, steady-state long-period seismic activity at Shishaldin has been shown to provide a plausible explanation for the observed volcanic behavior. The studies presented in this thesis further revealed that Shishaldin exhibits activity cycles: time periods of increased earthquake amplitudes lasting 1–2 months are separated by several months of background seismicity. The seismicity rate stays more or less constant throughout. The periods of elevated seismicity are characterized by an abundance of long-period events with highly similar waveforms, referred to as *repeating events*. The observed swarms of repeating events

have a distinct physical meaning: they represent time periods during which a dominant source process, being spatially confined, repetitive, and non-destructive, is activated. A mechanism, known as *choked flow* model (see Chapter 4), fulfills all the requirements implied by the observed repeating events, and therefore provides a plausible trigger mechanism for Shishaldin's long-period events. The nature of the swarms of repeating events suggests that the hydrothermal system at Shishaldin is multi-fractured, i.e. a network of small fractures may surround a main conduit that provided the eruption pathway in 1999. The pressure gradient within the uppermost conduit, required by the choked flow model, may be temporarily increased by the sealing of parallel flow pathways due to precipitates, a larger amount of debris within the main conduit and/or by increased gas influx into the hydrothermal system.

In this thesis we conclude that the driving forces behind Shishaldin's unusual seismic behavior are hydrothermal in nature. The volcano's persistent degassing activity from its summit vent indicates an efficient supply of gas to the upper conduit necessary for a fluid-flow induced seismic source mechanism. The presence of SO₂ in the plume is intimated by blue haze and was measured using satellite imagery and ground based techniques, suggesting that magmatic gases are at least partly involved in the generation of seismicity. The hydrogeological dynamics and resources, and the capacity of the underlying heat sources are unknown; pursuing the Shishaldin case study until the persistent activity terminates will give us a better general idea of what to expect for similar subduction zone stratovolcanoes.

Further progress in the interpretation of Shishaldin's seismicity will depend on a denser seismic network, preferably consisting of seismic broadband instruments, allowing source modeling and detection of potential very long-period (VLP; periods of 3–20 s) seismicity. Also higher resolution gas measurements of Shishaldin's plume as well as continuous GPS data, monitoring subtle movements induced by increasing pressurization of the system, would contribute to a more detailed picture of the dynamics and capacity of the volcanic system. A better understanding of the underlying magmatic system supplying the heat source for the hydrothermal activity is required. Geological studies that have the potential

to give more insights are in progress [*T. Plank, written communication, 2006*]; preliminary results indicate that the magma storage system is located at a depth ≤ 3 km that is unusually shallow for Aleutian volcanoes [*T. Plank, written communication, 2006*].

This thesis gives another good example for the importance of using multi-parameter datasets in scientific research and monitoring of volcanoes. The future challenge in advancing our understanding of subduction zone volcanoes like Shishaldin will be to further combine research efforts and to conduct detailed case studies at many individual volcanoes. We may discover that Shishaldin is not that unusual after all, and that we have to deploy seismometers in order to see earthquakes; for example, Mount Gareloi, a remote Aleutian stratovolcano, has continuously produced earthquakes since the moment a seismic instrument was switched on.

Appendix

Local infrasound observations of large ash explosions at Augustine Volcano, Alaska, during January 11–28, 2006¹

A.1 Abstract

We present and interpret acoustic waveforms associated with a sequence of large explosion events that occurred during the initial stages of the 2006 eruption of Augustine Volcano, Alaska. During January 11–28, 2006, 13 large explosion events created ash-rich plumes that reached up to 14 km a.s.l., and generated atmospheric pressure waves that were recorded on scale by a microphone located at a distance of 3.2 km from the active vent. The variety of recorded waveforms included sharp N-shaped waves with durations of a few seconds, impulsive signals followed by complex codas, and extended signals with emergent character and durations up to minutes. Peak amplitudes varied between 14 and 105 Pa; inferred acoustic energies ranged between 2×10^8 and 4×10^9 J. A simple N-shaped short-duration signal recorded on January 11, 2006 was associated with the vent-opening blast that marked the beginning of the explosive eruption sequence. During the following days, waveforms with impulsive onsets and extended codas accompanied the eruptive activity, which was characterized by explosion events that generated large ash clouds and pyroclastic flows along the flanks of the volcano. Continuous acoustic waveforms that lacked a clear onset were more common during this period. On January 28, 2006, the occurrence of four large explosion events marked the end of this explosive eruption phase at Augustine Volcano. After a transitional period of about two days, characterized by many small discrete bursts, the eruption changed into a stage of more sustained and less explosive activity accompanied by the renewed growth of a summit lava dome.

¹Published under the same title with authors T. Petersen, S. De Angelis, G. Tytgat, and S. R. McNutt in *Geophysical Research Letters*, 33, L12303, doi:10.1029/2006GL026491, 2006.

A.2 Introduction

Augustine Volcano is a 1260 m high cone-shaped island stratovolcano located in southern Cook Inlet, Alaska. Historical Augustine activity has been characterized by vigorous explosion events that produced ash clouds and pyroclastic flows, small lava flows and extrusion of lava domes. On January 11–28, 2006, Augustine’s most recent eruption exhibited 13 large explosive events with durations of 1–11 minutes that produced ash-rich plumes reaching heights of up to 14 km a.s.l. The explosion events generated strong infrasonic signals that were recorded on scale by a newly installed microphone located on the volcano.

In the last ten years, microphones located on many active volcanoes around the world have revealed a large variety of infrasound signals associated with different styles of volcanic degassing [Johnson *et al.*, 2004b]. For example, infrasonic degassing signals recorded at Stromboli [Vergnolle *et al.*, 1996] and Erebus [Rowe *et al.*, 2000] exhibited waveforms that are characterized primarily by a single, short-duration sinusoidal pulse associated with bubble bursts at the surface of a low-viscosity fluid body. In contrast, Arenal [Hagerty *et al.*, 2000], Karymsky and Sangay [Johnson and Lees, 2000] revealed complex codas lasting several minutes indicative of extended-duration degassing associated with Strombolian explosions in higher-viscosity volcanic systems.

The objective of this paper is to describe the strong infrasound signals associated with the Vulcanian-style eruptions that occurred in the period January 11–28, 2006 at Augustine Volcano. The acoustic data gathered during this sequence of explosive eruptions exhibit some unique features in comparison to other case studies found in the literature. This dataset provides one of the few examples of continuous monitoring of an entire eruptive sequence by use of a local sensor, as opposed to temporary campaigns where microphones are deployed for periods of days to weeks. In conjunction with Augustine infrasound recorded in the far-field (infrasound array I53US, Fairbanks) the dataset offers a unique opportunity for the infrasound community to enhance studies of acoustic propagation. Furthermore, the dataset provides observations for a type of eruption that is not frequently studied with acoustic sensing. Previous acoustic studies have mainly focused on Strombolian explosions,

lava lake degassing (e.g. Erebus [Rowe *et al.*, 2000]), silicic dome building eruptions (e.g. Santiaguito [Johnson *et al.*, 2004a]), and Subplinian plumes (Shishaldin, e.g. Vergnolle and Caplan-Auerbach [2005]). The eruptive activity at Augustine Volcano presents a rare case of waveforms associated with vigorous and continuous degassing activity during an energetic Vulcanian-type eruption.

A.3 Data acquisition

On January 4, 2006, we deployed a Chaparral Model 2.1 microphone at site AUE on the volcano's ENE flank at a direct distance of 3.2 km from the active summit vent (Fig A.1). The well calibrated pressure transducer system, consisting of the microphone, a Voltage Controlled Oscillator (VCO) and a discriminator, has a flat response between 0.1 and 50 Hz. In addition to a high-gain channel the system is equipped with a low-gain component that allows recording pressure waves with amplitudes as large as 298 Pa before saturating; the sensitivities of the high-gain and the low-gain systems are 0.171 and 0.0084 V/Pa respectively. A noise reduction system, consisting of eight microporous hoses spread out over a half circle, is connected to the microphone. This design provides a spatial filter to sum coherent acoustic energy and to filter out incoherent turbulent wind noise. In addition, the system is located in an area densely covered with alders providing excellent low-noise recordings of acoustic signals from the volcano. The microphone is co-located with a 1 Hz vertical-component S-13 geophone at station AUE. AUE is part of a seismograph network operated by the Alaska Volcano Observatory (AVO) that consisted of seven short-period and one broadband seismometer at the start of the eruption. The data from these stations are telemetered to the AVO data acquisition office in Homer, where they are digitized at 100 Hz with a 12-bit resolution.

All the major explosion events that occurred during January 2006 at Augustine were recorded in full and with a good signal-to-noise ratio on the pressure sensor at station AUE. The corresponding seismic signals saturated all short-period stations, but remained on scale on the broadband seismometer (Guralp CMG-40T) at station AUL that is located on the

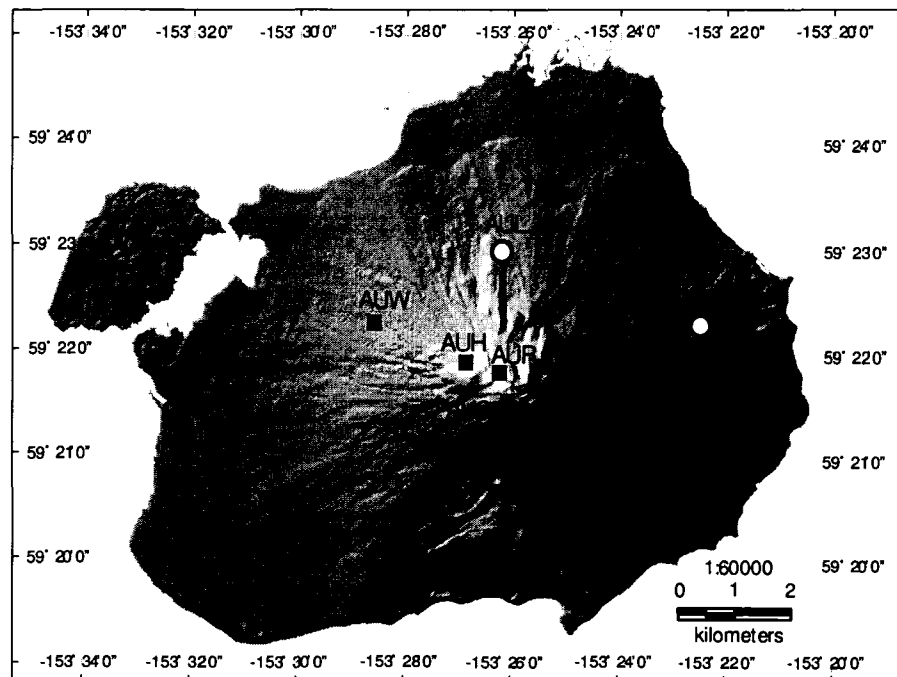


Figure A.1. Map of Augustine Volcano showing the permanent AVO monitoring network stations including broadband seismic station AUL and the pressure sensor co-located with a short-period seismic station at AUE (white circles). The active vent is located at the summit. The four summit stations and AUL were destroyed over the course of the eruption. Image modified from map provided by E. Thoms/USGS.

north flank of the volcano at 2.2 km from the active vent (Figure A.1). Station AUL ceased to operate on January 28, when it was destroyed by pyroclastic flows.

The National Weather Service (NWS) determined preliminary volcanic plume heights for the individual eruption events based on Doppler radar measurements [NWS, *personal communication*, 2006] (Table A.1). Although this method may not detect the uppermost highly diluted part of the plumes, it provides an approximation that is consistent throughout the explosive eruption sequence. Visual observations of the initial dynamic behavior of the volcanic plumes are not available, because clouds often obscured the volcano's summit and the majority of eruptions occurred at night.

A.4 Acoustic data

The acoustic signals recorded at station AUE during the January 2006 Augustine explosive activity had peak amplitudes ranging from 14 to 105 Pa (Figure A.2). Following a large pulse that accompanied the onset of the eruption phase on January 11, 2006, a sequence of events with increasingly larger peak pressures was recorded; the largest pulse was recorded on January 28, 2006 at 08:37:47 UT. The plume heights associated with the individual events of this explosive eruption phase exhibit no apparent correlation with the corresponding acoustic peak pressures. Following January 28, 2006, the occurrence of many small discrete explosions (0-peak pressures of 0.5–1 Pa; only distinguishable from noise on the high-gain channel) characterized a period that lasted about two days, and that marked the transition of the eruption to a more continuous and less explosive stage of activity. In Table A.1, we report peak amplitudes for the various explosion events as recorded at station AUE; we also list the respective sound pressure levels $SPL = 20 \log(\Delta P/2 \times 10^{-5})$ [Johnson, 2003] of atmospheric pressure perturbations (ΔP) relative to background atmospheric pressure ($\sim 10^5$ Pa) that were recorded at station AUE.

It is worth noting that the acoustic pulses associated with the explosive phase were large enough to be recorded by the infrasound array I53US located in Fairbanks, Alaska (at 675 km from the volcano); zero-to-peak amplitudes ranged from 0.04 to 0.42 Pa (Table A.1) and signal root-mean-square values between 0.0103 and 0.0796 Pa [Wilson *et al.*, 2006].

The waveforms recorded at AUE exhibit a great variety of different characteristics; representative examples are shown in Figure A.3. Although individual events differ significantly from each other, we can group them into two broad categories based on the appearance of the initial phase: *emergent events* and *impulsive events*. The two groups share a largely similar frequency content with the bulk of acoustic energy confined between 0.1 and 5 Hz. The *emergent events* are characterized by gradually increasing initial phases that reach peak amplitudes of 14–52 Pa before slowly tapering off (e.g., Figure A.3b); typical time durations are 100–170 s.

The *impulsive events* exhibit a sharp large-amplitude compression followed by a rar-

Table A.1. Parameters of Augustine January 11–28, 2006 explosive eruption events

Event No.	Date 2006	Event Onset ^a [UT]	Acoustic				Acoustic Energy [J]	SPL [dB]	AUL D _{seis} [s] ^e	Plume Height, km	Signal at I53US ^f [Pa]
			Onset ^b [UT]	Type ^c	[Pa] ^d	D _{acous} [s] ^e					
1	11-Jan	13:44	13:44:55	I	93	25	5.8×10^8	133	25	9	0.09
2	11-Jan	14:12	14:12:29	E	14	100	2.1×10^8	117	150	9	0.05
3	13-Jan	13:24	13:19:51	E	22	130	5.3×10^8	120	500	10	0.04
4	13-Jan	17:47	17:48:27	E	35	100	9.4×10^8	124	300	>9	0.09
5	13-Jan	20:22	20:22:15	I	32	150	14.6×10^8	124	300	11	0.16
6	14-Jan	01:40	01:40:38	E	29	150	14.3×10^8	123	280	10	0.05
7	14-Jan	03:58	03:58:15	E	52	170	38.0×10^8	128	300	9	0.08
8	14-Jan	09:14	09:13:37	I	65	100	27.0×10^8	130	200	No data	0.23
9	17-Jan	16:58	(16:58:28) 16:58:57	E+I	93	50	36.1×10^8	133	200	14	0.21
10	28-Jan	05:24	(05:31:05) 05:31:17	E+I	83	250	38.5×10^8	132	No data	9	0.31
11	28-Jan	08:37	08:37:47	I	105	20	7.1×10^8	134	No data	<3	0.10
12	28-Jan	11:04	11:04:26	I	66	150	21.5×10^8	131	No data	8	0.42
13	28-Jan	16:42	16:48:24	E	24	160	20.4×10^8	121	No data	8	0.10

^aAVO official start of eruption event based on seismic data.

^bAcoustic arrivals (± 1 s) at AUE; times in () indicate arrival of low-amplitude phase that precedes main pulse.

^cWaveform category *impulsive* (I) and *emergent* (E).

^dMaximum 0-to-peak pressure [Pa].

^eDuration of acoustic and seismic traces recorded at AUE and AUL, respectively, measured from signal onset until amplitude has decayed to background levels; AUL stopped functioning on January 28; listed acoustic duration was used for energy calculations.

^fPressure signal (0-to-peak) [Pa] recorded at infrasound array in Fairbanks [C. R. Wilson, *personal communication*, 2006].

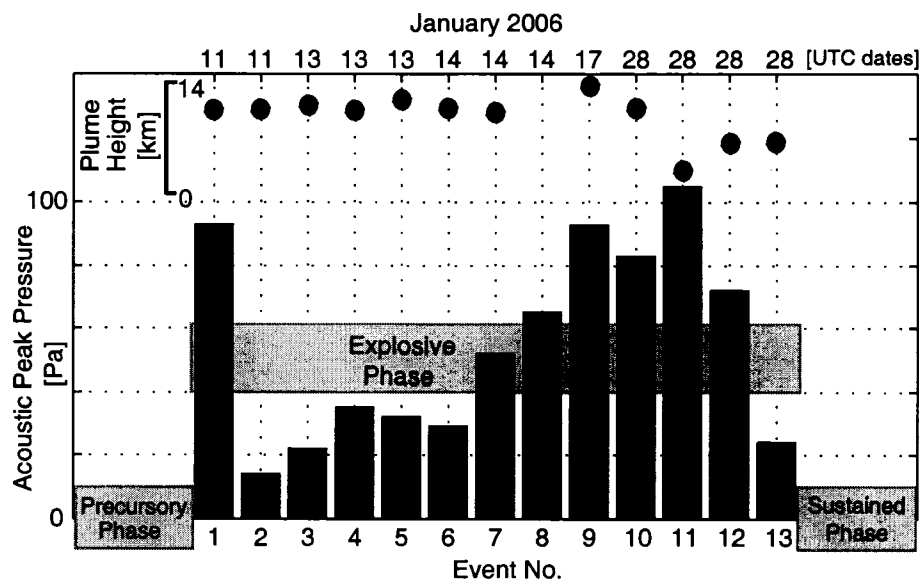


Figure A.2. Zero-to-peak pressures of the 13 acoustic signals associated with the explosive eruption phase (January 11–28, 2006). Preliminary plume heights determined by NWS are indicated by dots. Horizontal axis is event number, with dates shown at the top.

efaction; this characteristic N-shaped phase is followed by a lower amplitude coda (e.g., Figure A.3 a, c, d) lasting 20–150 s. These signals generally display large peak amplitudes (32–105 Pa); coda durations vary between 20 and 120 s, which may depend on how much the system was able to degas during the initial burst. The impulsive phase exhibits a higher frequency content with the dominant energy between 0.1 and 3 Hz; the coda waves have frequencies confined below 2 Hz (Figure A.4). If we reduce the recorded pressures to 1 km, assuming an inverse pressure decrease with radial distance from the vent, the largest acoustic pulse has a pressure of 336 Pa. The formation of shock waves for explosions with such large excess pressures seems likely, but could not be confirmed due to the limited visual observations.

The January 11 acoustic signal associated with the onset of the Augustine eruption sequence exhibits a strong impulsive initial compressional peak of 93 Pa (Figure A.5); the discrete peak is followed by a low-amplitude coda that lasts only 20 s. We suggest that this simple pressure pulse represents the initial vent-opening blast, i.e. the sudden uncorking

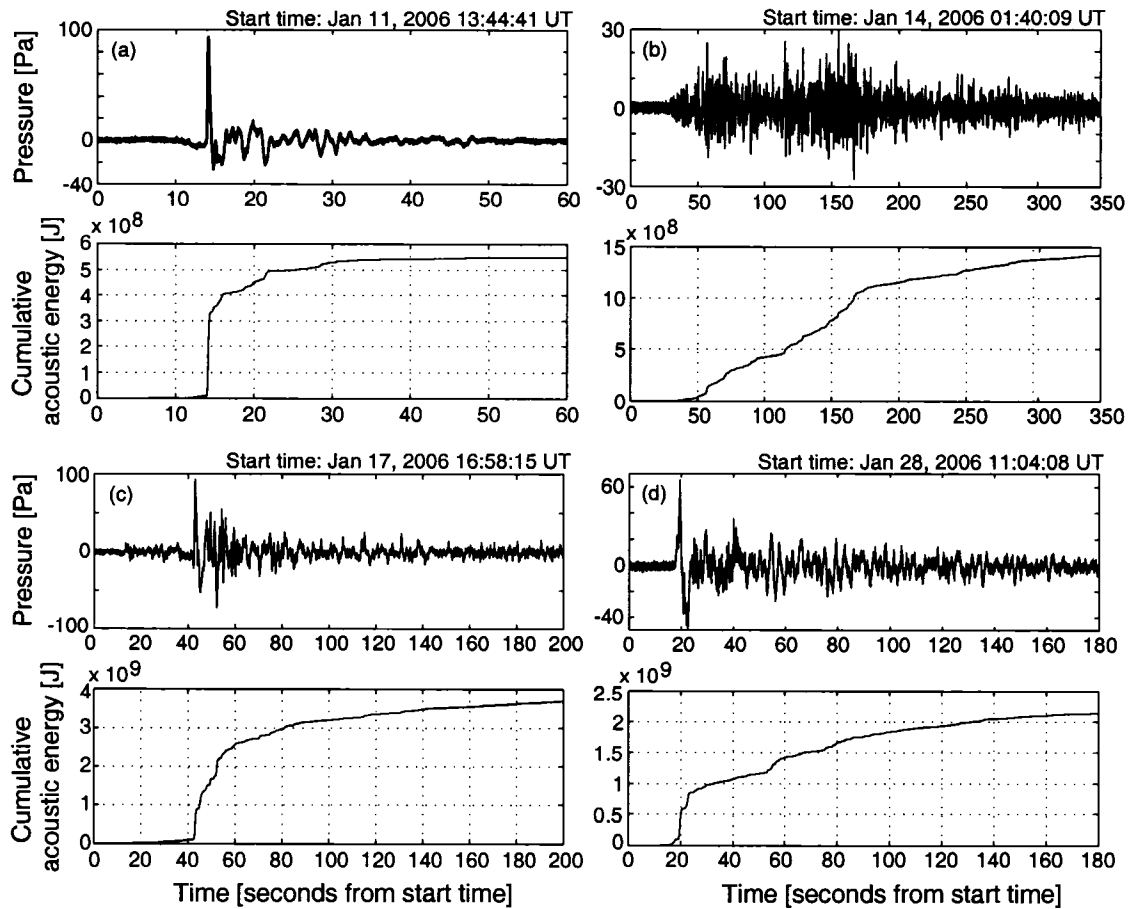


Figure A.3. Examples of traces and cumulative energies of acoustic signals associated with the Augustine January 2006 explosive eruptions recorded at AUE. The signals are high-pass filtered with a corner frequency of 0.1 Hz. a), c) and d) are *impulsive events*; b) gives an example for an *emergent event*. Note that impulsivity of the individual degassing events is clearly visible as the vertical part in the cumulative energy plots.

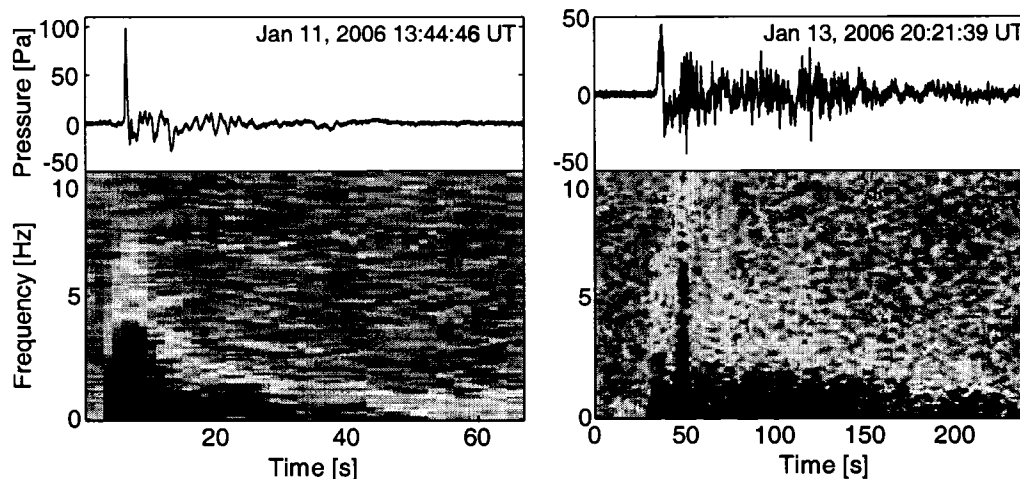


Figure A.4. Spectrograms for two of the impulsive pressure signals recorded at AUE in January 2006 (acoustic onsets: 11-Jan-06 13:44:55 UT and 13-Jan-06 20:22:15 UT; fft length: 1024 samples, 80% overlap). Black indicates the highest energies.

of the volcano. For a common seismo-acoustic source located at the vent, the expected time delay between the seismic and acoustic arrivals at station AUE is ~ 8 s (assuming that seismic and acoustic signals travel the same distance of 3.2 km, a seismic velocity of 3000 m/s, and an atmospheric acoustic velocity of 340 m/s). We measured a time lag of 14.0 ± 0.5 s. This discrepancy between the expected and measured time delays cannot be explained by a conjoint seismo-acoustic source, but exhibits strong evidence for precursory seismicity occurring about 6 s prior to sound generation.

In addition to acoustic peak amplitudes, the radiated elastic energy estimated from infrasonic pressure traces provides a useful parameter for comparison of eruptive activity at different volcanoes [Johnson, 2003]. The acoustic energy radiated by each of the Augustine explosive events can be approximated by assuming an isotropic radiation of a linear elastic wave propagating through a homogeneous atmosphere [Johnson and Aster, 2005] as:

$$E_{acoustic} = \frac{2\pi r^2}{\rho_{atmos} c_{atmos}} \int \Delta P(t)^2 dt \quad (A.1)$$

We assume an atmospheric sound velocity $c_{atmos} = 340$ m/s and an atmospheric density $\rho_{atmos} = 1.2$ kg/m³, and integrate over the entire duration of the acoustic pressure trace

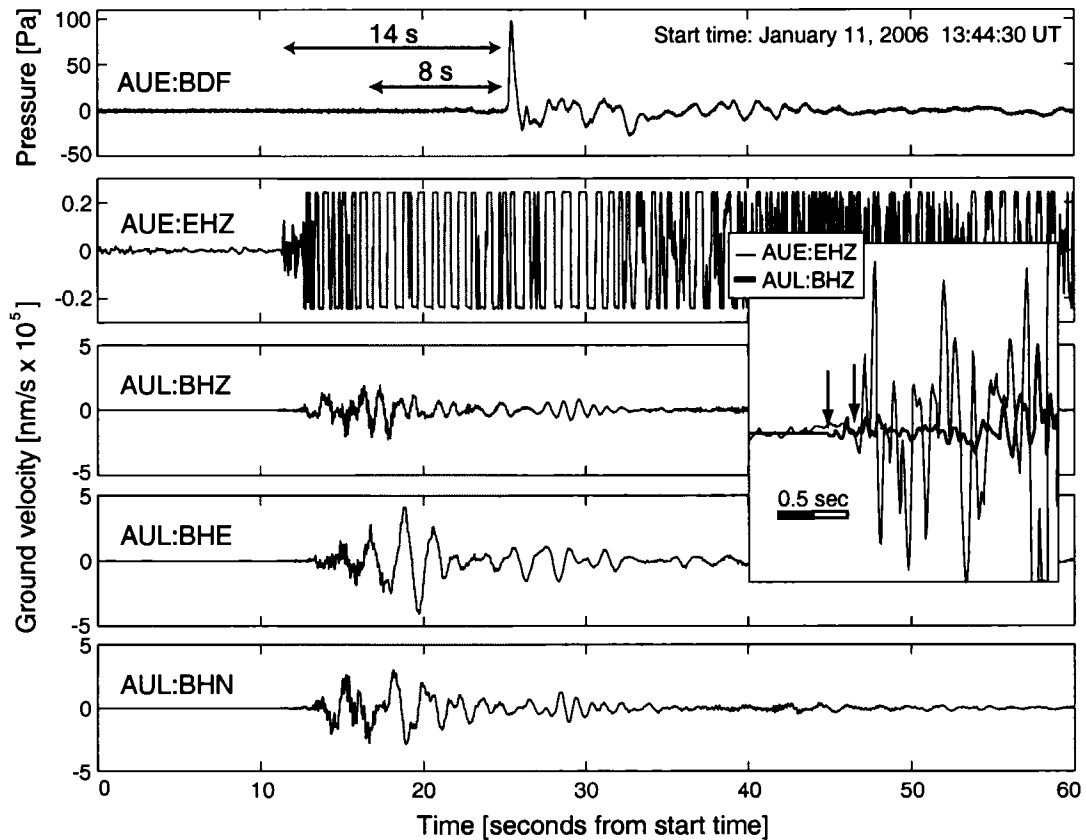


Figure A.5. The acoustic pulse associated with the initial vent-clearing event (acoustic onsets: 11-Jan-06 13:44:55 UT), recorded at AUE (acoustic and seismic) and three AUL broadband components (vertical = BHZ, east-west = BHE, north-south = BHN). The expected and measured time differences between seismic and acoustic arrivals at AUE, 8 and 14 s respectively, are marked in light grey. The impulsive acoustic onset does not correspond to the onset of the seismic signal, but is associated with a later part of the seismic waveform. Note that the seismic onset recorded at AUL is too small on the larger amplitude scale to be visible; the inset shows a 2.5-s close-up of the individually normalized seismic traces.

$\Delta P(t)$ recorded at a source-receiver distance $r = 3.2$ km. The acoustic waveforms have been high-pass filtered (> 0.1 Hz) using a 2-pole Butterworth filter before the energy calculation. Acoustic energies estimated for explosion events at Augustine range between 2×10^8 and 4×10^9 J (Table A.1). These are relatively high values compared to acoustic energies calculated for other volcanoes [Johnson, 2003]; for example, energy estimated from acoustic traces recorded at Stromboli [Ripepe and Marchetti, 2002] present a value of 1×10^5 J. Acoustic energies estimated for vigorous degassing activity at Sakurajima Volcano [Garcés *et al.*, 1999] have a value of 4×10^8 J. Although this value is comparable to energies estimated for Augustine, the corresponding acoustic waveforms have a significantly smaller peak excess pressure of 4 Pa at ~ 3 km from the vent; the Sakurajima infrasound is less intense but longer in duration.

A.5 Discussion

We have presented acoustic signals associated with large explosive Vulcanian-style eruption events at Augustine Volcano, Alaska, during January 11–28, 2006.

The substantial difference in degassing behavior between individual eruption events is reflected by the large variety of acoustic waveforms. A correlation between acoustic energy release and plume heights is not apparent. We observed a dramatic difference in character between emergent and impulsive events. The continuous nature of the emergent events reflects a non-impulsive extended release of the pyroclast-gas mixture that may be attributed to a combination of factors such as high magma viscosity, impediments at the vent and variable depths of fragmentation. The high-amplitude N-shaped phase of the impulsive events suggests an abrupt outward acceleration of gases and volcanic material from the vent, i.e. the explosive start of a volcanic plume, which may be initiated by a large overpressure. The seismic and acoustic sources associated with the impulsive initial vent-opening explosion event were not conjoint; the sudden uncorking of the volcano and initiation of the plume was preceded by precursory seismic activity. The pre-explosion seismic energy may have been related to fracturing or movement of material within the

over-pressurized sealed edifice prior to its arrival at the ground-air interface.

The acoustic signals recorded at Augustine have further demonstrated that microphones deployed on volcanoes provide a useful tool for eruption monitoring. The presence of large pressure pulses helps to distinguish between sub-surface seismicity and seismic events associated with explosive degassing from the vent. In contrast to seismic signals, impulsive acoustic waveforms give a direct measure of the onset of explosive volcanic plumes, which is especially helpful whenever visual observations are limited by remote settings or by cloud cover. The acoustic signal strength characterizes the impulsivity of the degassing source.

A.6 Acknowledgements

We are grateful to our colleagues from the Alaska Volcano Observatory including the USGS, DGGS and University of Alaska Fairbanks for the combined efforts put into the monitoring and eruption response. Special thanks go to Ed Clark for helping with the installation of the microphone and to Kay Lawson for helpful comments. We thank Jeff Johnson for his careful review that helped to improve the manuscript. This work was partially supported by the Alaska Volcano Observatory and the U.S. Geological Survey as part of their Volcano Hazard and Geothermal studies, and by additional funds from the State of Alaska.

References

- Garcés, M. A., M. Iguchi, K. Ishihara, M. Morrissey, Y. Sudo and T. Tsutsui (1999), Infrasound precursors to a Vulcanian eruption at Sakurajima Volcano, Japan, *Geophys. Res. Lett.*, *26*(16), 2537–2540.
- Hagerty, M. T., S. Y. Schwartz, M. A. Garcés and M. Protti (2000), Analysis of seismic and acoustic observations at Arenal Volcano, Costa Rica, 1995–1997, *J. Volcanol. Geotherm. Res.*, *101*, 27–65.
- Johnson, J. B. and R. C. Aster (2005), Relative partitioning of acoustic and seismic energy during Strombolian eruptions, *J. Volcanol. Geotherm. Res.*, *148*, 334–354.
- Johnson, J. B., A. J. L. Harris, S. Sahetapy-Engel, R. E. Wolf and W. I. Rose (2004a), Explosion dynamics of pyroclastic eruptions at Santiaguito Volcano, *Geophys. Res. Lett.*, *31*, L06610, doi:10.1029/2003GL019079.
- Johnson, J. B., R. C. Aster RC and P. R. Kyle (2004b), Volcanic eruptions observed with infrasound, *Geophys. Res. Lett.*, *31*, L14604, doi:10.1029/2004GL020020.
- Johnson, J. B. (2003), Generation and propagation of infrasonic airwaves from volcanic explosions, *J. Volcanol. Geotherm. Res.*, *121*, 1–14.
- Johnson, J. B. and J. M. Lees (2000), Plugs and chugs – seismic and acoustic observations of degassing explosions at Karymsky, Russia and Sangay, Ecuador, *J. Volcanol. Geotherm. Res.*, *101*, 67–82.
- Ripepe, M. and E. Marchetti (2002), Array tracking of infrasonic sources at Stromboli volcano, *Geophys. Res. Lett.*, *29*(22), L2076, doi:10.1029/2002GL015452.
- Rowe, C. A., R. C. Aster, P. R. Kyle, R. R. Dibble and J. W. Schlue (2000), Seismic and acoustic observations at Mount Erebus Volcano, Ross Island, Antarctica, 1994–1998, *J. Volcanol. Geotherm. Res.*, *101*, 105–128.

- Vergnolle S. and J. Caplan-Auerbach (2005), Basaltic thermals and Subplinian plumes: Constraints from acoustic measurements at Shishaldin volcano, Alaska, *Bull. Volcanol.*, doi:10.1007/s00445-005-0035-4.
- Vergnolle, S., G. Brandeis and J.-C. Mareschal (1996), Strombolian explosions: 2. Eruption dynamics determined from acoustic measurements, *J. Geophys. Res.*, 101(B9), 20449–20466.
- Wilson C. R., J. V. Olson, C. A. L. Szuberla, S. R. McNutt and G. Tytgat (2006), Infra-sonic Array Observations at I53US of the 2006 Augustine Volcano Eruptions, *InfraMatics* (www.inframatics.org), Newsletter No.13, March 2006.